CIVIL ENGINEERING STUDIES
Illinois Center for Transportation Series No. 24-010
UILU-ENG-2024-2010
ISSN: 0197-9191

Updates to Mechanistic-Empirical Design Inputs for Illinois Flexible Pavements

Prepared By
Ramez M. Hajj
Marshall R. Thompson
Renan Santos Maia
Yujia Lu
Abhilash Vyas
Babak Asadi
Bibek Regmi
University of Illinois Urbana-Champaign

Research Report No. FHWA-ICT-24-008

A report of the findings of

ICT PROJECT R27-233
Mechanistic-Empirical Design Procedures for Flexible Pavements

https://doi.org/10.36501/0197-9191/24-010

Illinois Center for Transportation

May 2024

TECHNICAL REPORT DOCUMENTATION PAGE

1. Report No.	2. Government Accession No.	3. Recipient's Catalog No.
FHWA-ICT-24-008	N/A	N/A

4. Title and Subtitle	5. Report Date
Updates to Mechanistic-Empirical Design Inputs for Illinois Flexible Pavements	May 2024
	6. Performing Organization Code N/A

7. Authors	8. Performing Organization Report No.
Ramez M. Hajj (https://orcid.org/0000-0003-0579-5618), Marshall R. Thompson, Renan Santos Maia (https://orcid.org/0000-0002-0877-4006), Yujia Lu (https://orcid.org/0000-0001-9472-199X), Abhilash Vyas (https://orcid.org/0000-0002-8713-7856), Babak Asadi (https://orcid.org/0000-0002-4946-8793), Bibek Regmi (https://orcid.org/0009-0008-8174-3952)	ICT-24-010 UILU-2024-2010

9. Performing Organization Name and Address	10. Work Unit No.
Illinois Center for Transportation Department of Civil and Environmental Engineering University of Illinois at Urbana-Champaign 205 North Mathews Avenue, MC-250 Urbana, IL 61801	N/A
	11. Contract or Grant No. R27-233

12. Sponsoring Agency Name and Address	13. Type of Report and Period Covered
Illinois Department of Transportation (SPR) Bureau of Research 126 East Ash Street Springfield, IL 62704	Final Report 5/16/21–5/15/24
	14. Sponsoring Agency Code

15. Supplementary Notes

Conducted in cooperation with the U.S. Department of Transportation, Federal Highway Administration.
https://doi.org/10.36501/0197-9191/24-010

16. Abstract

This study reviews the Illinois Department of Transportation's full-depth asphalt, limiting strain criterion, and asphalt over rubblized concrete design procedures, considering technological advancements in hot-mix asphalt—namely, the increased use of recycled materials and modified asphalt binders. The researchers evaluated the current |E*| algorithm by conducting laboratory tests with four mix designs and seven asphalt binders of different Superpave performance grades. They compared predictive models, including the current Illinois modulus algorithm as well as the Witczak, Hirsch, and newly developed Illinois Center for Transportation (ICT) Bayesian neural network (BNN) models. The ultrasonic pulse velocity (UPV) nondestructive test for modulus and field modulus measurements was evaluated as well. Subsequent tasks involved reviewing current fatigue endurance limit (FEL) criteria from an adapted protocol for the four-point bending beam fatigue test. This study found that typical hot-mix asphalt modulus values in Illinois are underestimated compared to modern mixes, suggesting potential savings by allowing an increased modulus value to be used, reducing layer thickness design. Low-temperature performance grades significantly influenced modulus, and the developed ICT BNN predictive model outperformed traditional ones. While UPV was promising for modulus screening, challenges related to material properties assumptions were identified. The current stage of research on assessing modern mixes' FEL reveals the complexity of observing FEL using simplified methods. To advance this objective, a concept of acceptable stiffness ratio (SR) is introduced. In these cases, exceptionally long fatigue life would be obtained for mixes that demonstrate an acceptable drop in SR within 10,000 cycles, with no apparent evolution of the damage state. The most conservative estimation of strain level that would result in acceptable SR aligned with IDOT's current 70 microstrain FEL criteria. On the less conservative side, allowing a 10% drop in SR within 10,000 loading cycles could increase the acceptable SR < 1 strain level as high as approximately 180 microstrain, with caution needed regarding evolving mobility trends and environmental stressors including the changing climate.

17. Key Words	18. Distribution Statement
Asphalt, Fatigue Endurance Limit, Dynamic Modulus, Traffic Speed Deflectometer	No restrictions. This document is available through the National Technical Information Service, Springfield, VA 22161.

19. Security Classif. (of this report)	20. Security Classif. (of this page)	21. No. of Pages	22. Price
Unclassified	Unclassified	59 + appendix	N/A

ACKNOWLEDGMENT, DISCLAIMER, MANUFACTURERS' NAMES

This publication is based on the results of **ICT-R27-233: Mechanistic-Empirical Design Procedures for Flexible Pavements**. ICT-R27-233 was conducted in cooperation with the Illinois Center for Transportation; the Illinois Department of Transportation; and the U.S. Department of Transportation, Federal Highway Administration.

Members of the Technical Review Panel (TRP) were the following:

- Charles Wienrank, TRP Chair, Illinois Department of Transportation
- Brian Hill, TRP Co-Chair, Illinois Department of Transportation
- Dennis Bachman, Federal Highway Administration
- Kevin Burke, Illinois Asphalt Pavement Association
- Tim Peters, Illinois Department of Transportation
- John Senger, Illinois Department of Transportation
- Heather Shoup, Illinois Department of Transportation
- Filiberto Sotelo, Illinois Department of Transportation
- Steve Worsfold, STATE Testing

EXECUTIVE SUMMARY

The Illinois Department of Transportation's last major modification on full-depth asphalt pavement mechanistic-empirical (M-E) design procedures and policies was in 2008. Significant changes and improvements in hot-mix asphalt (HMA) and other material technologies have taken place since that date, including the widespread use of recycled materials (reclaimed asphalt pavement [RAP] and reclaimed asphalt shingles [RAS]) and modified asphalt binders. To address the need for reviewing the current design framework, two main concepts for standard full-depth and limiting strain criterion asphalt pavement design were revisited: the HMA dynamic modulus (|E*|) algorithm and the fatigue endurance limit (FEL) criteria.

The initial tasks of this research were dedicated to updating IDOT's current |E*| algorithm to account for the presence of recycled asphalt and binders modified with styrene-butadiene-styrene (SBS). |E*| tests were conducted for all combinations of four mix designs and seven asphalt binders with different performance grades (PGs). The |E*| values were compared to the outputs of different models: the current Illinois M-E design algorithm as well as the Witczak, Hirsch, and newly developed Illinois Center for Transportation (ICT) Bayesian neural network (BNN) |E*| models. Furthermore, an alternative method to measure modulus using the ultrasonic pulse velocity (UPV) nondestructive test was evaluated. This project also involved field modulus measurements to evaluate this property in practical field conditions. These measurements aimed to assess the tensile strain levels observed in real-world field scenarios, considering that these pavement sections were designed based on past versions of IDOT's *Bureau of Design and Environment (BDE) Manual*, Chapter 54 (Pavement Design).

Subsequent tasks reviewed the current pavement M-E design FEL criteria. An adapted protocol for the four-point bending beam fatigue (4PBBF) test (AASHTO T 321-22) was applied to an experimental matrix combining three mixes and seven asphalt binders. Two distinct rest period conditions were considered: a 1-second rest period and a 0-second rest period. The first condition mirrors traffic patterns typically observed in real-world field conditions, where longer rest periods exist between successive load applications. The second scenario, however, is more severe and can be linked to situations where platoonable roadway sections could experience short rest periods between successive load applications. Ideas are presented regarding the appropriateness of the existing tensile strain limit of 70 microstrain for limiting strain criterion pavement design. Furthermore, alternative approaches were explored to evaluate an "acceptable level of damage" that could be defined through a reduced and simplified protocol within the four-point bending beam machine. The significance of this activity is paramount, as the existing protocols for assessing the fatigue behavior of asphalt mixtures under low strain levels and rest periods longer than zero are impractical due to excessively long test durations. Finally, findings from various scales—spanning binder-level assessments to modulus, fracture, and fatigue laboratory tests on mixtures to field data—were combined and analyzed in depth. Relationships and trends within the compiled data were further explored.

Overall, this study observed that typical HMA modulus values used in Illinois for asphalt mixes are underpredicted when compared to modern mixes incorporating recycled materials and modified binders. Assuming higher modulus values could yield cost and environmental savings by allowing for

reduced layer thicknesses in full-depth pavement design. However, the effects of climate change may also have substantial effect on decreasing the modulus, which needs to be studied further and integrated with changing climate models. Furthermore, low temperature PG of asphalt binders demonstrated a crucial role for modulus determination within the frequency and design temperature range of interest for the state of Illinois. The ICT BNN model outperformed the traditional and well-known Witczak and Hirsch models in terms of modulus modeling. Another benefit of the BNN approach is its simplified application, relying solely on the PG label without the need for extensive binder testing. This research suggested this model holds potential as a supplement to the current IDOT modulus algorithm. On the nondestructive testing side, while the UPV test shows promise for quick screening of asphalt modulus, challenges arise from assumptions about Poisson's ratio (PR) and shift factors (SF), leading to consistently higher predicted modulus values than those obtained from actual laboratory tests.

Although the modulus study demonstrated potential for reducing flexible pavement design thickness, assessing the impact of recycled materials on mix stiffening and fatigue life is paramount. The ongoing stage of this research involved a comprehensive fatigue evaluation, refining approaches for the definition of a FEL analysis protocol that combined solid theoretical background and simplicity for practical application. Inspired by NCHRP report 9-44A (Witczak et al., 2013), this research proposed an adaptation to the 4PBBF test standard that accounted for varying strain levels and rest periods. However, defining a FEL value remains an open and ongoing research question, considering challenges in test geometry, loading characteristics, and the asphalt mix viscoelastic behavior. This project proposed, so far, an acceptable SR < 1 value for mixes instead of an FEL value. This condition would be achieved when a mix indicates an exceptionally long fatigue life as it exhibits an acceptable drop in SR within 10,000 cycles and a very stable (flat line) SR value within its final loading cycles. From the four scenarios of acceptable SR < 1, the most conservative estimated FEL converged to the current IDOT standard value of 70 microstrain, suggesting that this might be a conservative criterion. This case would correspond to a tensile strain value that would lead the mix to its peak SR under the critical 0-second rest period condition. On the less conservative side, considering a scenario where a 10% drop in SR within 10,000 cycles was allowed, the acceptable SR < 1 could be increased to approximately 180 microstrain. However, the agency needs to consider relaxing such limits with great care, as the world is facing rapid changes in mobility trends, such as platooning and electric vehicles with heavy loads, as well as increasingly critical environmental stressors due to climate change. These combined factors demonstrate the need for further evaluation of the modulus criteria and comprehensive study of materials from various sources and including a wider range of mix design factors.

TABLE OF CONTENTS

LIST OF FIGURES

LIST OF TABLES

CHAPTER 1: INTRODUCTION

It is important to continue to review and modify, as appropriate, IDOT's mechanistic-empirical (M-E) flexible pavement design procedures and policies, as many significant factors continue to change. Hot-mix asphalt (HMA) modulus and fatigue data developed in ICT-IDOT project R27-161 (Lippert et al., 2017) show that the currently utilized modulus and fatigue algorithms do not adequately capture the impact of SBS-modified binders and recycled asphalt (reclaimed asphalt pavement [RAP] and reclaimed asphalt shingles [RAS]) on these inputs for flexible pavement thickness design. The last major modification to Chapter 54 (Pavement Design) in IDOT's *Bureau of Design and Environment (BDE) Manual* was based on research conducted in 2008, and significant changes and improvements in HMA and pavement technology have been achieved since that date. To maximize the impact of IDOT's M-E flexible pavement design procedures and maintain their applicability, current technology should be reflected (as applicable for IDOT conditions).

The objective of the project is to conduct those activities relevant to establishing and utilizing the best demonstrated available technology as related to IDOT's flexible pavement design procedures and policies. The main focus of this study was revising the current inputs used for modulus and fatigue endurance limit (FEL) in full-depth asphalt pavement design. The objectives are to update the modulus measurements and calculations to account for new materials in HMA mixes and apply this knowledge to fatigue-related asphalt layer thickness design to account for these updated material properties. In addition, the research team continued to monitor literature, structural testing data from the field, and ongoing projects to ensure the performance of full-depth asphalt and asphalt over rubblized concrete flexible pavements.

RESEARCH OBJECTIVES

The objectives of this research were as follows:

- Use traditional techniques (dynamic modulus test) and novel methods (e.g., ultrasonic pulse velocity) to conduct a wide range of modulus measurements with field- and laboratory-compacted mixes.
- Determine the effectiveness of various predictive fatigue algorithms including binder and mixture-based predictive algorithms.
- Explore the dependency of the fatigue endurance limit on different mix variables, including the use of RAP and polymer-modified binder.
- Determine if a fundamental or empirical relationship can be established between the Illinois Flexibility Index Test (I-FIT) or other test methods and the fatigue endurance limit.

CHAPTER 2: THEORETICAL BACKGROUND AND LITERATURE REVIEW

IDOT'S ASPHALT PAVEMENT M-E DESIGN PROCEDURE: CURRENT STATE AND CHALLENGES

The Illinois Department of Transportation's design of full-depth HMA pavement as well as HMA pavement placed on top of rubblized Portland cement concrete (PCC) is based on IDOT's *Bureau of Design and Environment Manual*, Chapter 54. The latest version of this protocol was updated based on research completed in 2008. The design concept followed in this procedure is based on three main inputs: (i) a subgrade support ratio (SSR), ranging from poor (worst quality) to granular (best quality); (ii) a facility class, ranging from Class I (highest traffic volume) to Class IV (lowest traffic volume); and (iii) an HMA mixture design temperature, ranging from 73°F (northern Illinois) to 81°F (southern Illinois) based on mean monthly pavement temperature corrected for May–June for standard designs and July for limiting strain criterion designs.

According to Chapter 54 of the *BDE Manual*, the definition of the SSR classification is based solely on the percentage of sand, silt, and clay fractions within the subgrade soil. The traffic factor is a function of the design period in years as well as the composition of the traffic for the design lane. When it comes to HMA characterization for design, the manual directly relates the asphalt binder Superpave PG to a theoretical HMA modulus considering a range of design temperatures (from 73°F to 81°F). This algorithm is divided into two groups: for PG 64-28 and PG 70-28, the HMA modulus is assumed to be lower, ranging from 400 to 600 ksi, whereas for PG 64-22, PG 70-22, PG 76-22, and PG 76-28, the HMA modulus is assumed to vary between 500 and 750 ksi. PG 58-28 was not considered in this algorithm because the algorithm does not factor in the use of recycled materials, which is the only case in which PG 58-28 is used, although most mixes use recycled materials today. The final design thickness is a function of a design strain directly related to the traffic factor. Once the assumed HMA modulus at the design temperature and the design strain are defined, the HMA design thickness is determined for each SSR type. For limiting strain criterion pavements (full-depth HMA and HMA placed on top of rubblized PCC), the HMA design thickness is determined assuming a design tensile strain of 70 microstrain, termed the "fatigue endurance limit" or "FEL."

One of the main inputs for M-E pavement design approaches is the asphalt mixture elastic modulus. The dynamic modulus (|E*|) is a measure of material stiffness, which increases as asphalt binder ages and recycled material content increases, as recycled materials are aged significantly. This results in a simple assumption that an increase in asphalt mixture modulus leads to a reduction in pavement critical responses when linear elastic analysis is considered within the asphalt layer. From one point of view, this appears beneficial for pavement performance. However, asphalt binders with increased stiffness resulting from a higher degree of aging are susceptible to cracking due to their increased brittleness. This is the case for asphalt mixtures using RAP and RAS (Al-Qadi et al., 2007; Ma et al., 2022). Therefore, the future of any pavement design algorithm must consider the use of these materials from multiple perspectives.

The use of recycled materials (especially RAP) is already ubiquitous in asphalt mixtures in Illinois and around the world. This topic has gained momentum since the early 2000s, with several remaining challenges. The demand for recycling asphalt presents potential savings for contractors and agencies because reusing existing asphalt binder, generally the most expensive component of HMA, will reduce its demand. Over time, the composition of asphalt binder has become increasingly variable and complex. This is, in part, a function of the wider use of RAP and additives such as polymer modifiers and rejuvenators (termed softener modifiers in IDOT specifications). In summary, the final composite asphalt binder, made of recycled and virgin asphalt, tends to vary widely in terms of its chemical composition and performance, leading to variable performance of the corresponding mix. Therefore, the present study approaches the issues presented by recycled materials and new asphalt binder formulations by analyzing comprehensively both fatigue and modulus performance of mixes with varying mix design factors.

HMA MODULUS MEASUREMENT AND MODELING

Dynamic Modulus Concept

Since the 1960s, the complex modulus (E*) has been researched as an alternative to the use of the resilient modulus for the characterization of asphalt mixture stiffness. Fundamental studies (Papazian, 1961; Witczak & Root, 1974; Bonnaure et al., 1977; Christensen, 1982; Daniel et al., 1998) demonstrated that applying sinusoidal loading to specimens at controlled temperatures and various frequencies, and measuring the respective displacements, enables the linear viscoelastic characterization of asphalt mixtures. The outcome of this process is the material stress–strain constitutive law under continuous sinusoidal loading (Witczak, 2002). The mathematical formulation of the complex and dynamic modulus is described in Figure 1 to Figure 7.

$$\sigma = \sigma_0 \sin(\omega t)$$

Figure 1. Equation. Sinusoidal stress function.

$$\omega = 2\,\pi\,f$$

Figure 2. Equation. Angular frequency.

$$\varepsilon = \varepsilon_0 \sin(\omega t - \delta)$$

Figure 3. Equation. Sinusoidal strain function.

$$|E^*| = \frac{\sigma_0}{\varepsilon_0}$$

Figure 4. Equation. Dynamic modulus.

$$E' = \frac{\sigma_0 \ cos(\delta)}{\varepsilon_0}$$

Figure 5. Equation. Storage modulus.

$$E'' = \frac{\sigma_0 \ sin(\delta)}{\varepsilon_0}$$

Figure 6. Equation. Loss modulus.

$$E^* = E' + i\,E''$$

Figure 7. Equation. Complex modulus.

Where: σ = stress

ε = strain

σ_0 = stress amplitude

ω = angular frequency

f = frequency

ε_0 = strain amplitude

δ = phase angle

E' = storage modulus

E'' = loss modulus

i = imaginary number ($\sqrt{-1}$)

|E*| = dynamic modulus

The dynamic modulus (|E*|) is the stiffness property of asphalt mixtures and is most used as an input parameter in the M-E design of asphalt pavements. It is the primary input in all three hierarchical levels in AASHTO's *Mechanistic–Empirical Pavement Design Guide* (*MEPDG*) (AASHTO, 1993). Mechanistic-empirical design frameworks involve applying transfer functions to relate critical pavement responses (a stress and strain determined as a function of the applied load, pavement geometry, and the material properties) to empirical measurements of distresses (mainly rutting and fatigue cracking) observed in the field (Witczak, 2002; AASHTO, 2008). Previous literature has shown |E*| to correlate consistently with pavement distresses (Witczak, 2002; Zhang et al., 2013; Bech & Vandenbossche, 2023). Dynamic modulus significance extends beyond direct pavement design applications to numerical simulations and the development of viscoelastic/viscoplastic constitutive

relationships within HMA layers (Hernandez et al., 2016; Darabi et al., 2020). However, dynamic modulus measurement still presents a challenge due to its expensive and time-consuming testing procedures—namely, AASHTO T 342-22 (2022) and T 378-22 (2022). Nonetheless, accurate predictive modeling of |E*| is crucial for research, industry, and agencies. Consequently, numerous predictive models have emerged over the past few decades to address this concern.

Dynamic Modulus Predictive Models

In the context of M-E design, the accuracy of |E*| is crucial. Moreover, once a design framework relies on |E*| prediction, it becomes imperative to continuously update and refine the associated algorithms to consider the materials most widely used. This is especially true considering the widespread use of recycled asphalt and modified asphalt binders that have become commonplace in the last decades, which add more uncertainty to existing predictive models that did not consider these items. Several |E*| models are available in the literature. The original Witczak model (Witczak & Fonseca, 1996) and revisions (Bari & Witczak, 2005), used in the 1.0 version of AASHTO's *MEPDG* software (Witczak et al., 2007), and Hirsch (Christensen Jr et al., 2003) models are the most widely known models. These models use empirical data to predict |E*| using binder properties and volumetric mix design parameters. Other models, such as the one proposed by Al-Khateeb et al. (2006), have the advantage of simplicity by considering fewer variables as inputs: asphalt binder complex shear modulus (G*) and voids in the mineral aggregate (VMA). Research conducted in Illinois showed agreement and similar accuracy between Witczak and Hirsch models while noting that the Hirsch model is simpler (Garcia & Thompson, 2007).

Over time, an increase in available data and innovations in data science and machine learning have enabled the development of newer predictive models. To address some of the inconsistencies of |E*| predictions within empirical models, researchers try to calibrate these models for local materials and conditions (Birgisson et al., 2005; Bennert, 2009; Mohammad et al., 2014). Also, numerous machine learning–based models for |E*| prediction have been developed (Behnood & Daneshvar, 2020; Ceylan et al., 2008; Far et al., 2009; Singh et al., 2013). In this context, this research effort proposed a prediction model by means of the BNN approach (Asadi et al., 2023). The authors incorporated an extensive dataset and took into consideration model uncertainties using the BayesByBackprop algorithm (Blundell, 2015), which showed potential to outperform traditional and machine learning–inspired models. It presented several advantages, including the replacement of binder linear viscoelastic parameters (binder complex shear modulus, G*, and phase angle, δ) by simple PG, as well as the consideration of RAP content. Chapter 3 presents more details about this model.

Nondestructive Testing for Modulus Using the Ultrasonic Pulse Velocity Method

Nondestructive techniques facilitate the characterization of materials, either in the field or in the laboratory. These techniques are beneficial in terms of their simplicity and cost-effectiveness. Ultrasonic pulse velocity is a nondestructive technique that can be applied to predict different material properties. Originally, UPV was utilized mainly to evaluate the material properties (mostly regarding stiffness) of HMA and PCC. In the laboratory, |E*| can be obtained from the application of standards AASHTO T 342-22 (2022) and T 378-22 (2022). In the field, the falling weight deflectometer (FWD) is the most widely known device for the determination of HMA, unbound aggregate base, and subgrade layer moduli. However, both tests can be time and resource intensive.

In the laboratory, portable devices such as UPV can be extremely useful. Birgisson et al. (2003) used UPV to investigate the impact of moisture on asphalt integrity. Arabani et al. (2009) evaluated filler content, binder content, and compaction level by applying the UPV technique. Material properties including strength (Mata et al., 2023), modulus (Van Velsor et al., 2011; Medina et al., 2018), and Poisson's ratio (Pal, 2019) of construction materials have been measured, and these measurements have been validated using traditional techniques.

ASTM C597-22 (2022) is the main reference for performing modulus tests using UPV. Although the standard method is specific for PCC, several authors have adapted this protocol for HMA (Tavassoti-Kheiry et al., 2017; Medina et al., 2018). Although the application of UPV can be straightforward, the reliability of UPV for assessing HMA stiffness is limited because some parameters, most frequently the Poisson's ratio (Jiang et al., 2006), must be assumed. Further complexity exists given that Poisson's ratio is dynamic for viscoelastic materials and depends on the loading frequency (Di Benedetto et al., 2016; Nguyen et al., 2021). There are frameworks for Poisson's ratio determination using direct and semi-direct wave speed measurement (Carrillo et al., 2019). However, these frameworks are suitable for concrete cubic samples and are not practical for cylindrical specimens, which are most commonly obtained in the lab using the Superpave gyratory compactor or from the field using coring systems.

FATIGUE ENDURANCE LIMIT CONCEPT

Bottom-up fatigue cracking is expected not to occur for limiting strain criterion asphalt pavement designs, either full-depth HMA or HMA placed over rubblized PCC. The rationale is that the asphalt thickness is high enough (full-depth asphalt) or the base layer is stiff enough (HMA over rubblized concrete) to reduce the tensile strain to a point that the HMA layer will recover fully after each load application. The concept of FEL was established based on this rationale. It is defined as the limiting strain criterion below which there is no cumulative damage in an indefinite number of loading cycles. IDOT uses 70 microstrain as the FEL for its limiting strain criterion design, which dates back to the earliest work on FEL in California (Monismith et al., 1961). However, this criterion is on the conservative end, as previous studies of Illinois materials have shown that the existence of a single endurance limit is not applicable for all mixes, and some show substantially higher FELs (Carpenter & Shen, 2006; Shen & Carpenter, 2005). Note that when it comes to highway construction costs, even a marginal increase in FEL criteria can represent substantial cost savings due to a reduction in total HMA thickness.

Prowell et al. (2010) applied a protocol based on the four-point bending beam fatigue (4PBBF) testing scheme for 19.0 mm nominal maximum aggregate size (NMAS) mixtures made of four different asphalt binders at varying binder content designs. FEL determined using this methodology ranged from 75 to 200 microstrain. The presence of stiffer asphalt binders led to higher obtained FELs. Also, when the observed binder content was higher than the optimum binder content designs (lower air voids), FEL also increases. National Cooperative Highway Research Program (NCHRP) Project 9-44A (Witzcak et al., 2002) aimed to evaluate the relationship of FEL to asphalt binder rheology, air voids, asphalt content, temperature, strain level, number of load cycles, and rest period (RP) between load cycles. This research also observed that after the application of any number of load cycles, *N*, at the

FEL, the stiffness ratio (SR) would be a constant of 1, as shown in Figure 8. The authors also highlighted that rest periods would induce a Healing Index (*HI*), increasing the number of cycles to failure (SR = 0.5) (Witczak et al., 2013). They developed a model (Figure 9, R^2 = 0.891) for the prediction of SR using several variables. The authors determined FEL values based on ε_t values that would result in a SR of 1 for different values of E_0, *N* (later fixed as 200,000 load cycles), and rest period.

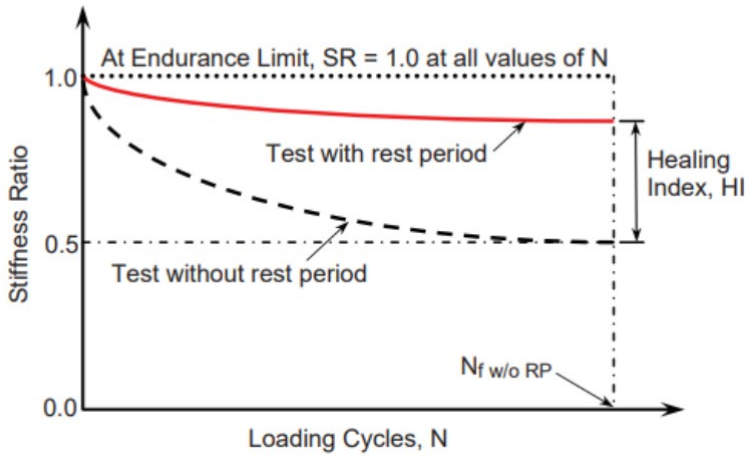

Figure 8. Graph. Endurance limit concept.

Source: Witczak et al. (2013)

$$SR = 2.0844 - 0.1386 * \log(E_0) - 0.4846 * \log(\varepsilon_t) - 0.2012 * \log(N) + 1.4101 * \tanh(0.8471 * RP)$$
$$+0.0320 * \log(E_0) * \log(\varepsilon_t) - 0.0954 * \log(E_0) * \tanh(0.7154 * RP) - 0.4746 * \log(\varepsilon_t) * \tanh(0.6574 * RP)$$
$$+0.0041 * \log(N) * \log(E_0) + 0.0557 * \log(N) * \log(\varepsilon_t) + 0.0689 * \log(N) * \tanh(0.2590 * RP)$$

Figure 9. Equation. Stiffness ratio equation from NCHRP Report 9-44A.

Source: Witczak et al. (2013)

Where: E_0 = Initial flexural stiffness (ksi)

ε_t = Tensile strain (10^{-6} in/in)

RP = Resting period(s)

N = Number of loading cycles

Isied and Souliman (2019) extracted the data points from the 4PBBF test matrix performed in the NCHRP 9-44A project to propose an artificial neural network (ANN) model for determining SR values. The trained ANN model was simplified into a stand-alone equation (Figure 10). By setting SR = 1 and Nf = 20,000, the endurance limit (EL) value could be determined (Figure 11). Note that these equations are based on data from the NCHRP 9-44A report, and local calibration would be required for their application to modern materials and those used in states outside the scope of the study.

$$\varepsilon = 10^{-0.28256 \log(E_0) + 0.1058 \tanh(RP) - 0.06934 \log(Nf) - 0.11089 (SR) + 3.40365}$$

Figure 10. Equation. ANN-derived stand-alone equation.

Source: Isied & Souliman (2019)

$$EL = 10^{-0.28256 \log(E_0) + 0.1058 \tanh(RP) + 2.99452658}$$

Figure 11. Equation. Endurance limit stand-alone equation.

Source: Isied & Souliman (2019)

Where: E_0 = Initial flexural stiffness (ksi)

ε = Applied strain (microstrain)

RP = Resting period (s)

N_f = Number of loading cycles to failure

SR = Stiffness ratio

Shen and Carpenter (2006) applied the concepts of healing and endurance limit to the analysis of the fatigue life of airport pavements. The theoretical background of this study involved the dissipated energy approach. The energy input by loading can be computed as the area under the stress–strain curve, and the sum of the energy of a loading/unloading cycle should be zero for purely elastic materials. However, when it comes to non-elastic materials, this sum is not zero, indicating that energy has been dissipated within the loading cycle. Fatigue damage mechanisms are associated with the energy dissipation phenomena. Note that the existence of dissipated energy in a system does not necessarily represent a damage-state cycle, given that not all dissipated energy can be translated into cracking. Previous studies indicated that non-deteriorating cycles will generate stable hysteresis loops (Schapery, 1984; Si et al., 2002). On the other hand, cycles with changing hysteresis loops are associated with ratios of dissipated energy change (RDEC). According to this concept, the energy loss that is not related to damage remains approximately constant; therefore, potential changes in dissipated energy are associated with damage development. Shen and Carpenter (2006) used the RDEC approach, meaning that a plateau value (PV) corresponding to a RDEC value at 50% initial stiffness reduction represents an energy plateau where an approximately constant rate of energy is converted into damage in each cycle. The authors observed the existence of a fundamental relationship between PV and fatigue life. Shen (2006) suggested the use of an energy-based FEL criterion, based on a plateau value (PV_L) for which any PV below this level would represent a mixture having an "extraordinarily long" or "unlimited" fatigue life. A typical PV_L for HMA mixtures was 6.74×10^{-9}. Still, the number of cycles within the 4PBBF test machine required to obtain such information could be considerably long. They stated that 8 million load repetitions at 10 Hz frequency were required, meaning the tests would need to be run for approximately 10 days.

Fatigue tests are valuable for comparing and ranking different materials. However, several drawbacks have been identified, such as their prolonged duration and the fact that the mechanism and mode of fracture initiation and propagation are not often well-defined. Reaching load repetitions in the order of tens of millions becomes time-consuming, especially when dealing with low strain levels. Exploring alternatives to establish strain levels that will lead to prolonged fatigue life during the initial load application cycles would be highly beneficial for researchers and practitioners. Notably, NCHRP 9-44A did attempt this, proposing that FEL values can be estimated within a protocol that combines different strain levels, rest periods, and the reasonable range of 20,000 load application cycles. This will be explored further in Chapter 5 of this report.

CHAPTER 3: MATERIALS AND METHODS

MATERIALS

Asphalt Binders

Seven asphalt binders were collected from a single source to ensure relative similarity in terms of composition. The binders differed in terms of the Superpave PG. Two out of seven were neat binders (PG 58-28 and PG 64-22), and five were binders modified with styrene-butadiene-styrene (SBS) (PG 64-28, PG 70-22, PG 70-28, PG 76-22, PG 76-28) (Table 1). It is important to highlight that SBS is the only polymer currently used for modification of asphalt binders in the state of Illinois. As per a 2023 IDOT special provision, ground tire rubber and softener modification are also allowed for asphalt binder modification, but these modifiers were outside the scope of the current project.

Table 1. Asphalt Binders

PG	Polymer Modification
58-28	None
64-22	None
64-28	SBS
70-22	SBS
70-28	SBS
76-22	SBS
76-28	SBS

For quality control throughout this project, the asphalt binders were initially collected into 5-gallon metallic buckets and kept in cold storage to mitigate aging. Then, the asphalt binders were fractionated into quarter-gallon cans. For fractionation, the asphalt binders were heated to 140°C for at least 4 hours, with stirring performed after 2 hours. Stiffer asphalt binders required more heating time to flow and homogenize enough for fractionation. The quarter-gallon cans were sealed and stored on a shelf at room temperature in the lab. To ensure there was no significant aging during this storage process, all binders were tested for high and low PG after six months. The asphalt binder cans were discarded if they were stored for more than one year, and a new fractionation process was performed with the asphalt binders properly stored in the cooler.

Mineral Aggregates, RAP, and RAS

The mineral aggregates and recycled asphalt materials (RAP and RAS) were obtained from four asphalt mixture plants in Illinois. Each aggregate source was sampled based on mix designs approved by IDOT and which were to be replicated in the laboratory. For this report, the sources/mixes were named as follows based on nominal maximum aggregate size, asphalt binder replacement (ABR), and number of design gyrations in the Superpave gyratory compactor:

- Source 1 (District 1): 19.0 mm N90 high ABR mix with RAS
- Source 2 (District 7): 19.0 mm N90 lower ABR mix
- Source 3 (District 1): 19.0 mm N90 medium ABR mix
- Source 4 (District 5): 19.0 mm N50 high ABR mix

The aggregates were collected from each plant and transported to the Illinois Center for Transportation laboratory in Rantoul, Illinois. The mineral aggregates were dried at 110°C for 24 hours. The recycled materials were dried at 50°C for 72 hours (with stirring performed every 24 hours). Then, the aggregates were fractionated according to IDOT practices for each stockpile. For RAP and RAS, fractionation was adapted according to the apparent gradation to ensure better control during the batching procedures. Illinois State Geological Survey publications (Lasemi, 2015; Miao et al., 2016) were used for identifying the mineralogy of each aggregate type used in all four mixtures. In general, most mixes were comprised of limestone/dolomitic aggregates, as expected for Illinois lower binder, dense-graded mixes.

Mix Design and Laboratory Mix Control

The four mixes were originally designed by contractors and approved by IDOT sometime over the last decade. All mixes had similar NMAS (19.0 mm), design air voids (4%), and use (as a lower lift, binder course). Each mix had different contents of recycled material (RAP and RAS). Mix 1 had both RAP and RAS as constituents. Mixes 2 and 3 had only RAP (with mix 2 having the lowest RAP percentage). Mix 4 had the highest RAP content, but this mix was designed at 50 gyrations and included in the study for local agency type applications. Mixes 1, 2, and 3 were designed at 90 gyrations and included in the study for interstate/higher traffic applications. Table 2 summarizes the mix design information.

Table 2. Mix Designs

Mix	NMAS (mm)	Number of Gyrations	RAP (%)	RAS (%)	Binder Content (%)	Virgin Binder (%)	Recycled Binder (%)	ABR (%)	Air Voids (%)	VMA
1	19	90	22.0	2	5.4	3.66	1.63	30.3	4.0	13.7
2	19	90	15.0	0	5.0	4.20	0.78	15.7	4.0	13.6
3	19	90	25.0	0	5.2	4.15	1.04	20.0	4.0	14.2
4	19	50	38.3	0	5.4	3.91	1.53	28.1	4.0	13.8

IDOT's approved mix designs were taken as a reference. To evaluate the effect of different asphalt binders for the experimental matrix of this research, the reference design was kept constant in terms of the proportions of materials for the seven asphalt binders analyzed. The control of the mix properties was based on gradation, binder content, bulk specific gravity (G_{mb}), and theoretical maximum specific gravity (G_{mm}) at the number of design gyrations (N_{design}) for the reference asphalt binder. Once the laboratory-prepared mixes based on the reference asphalt binder were accepted, G_{mm} was measured for all source and binder combinations (28 total). Then, the G_{mm} obtained for each specific combination of asphalt binder and aggregate source was used as a reference to produce all

specimens for the mechanical tests. Figure 12 presents the gradation curves for the field and laboratory gradations, showing the control of this property was acceptable for the mechanical tests performed later.

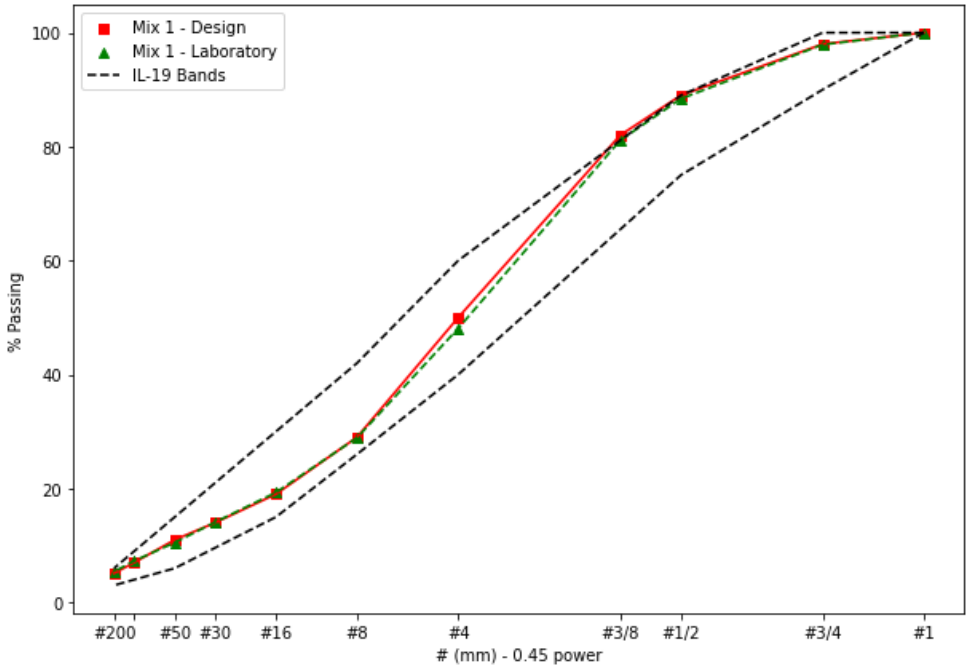

(A) Mix 1

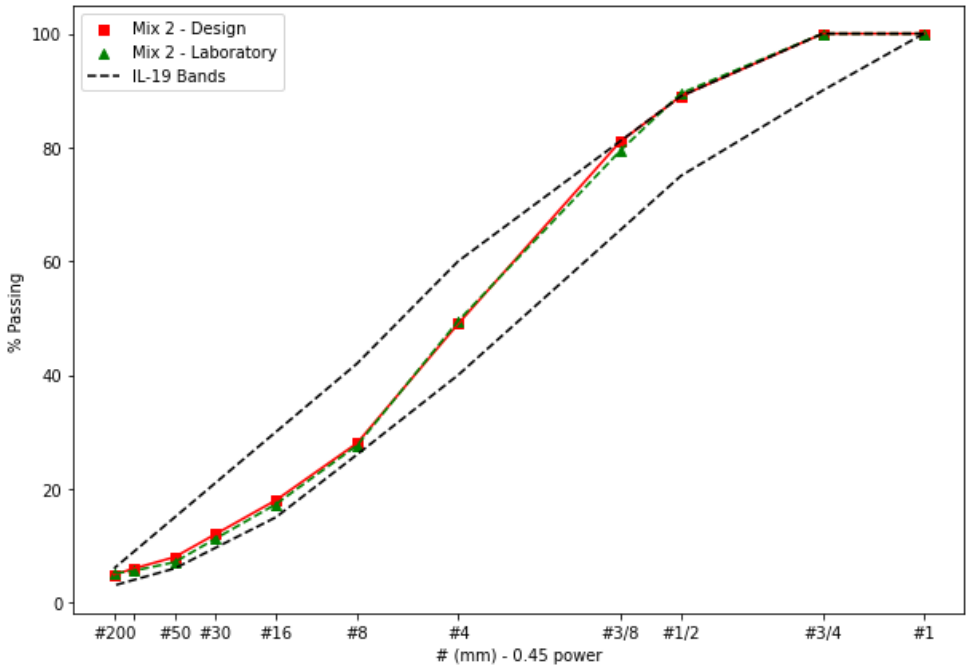

(B) Mix 2

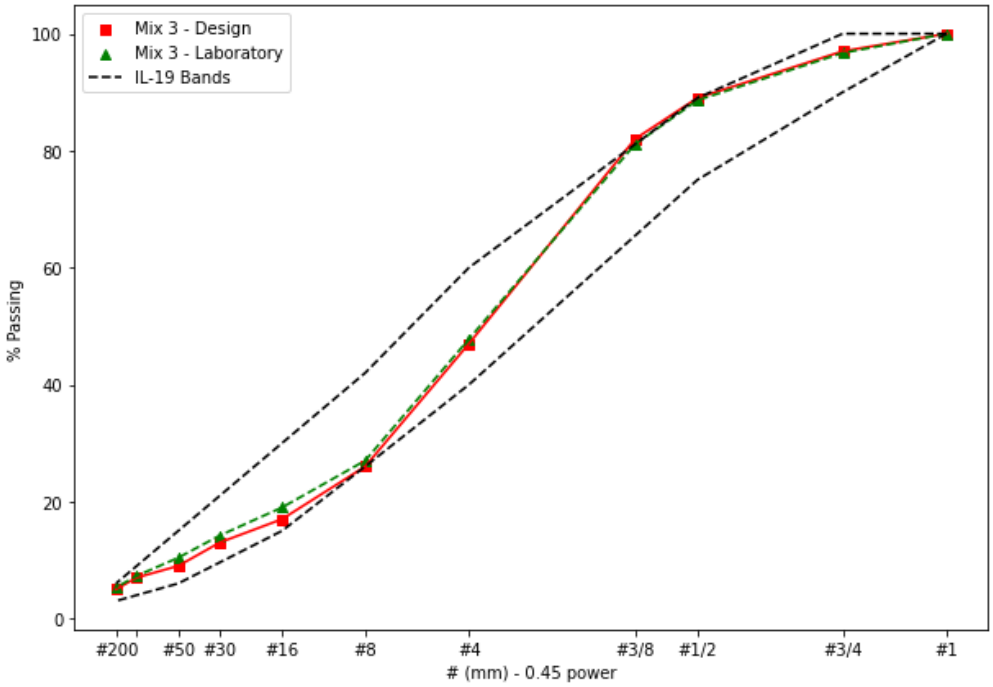

(C) Mix 3

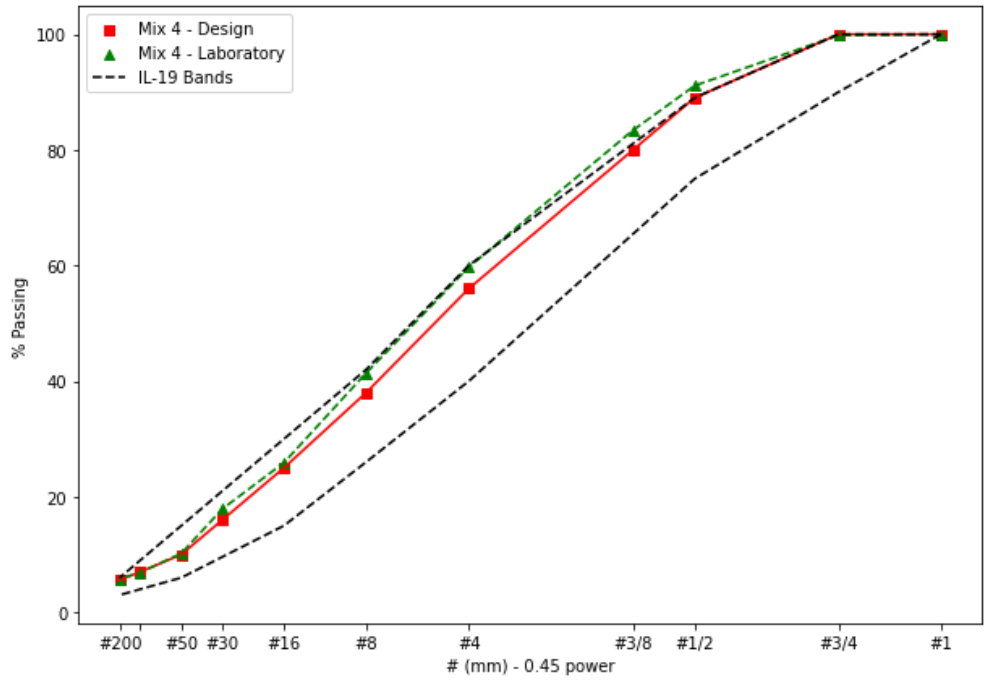

(D) Mix 4

Figure 12. Graph. Design and laboratory gradations.

To prepare the mixes, the aggregates were batched based on the proportions in the design for each fraction of each material (allowing a variation of no more than 1 g). The amount of material to be

compacted was calibrated for the specimens to meet the targeted air void content. The mixing, short-term aging, and compaction processes were performed based on AASHTO specifications (AASHTO T 312-22, AASHTO R 30-22, AASHTO R 83-22) and IDOT modifications (IDOT *Manual of Test Procedures for Materials*) (IDOT, 2021). The aggregates and asphalt binders were heated to a mixing temperature of 146°C for unmodified binders and 163°C for modified binders. All mixes were subjected to 1 hour of short-term aging at their compaction temperature (146°C for unmodified binders and 152°C for modified binders) before the manual separation for G_{mm}, the compaction of cylindrical specimens for mechanical testing using the Superpave gyratory compactor or beams using the rolling wheel compactor. Once the compacted specimens were obtained, volumetrics were checked, and the proper sawing protocols were applied for each test to be performed (dynamic modulus, Illinois Flexibility Index Test, and 4PPBF).

ASPHALT BINDER TESTING

All binders were tested in terms of frequency sweep for unaged, rolling thin film oven (RTFO), and pressure aging vessel (PAV) aged conditions. The multiple stress creep and recovery test was performed to get a sense of the nonlinear performance of the asphalt binder. To assess the nonlinear cracking potential of asphalt binders, the poker chip test was used to evaluate the tensile strength and ductility of the asphalt binder at room temperature. This test involves sandwiching the asphalt binder between two metal plates and pulling the top plate apart by means of a monotonic uniaxial loading rate of 2 N/s. Three spacers, 0.016 in diameter and spaced 120° apart, are used to control the film thickness, which in turn forces cohesive failure by fracture of the asphalt binder sample. Studies have shown that poker chip ductility of asphalt binder correlates well with cracking resistance of asphalt binders in the lab and field (Clark, 1958; Doyle, 1958; Glover et al., 2005; Mohanraj et al., 2023). However, most traditional ductility tests put less importance on the critical stress state that the binder is subjected to within the asphalt mixture. The poker chip test measures ductility of the asphalt binder by subjecting it to a realistic stress state, with high shear and confinement. This better represents a thin film of asphalt binder confined between two aggregates. A stress–strain curve is derived after completion of the test. The tensile strength parameter is the peak stress in the curve, while the ductility parameter is the strain at 80% peak stress (20% reduction after peak), denoted as a percentage. More information about this test can be found in the existing and recent literature (Filonzi et al., 2022).

DYNAMIC MODULUS TESTING AND MODELING

Dynamic modulus tests were conducted per AASHTO standards T 342-11 (2022), T 378-17 (2022), and R 84-17 (2017). The AASHTO T 378-17 (2022) standard was the main reference for performing the |E*| test by means of the Asphalt Mixture Performance Tester (AMPT) for determination of stiffness and phase angle at different temperatures and frequencies. The test was carried out for each specimen at −10.0, 4.4, 21.1, 37.8, and 54.4°C, at six loading frequencies: 0.1, 0.5, 1.0, 5.0, 10.0, and 25.0 Hz. Peak-to-peak strains were fixed between 75 and 150 microstrain to ensure that the mixes were evaluated within the linear viscoelastic region, and no damage was induced during testing. Master curves for each mix were built based on the time-temperature superposition principle. The sigmoidal function (Figure 13) was employed to fit the master curves at a reference temperature of

21.1°C. The Williams-Landel-Ferry (WLF) equation (Figure 14) (Williams et al., 1955) was employed to determine shift factors.

$$\log|E^*| = \delta + \frac{\alpha}{1 + e^{\beta + \gamma(\log f_r)}}$$

Figure 13. Equation. Sigmoidal function.

Where: f_r: reduced frequency

δ, α, β, γ: curve fitting coefficients

$$\log a_T = \frac{C_1 (T - T_0)}{C_2 + T - T_0}$$

Figure 14. Equation. Williams-Landel-Ferry (WLF) equation.

Where: C1, C2 = fitting coefficients

T_0 = reference temperature (21.1°C)

T = temperature to be shifted

ICT Bayesian Neural Network Model

An overview of previous machine learning (ML)-based approaches for |E*| prediction is detailed by Asadi et al. (2023). Note that most ML models often focus on a specific dataset, such as previous NCHRP project data or local databases, which may be outdated and lack recent mix design components such as polymer-modified binders and RAP. The application of these models to new data, especially from various labs or geographic locations, has infrequently been reported. Furthermore, the bulk of previous ML studies have presented deterministic models without addressing model uncertainty. Aleatoric uncertainties are inherent to the randomness in a system's physical attributes, stochasticity in its input excitations, and high noise levels in the accompanying experimental data (Olivier et al., 2021). Variations in |E*| measurements may be attributed to factors such as testing equipment, specimen preparation, or operator influence. However, uncertainty quantification has been overlooked in most ML-based |E*| models.

Kim et al. (2011) found that the average |E*| values obtained for the same HMA mixtures determined by AASHTO T 378 are systematically lower than those obtained using AASHTO T 342-11. The reported difference between the two procedures was approximately 13%. The significant variance in |E*| results for identical HMA mixtures tested in different laboratories has also been reported (Bennert et al., 2009). Developing neural network-based |E*| models also involves epistemic or model uncertainty, often stemming from a lack of training data or knowledge about the problem. To tackle this concern, this study established a probabilistic Bayesian deep neural network (BNN) using the BayesByBackprop algorithm to predict |E*| that incorporates aleatoric and epistemic

uncertainties for various HMA mixes, including those with RAP. A total of 9,017 data points were gathered from reports and studies in the existing literature spanning 18 states (Figure 15) to train the BNN, with more than one-third of the HMA mixes considered including RAP. All data were publicly available in the literature, except those inherent to Illinois Center for Transportation from previous IDOT studies.

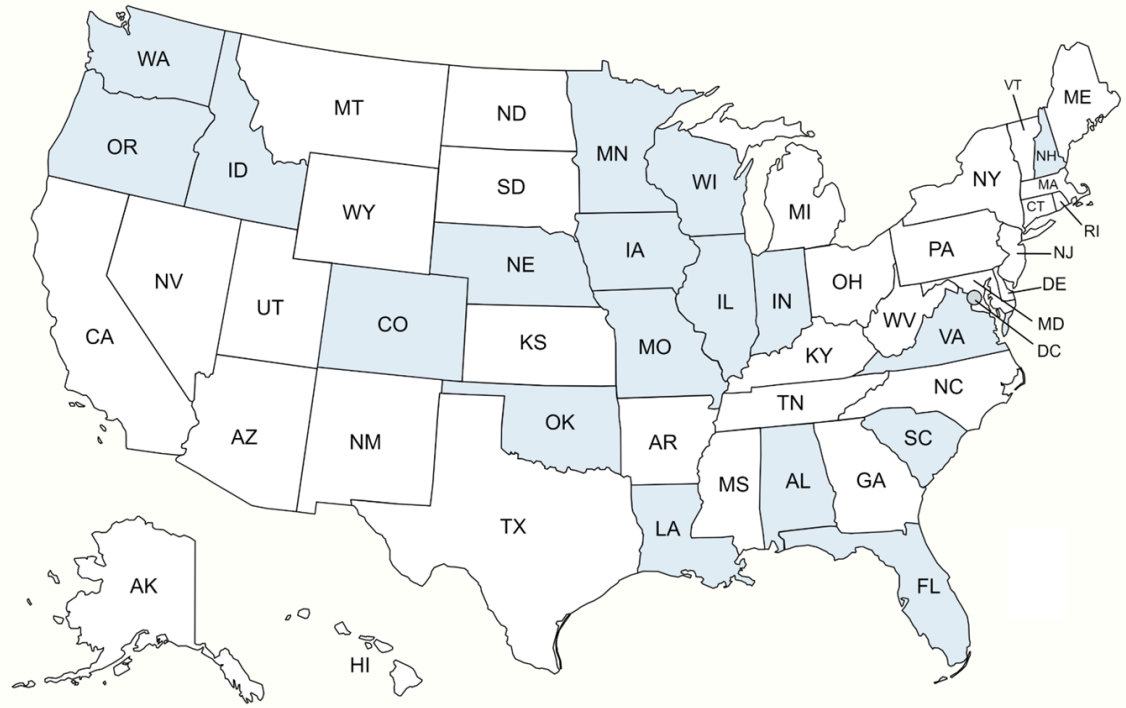

Figure 15. Map. Collected dataset from different states to deploy the BNN.

To the best of our knowledge, this is the most extensive dataset on which an ML model for predicting |E*| has been trained. Table 3 presents the model inputs along with the summary statistics of the dataset.

Table 3. Summary of BNN-Model Dataset Statistics

Category	Variable	Symbol	Mean	Std. Dev.	Min.	Max.
Gradation	% retained in 3/4 in. (19.0 mm) sieve	$p_{3/4}$	0.74	1.94	0	16.00
Gradation	% retained in 3/8 in. (9.5 mm) sieve	$p_{3/8}$	17.02	8.67	1	55.30
Gradation	% retained in #4 sieve	p_4	40.69	12.13	0	78.00
Gradation	% passing #200 sieve	p_{200}	5.16	1.52	0	9.30
Volumetrics	Air voids (by volume of mix) (%)	V_a	4.77	1.61	2.6	15.20
Volumetrics	Effective asphalt content (by volume) (%)	V_{beff}	10.61	2.04	3.50	15.30
Volumetrics	Voids in mineral aggregate (%)	VMA	15.62	2.41	11.90	27.23
Asphalt Binder	High-temperature PG (°C)	PG-HT	64.99	6.26	52.00	82.00
Asphalt Binder	Low-temperature PG (°C)	PG-LT	-26.95	3.46	-34.00	-22.00
RAP	RAP content (by weight of mix) (%)	RAP	9.59	15.08	0.00	53.00
Testing Condition	Test temperature (°C)	T	21.72	20.89	-12.20	58.00
Testing Condition	Loading frequency (Hz)	f	6.57	8.48	0.01	25.00
Material Property	Dynamic modulus of mixture (psi)	|E*|	1.07E6	1.10E6	2531	6.21E6

While most previous research has considered binder shear modulus and phase angle (|G*| and δ, respectively) as inputs, this study used high and low PG of the asphalt binder. This was determined to reduce the need for conducting a time-consuming frequency sweep test using the dynamic shear rheometer and to allow for the consideration of asphalt binder substitutions, which commonly occur at the mix production stage and can include changing of producer source. This also enables more simplistic incorporation of the grade bumping concept, where a lower grade is used to compensate for recycled material content, into this predictive algorithm.

Bayesian neural networks (BNNs) can be regarded as an extension of plain neural networks combined with Bayesian inference. Instead of optimal single values for the weights as in a standard neural net, weights in the BNN are assigned a probability distribution used to take the uncertainty introduced by the model (i.e., epistemic uncertainty) into account. In other words, training a BNN leads to learning the parameters of these probability distributions rather than the point estimate of the weights directly. A detailed mathematical explanation of this model and the selected hyperparameters are presented in Asadi et al. (2023). The primary advantage of this model lies in its capability to provide uncertainties concerning the predictions, while simultaneously enhancing accuracy in comparison to a standard neural network. Given the quantified model uncertainty and intrinsic variability in the |E*| test, the predictive BNN values are highly reliable. In practice, predicted moduli could be as accurate and effective as measured values. The results demonstrated that the developed BNN model performed exceptionally well in predicting |E*| for four unseen datasets outside of the training data, achieving an R^2 greater than 0.93 and a Se/Sy (standard error over standard deviation of the residuals) less than 0.26. Furthermore, the BNN model outperformed all other empirical and available ML models in the literature. Finally, a web API was created, making the BNN accessible to anyone with mix design data. The tool can be found at https://dmict.herokuapp.com/.

Modulus Nondestructive Testing—Ultrasonic Pulse Velocity

All |E*| samples were tested using the UPV method with a Portable Ultrasonic Nondestructive Digital Indicating Tester (PUNDIT) equipment with flat transducers (Figure 16). Following the ASTM C597-22 (2022) standard, five temperatures were applied (4.4, 21.1, 37.8, 54.4, and 60.0°C). Transducer frequency and signal width were fixed at 54 kHz and 9.3 μs, respectively. The average time mode was applied, given that the highest resolution is 0.1 μs, with this mode being suitable for shorter path measurements (PUNDIT LAB, 2017). The direct transducer arrangement was applied for all tests, after discussions that indicated that indirect measurements would not be reliable due to interference. As a first step, verification of the device calibration was conducted on a regular basis by comparing the expected transit time of a calibration rod and its measured transit time. Velocity accuracy within one decimal was considered valid. As per ASTM C597-22 (2022), the relation between pulse velocity, elastic modulus, and Poisson's ratio (PR) is presented in Figure 17. In this equation, pulse velocity is the only known parameter, so the accuracy of modulus and PR prediction is interdependent. The direct form of modulus calculation for different test temperatures is shown in Figure 18, depending on the assumption of PR value.

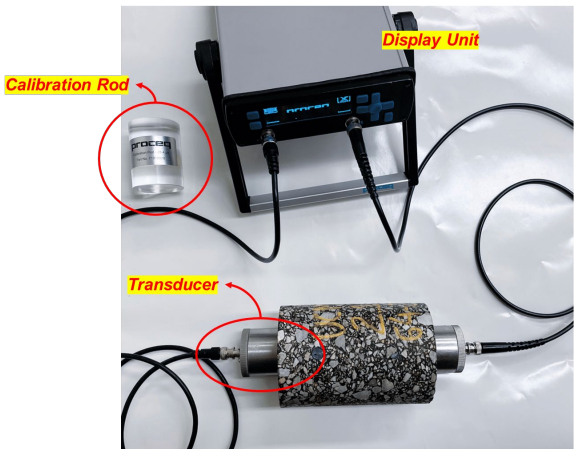

Figure 16. Photo. UPV device.

$$V = \sqrt{\frac{E(1-\mu)}{\rho(1+\mu)(1-2\mu)}}$$

Figure 17. Equation. Wave speed relationship with modulus, PR, and density.

$$E = \frac{V^2\rho\,(1+\mu)\,(1-2\mu)}{1-\mu}$$

Figure 18. Equation. Modulus relationship with wave speed, PR, and density.

Where: E = modulus

V = transmit speed of P-wave transmission across the sample

μ = dynamic Poisson's ratio

ρ = bulk density

ENDURANCE LIMIT ANALYSIS

Four-Point Bending Beam Fatigue

The procedure followed in this research for 4PPBF testing was based on both the AASHTO T 321-22 standard and the protocol used in NCHRP Project 9-44A (Witczak, 2002). The protocol was conducted for a partial factorial matrix of materials from both field and lab mixes, as shown in Table 4. The field mixtures were collected from two sources (asphalt mixture producers of mix 1 and mix 2) and stored in a cooler at 10°C to prevent aging. For compaction, the loose mixes were heated to 140°C and homogenized using a splitter. The loose mixes were separated into 2.5 kg samples for a G_{mm} check (two replicates). The loose mixes were heated to the compaction temperature (152°C for mix 1 and 146°C for mix 2) and compacted using the rolling wheel machine (Figure 19) at ICT. The beams were

sawed to the standard dimensions of AASHTO T 321-22 (Figure 20), and air voids were evaluated. Any specimen with air voids deviating by more than 1% from the target value of 7% was rejected. Laboratory mixtures were produced for the three N90 sources (mix 1, mix 2, and mix 3). The mixes were heated to mixing temperatures (146°C for unmodified and 163°C for modified binders) and short-term aged for 1 hour in a draft oven at compaction temperature. The same procedure in terms of sawing and air void evaluation was followed.

Table 4. Beam Fatigue Test Matrix

Mix	PG 58-28	PG 64-22	PG 64-28	PG 70-22	PG 70-28	PG 76-22	PG 76-28
1	X	X			Field	X	X
2	X	Field	X		X		X
3	X	X		X			

Figure 19. Photo. ICT rolling wheel compactor.

Figure 20. Photos. Examples of compacted and sawed beams.

The temperature for the testing procedure was set to 20°C. The first part of the fatigue testing matrix was dedicated to a 1-second rest period, for which the strain levels of 70 and 100 microstrain were evaluated. These values were selected based on assumptions that the fatigue endurance limit final criterion will likely fall at or between these values. A 10-minute interval between the application of the different strain levels was ensured to allow for "full" healing. The second part of the fatigue testing was dedicated to a 0-second rest period, which is the more extreme condition in terms of fatigue (as it allows for no rest period for healing). The tests were run at 50, 70, 90, 100, 125, 150, 175, 200, 250, and 500 microstrain. These strain values were related to tensile strain at the bottom of the beam; therefore, the input peak-to-peak strain was twice the value of the tensile strain, given the sinusoidal form of the loading stress wave (Witczak et al., 2013). For the calculation of SR, initial flexural stiffness (E_0) was determined as an average of the first 100 cycles after the 100th cycle. SR was calculated for each new cycle until 10,000 cycles were reached.

The strain level versus $SR_{(10,000)}$ data were plotted and analyzed. The test geometry, loading nature, and asphalt mixture viscoelastic behavior are unlikely to result in SR = 100%, specifically at 0-second rest periods. For instance, during the initial cycles, material consolidation can occur, causing stiffening (or strain hardening). The loading nut's positioning also plays a role, as small displacements relative to the beam's center can lead to asymmetrical loading. Additionally, the absence of confinement hinders healing and recovery compared to field conditions. In this context, four strain levels were identified for each mix, representing the threshold that results in an acceptable SR value after 10,000 cycles:

- The acceptable tensile strain at 0-second RP would align with the minimum SR obtained for 1-second RP, under the assumption that this represents a scenario where no damage accumulates during subsequent load applications in a stable state.
- The acceptable tensile strain at 0-second RP would correspond to the strain level associated with the peak SR value among all levels tested at 0-second RP.
- The acceptable tensile strain at 0-second RP would be identified as the strain level corresponding to an SR greater than 90%.
- The acceptable tensile strain at 0-second RP would be determined based on the strain level corresponding to an SR greater than 95%.

Illinois Flexibility Index Test

The I-FIT determined fracture energy, slope, and flexibility index (FI) for all combinations of mixes 1, 2, and 3, and binders (seven binders), at aged and unaged conditions. I-FIT uses a semi-circular bending HMA specimen geometry, with a 50 mm thickness, 150 mm diameter, and 15 mm vertical notch at the center of the base. The procedure involves subjecting the semi-circular bending specimen to three-point bending by placing it symmetrically over two fixed rollers and applying a monotonic load along the vertical diameter of the specimen, at a load-line displacement control rate of 50 mm/min administered by a linear variable differential transformer. A vertical notch, created along the symmetric axis of the semi-circular HMA specimen, is critical for ensuring Mode I fracture. When evaluating the cracking potential of HMA at intermediate temperatures, fracture tests like I-FIT are useful because the notch limits the energy dissipation to the creation of new surfaces. In contrast, strength tests are useful for predicting the cracking potential of brittle HMA at low temperatures or with high RAP/RAS content (Al-Qadi et al., 2022). Some scholars have pointed out the variability (Batioja-Alvarez et al., 2019; Romero & VanFrank, 2019; Yan et al., 2020) in the results, which can cause trouble in terms of drawing conclusions. However, variability is inherent to HMA due to its heterogeneous nature. Hence, specimen preparation, variability, and non-repeatability in the test result often remain topics of debate among researchers. Other than that, I-FIT has proven to be a potential test to screen HMA mixes based on cracking resistance, especially mixes with high recycled material content.

First, asphalt binders and aggregates were heated in an oven to the required mixing temperature as specified by IDOT. Using a mechanical stirrer, a loose HMA mix was prepared. The loose mixture was short-term aged (STA) by conditioning in the oven for 1 hour until it reached the required compaction temperature based on Illinois Modified AASHTO R 30-22 (IDOT, 2021). Using the Superpave gyratory compactor, the conditioned loose mixture was compacted into cylindrical specimens of 150 mm diameter and 160 mm height. Air voids of the specimens were computed, and the cylindrical specimens were cut into test specimens for I-FIT as specified by Illinois Modified AASHTO T 393-22. A long-term aging procedure was performed on I-FIT specimens as defined in Section 7.3 of Illinois-modified AASHTO R 30-22. Some specimens within the required air void range of 7 ± 1% were aged in a forced-draft oven at 95°C for 3 days for long-term aging (LTA). After the LTA cycle, specimens were measured for thickness, notch depth, and ligament length, which were used in data analysis. Specimens that met dimension requirements in accordance with Illinois Modified AASHTO T 393-22 were conditioned in a water bath for 2 hours at 25°C before the test was run. Please note that LTA is not required by IDOT specifications for IL-19.0 mixtures. This testing was completed during the research study to have additional data results for mixture comparison purposes.

The specimens were tested within 10 minutes after the conditioning cycle was over. A vertical crack driven from the notch was formed in the specimen during testing. Load and displacement data were recorded and plotted to produce a load-displacement curve for each specimen. One output is the FI value, which is computed by first calculating fracture energy. According to the work of fracture method, fracture energy (in units of joules per square meter, J/m^2), is defined as the area under the load-displacement curve until the material is damaged. The work of fracture is calculated as the area under the load-displacement curve using a numerical integration technique. The work of fracture is used to calculate fracture energy, which ultimately is used to compute the FI value, defined as the

fracture energy divided by the slope of the curve at the post-peak inflection point multiplied by a constant.

Currently, IDOT specifies a minimum FI threshold of 8.0 for STA IL-19.0 mixes according to the 2022 IDOT standard specifications. With aging, the FI value reduces drastically. Aging rate, a parameter that quantifies this decrease, was computed as per Zhu et al. (2020). For the lower-lift binder course, IDOT does not specify a threshold for FI. As demonstrated by Singhvi et al. (2022), this segment of the HMA layer does not undergo significant aging over time, particularly in the context of full-depth asphalt structures. However, this parameter was still assessed in this study to obtain more effective comprehensive data about the selected materials.

FIELD MODULUS DATA COLLECTION USING FWD AND TSD

Deflection testing has been conducted on in-service pavements over the last several decades to assess their structural health. Traditionally, nondestructive deflection testing is performed using a falling weight deflectometer (FWD). The FWD applies a short pulse load (approximately 10 milliseconds in duration) which simulates the moving load of a tire passing over a pavement section. Deflections are measured based on surface accelerations at specified distances from the dropped weight, which typically range from 0 to 100 mils. These deflections form a deflection basin, which can in turn provide information about the structural integrity of the pavement. These include back-calculated layer moduli and design coefficients as well as parameters related to the shape of the deflection basin, which correlate well to pavement critical strain levels. For example, the area under the pavement profile (AUPP) is correlated directly to the tensile strain at the bottom of the HMA layer (Alvarez & Thompson, 1998).

Despite the benefits and reliability of FWD testing, a major drawback of FWD testing is that it is difficult to use at the network level because the test must be done in a stationary position, requiring traffic control in the testing lane. As an alternative, a range of devices have been developed that measure deflections due to moving loads at traffic speeds. These devices include the traffic speed deflectometer (TSD), rolling wheel deflectometer, airfield rolling wheel deflectometer, curviameter, and road deflection tester (Flintsch et al., 2012). Among these, the TSD is the most widely implemented and has been the only device to see adoption into potential pavement management schemes over the last 10 years (Katicha et al., 2022). The TSD applies the deflection load while moving at speeds up to 60 mph and measures the deflection basin using line laser velocities instead of deflections, which are then converted to deflections by integration.

Recently, Illinois was one of 28 agencies participating in a pooled fund study focused on pavement structural evaluation using TSD. ARRB Systems collected TSD data on many interstates and state routes in Illinois over the last two years and has delivered much of this data to IDOT. As part of this ICT-IDOT project, the research team reviewed this data and analyzed sections for which structural information was known. In addition to the lab testing discussed above, Chapter 6 of this report provides analyses of this portion of the study.

CHAPTER 4: BINDER-SCALE ANALYSIS

FREQUENCY SWEEP—COMPLEX MODULUS MASTER CURVES

Temperature/frequency sweep tests were conducted using a dynamic shear rheometer. Complex modulus master curves (Figure 21) at three aging levels were constructed by shifting curves at each temperature to a reference temperature of 21.1°C. Testing was completed at six temperatures with variable strain levels and 16 frequencies ranging from 0.1 rad/sec to 100 rad/sec. An 8 mm diameter parallel plate geometry was used for temperatures 10°C, 22°C, and 34°C, while a 25 mm diameter plate was used for 46°C, 58°C, and 70°C. Peak strain levels were limited to the presumed linear viscoelastic range to ensure that no damage occurred in the asphalt binder. Master curves were constructed using a symmetrical sigmoidal model (Rowe et al., 2009). The WLF equation was used to obtain shift factors for each temperature.

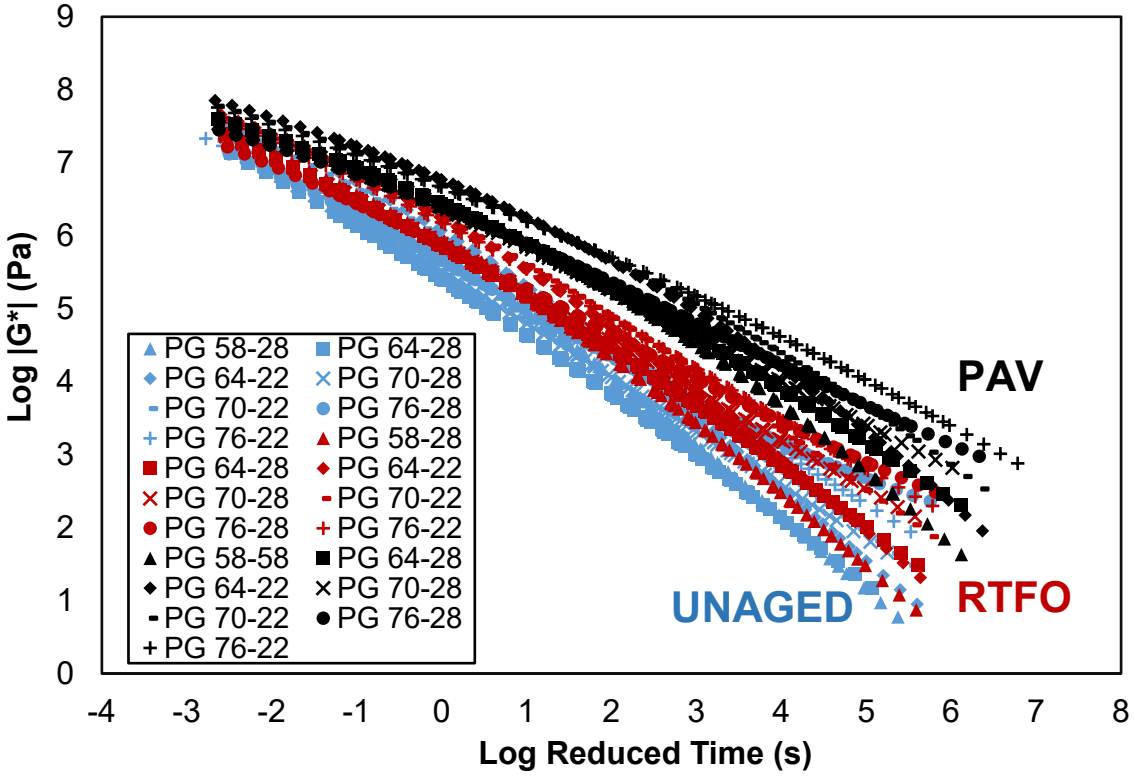

Figure 21. Graph. Binder master curves for unaged, rolling thin film oven (RTFO) aged, and pressure aging vessel (PAV) aged materials.

Numerous observations about the behavior of asphalt binders with frequency of loading could be drawn from the master curves. Complex shear modulus is higher at higher frequencies and lower at lower frequencies, as expected. At high frequencies, all asphalt binders show approximately the same complex modulus values. However, as frequency of loading decreases, a clear distinction between polymer-modified asphalt binders and unmodified asphalt binders was observed. This depicts the ability of modified asphalt binders to show higher stiffness and superior performance against rutting.

This finding is consistent with previous studies, which showed that polymer modification helps to retain stiffness at lower frequencies and higher temperatures (Ferry, 1980; Airey, 2003; Sultana & Bhasin, 2014). Stiffness increases with aging, as is depicted by an increase in complex modulus. For unaged and RTFO-aged conditions, PG 58-28 and PG 76-28 had the lowest and highest complex modulus, respectively. For PAV aging, PG 76-22 had the highest and PG 58-28 had the lowest complex modulus values. High PG binders (PG 76-22, PG 76-28, PG 70-22, and PG 70-28) showed higher complex modulus and stiffness than other asphalt binders at all aging levels and frequencies.

For RTFO-aged asphalt binders (21.1°C reference temperature), two clusters of asphalt binders were observed at the frequency range of interest for dynamic modulus in terms of the pavement design algorithm (10 Hz or 0.1-second loading time). Low PG -22 asphalt binders showed higher stiffness than low PG -28 asphalt binders. Among low PG -22 asphalt binders, PG 64-22 and PG 70-22 were slightly stiffer than PG 76-22, which could be a function of the base binder before modification or other factors used to obtain the PG 76-22 via modification. Figure 22 shows this trend.

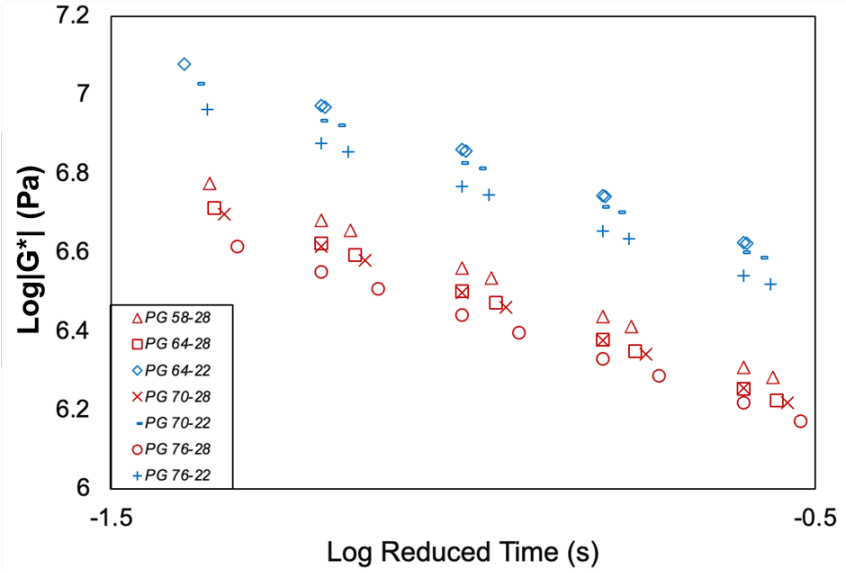

Figure 22. Graph. Binder master curves at 21.1°C and frequency range of 10 Hz.

POKER CHIP—TENSILE STRENGTH AND DUCTILITY

Forty-two poker chip tests on seven asphalt binders were conducted at room temperature. Using a 2 N/s monotonic loading rate, two replicates were tested for each asphalt binder at each aging level, and variation in tensile strength and ductility values was evaluated. Stress–strain curves at unaged and RTFO-aged conditions consisted of a nonlinear ascending branch followed by a gradually developing descending branch. However, the descending branch is not always observed at PAV aging levels, and, instead, a sudden fracture is observed, which represents the loss of ductility and increase in brittleness with aging. The branches are separated by an ultimate stress point that depicts the cohesive failure of the asphalt binder specimen. The shape of the curve varies from asphalt binder to asphalt binder and is dependent on the properties of the asphalt binder and the loading rate at which the test is conducted.

Force-displacement data were recorded and used to construct stress–strain curves. Tensile strength (kPa), ductility (%), and delta ductility (%) parameters for each asphalt binder at three aging levels were computed (Figure 23). Note that delta ductility was defined herein as the percent drop in ductility between RTFO- and PAV-aged conditions for a single asphalt binder. Per Figure 23, tensile strength increased and ductility decreased with aging for all asphalt binders. No clear trend for the strength parameter was observed. The strength value of polymer-modified asphalt binders was in the same range as unmodified asphalt binders. However, a clear distinction in ductility values was observed. Polymer-modified asphalt binders showed significantly higher ductility values than unmodified asphalt binders at both unaged and RTFO levels. For example, PG 76-28 had almost 4.5 times the ductility than that of PG 58-28. Based on this, polymer-modified binders are postulated to have superior cracking resistance at unaged and short-term aging conditions. This is mainly due to the polymer cross-linking phenomenon making them much more elastic and ductile than a neat asphalt binder, which in turn dissipates more energy into deformation. For long-term aged PAV levels, ductility values of polymer-modified asphalt binders decrease, approaching those of unmodified asphalt binders, but are still generally higher.

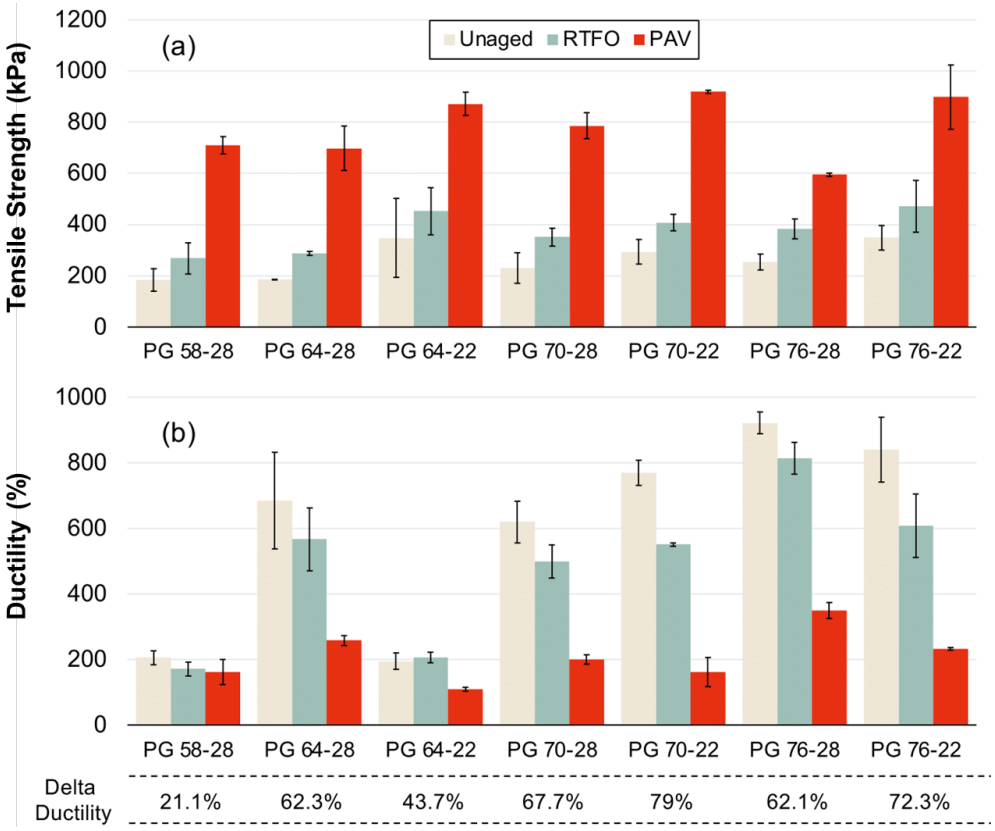

Figure 23. Graph. Binder poker chip tensile strength and ductility.

The ductility of the asphalt binders dropped with aging, with PG 70-22 and PG 58-28 showing the highest (79.0%) and lowest (21.1%) decrease, respectively. While unmodified asphalt binders showed a lower reduction, ductility of polymer-modified asphalt binders decreased significantly with long-term aging. For PG 70-22, ductility decreased from 770% to 162% approximately, which is a 79.0%

drop. This is potentially due to the degradation of polymer with aging in polymer-modified asphalt binders. However, this is not necessarily a problem, as this asphalt binder still had higher ductility than PG 64-22 unmodified binder at PAV aging level. Furthermore, as mentioned above, aging is not a concern for bottom-up cracking of full-depth asphalt pavements.

CHAPTER 5: IDOT MODULUS ALGORITHM STUDY

LABORATORY ANALYSIS OF IDOT MIXES

Dynamic modulus tests were performed at five temperatures and six frequencies, as detailed in Chapter 3. Using the time-temperature superposition concept, the data points were shifted to the reference temperature of 21.1°C in master curves using the sigmodal and WLF functions. The frequency sweep and the master curve sigmoidal equation parameters for each mix are presented in Figures 24–27 and Tables 5–8. Phase angle master curves and black space diagram (|E*| vs. phase angle) curves can be found in the appendix.

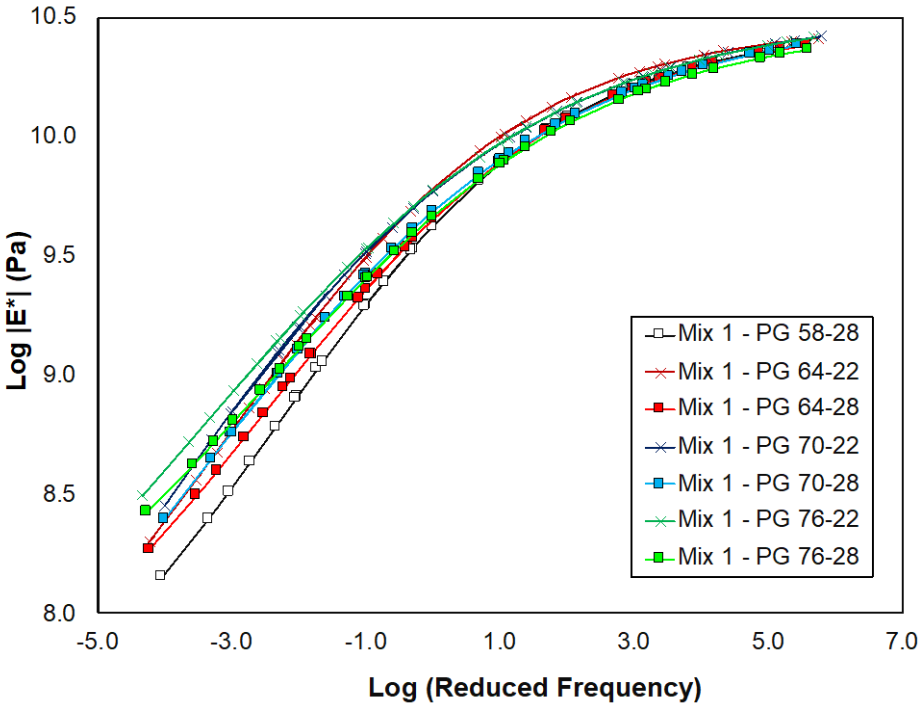

Figure 24. Graph. Master curves for mix 1 (reference temperature = 21.1°C).

Table 5. Sigmoidal and WLF Equations Parameters for Mix 1

Parameter	PG 58-28	PG 64-22	PG 64-28	PG 70-22	PG 70-28	PG 76-22	PG 76-28
α	3.330	3.401	3.222	4.529	3.967	3.468	3.081
β	-1.086	-1.360	-1.066	-1.593	-1.323	-1.290	-1.032
δ	7.136	7.073	7.258	6.007	6.556	7.057	7.394
γ	0.472	0.457	0.437	0.358	0.367	0.377	0.403
C_1	-20.0	-17.1	-23.8	-18.5	-22.4	-26.3	-26.1
C_2	182.0	150.1	209.1	161.2	201.2	222.2	224.7
T_r	21.1	21.1	21.1	21.1	21.1	21.1	21.1

For mix 1 (ABR = 30.3%), the master curves show that, at low frequencies/high temperatures, the ranking of PGs in terms of stiffness follows an expected trend. Higher PG asphalt binders resulted in stiffer mixes in the low frequency zone (stiffness of PG 76-XX > PG 70-XX > PG 64-XX > PG 58-XX). At 10 Hz frequency, |E*| values cluster together into two groups based on low PG: mixtures using asphalt binders with PG XX-22 were stiffer than ones using asphalt binders with PG XX-28.

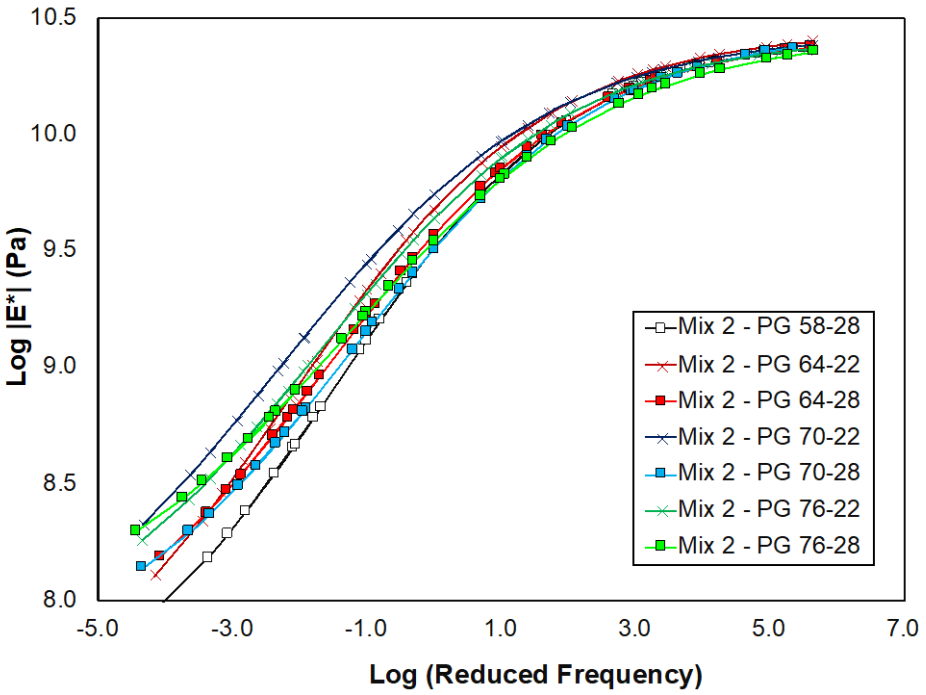

Figure 25. Graph. Master curves for mix 2 (reference temperature = 21.1°C).

Table 6. Sigmoidal and WLF Equations Parameters for Mix 2

Parameter	PG 58-28	PG 64-22	PG 64-28	PG 70-22	PG 70-28	PG 76-22	PG 76-28
α	3.007	3.137	2.840	2.893	2.740	2.706	2.587
β	-0.815	-1.121	-0.821	-1.140	-0.641	-0.889	-0.640
δ	7.426	7.315	7.599	7.550	7.714	7.721	7.851
γ	0.567	0.533	0.531	0.496	0.537	0.526	0.498
C_1	-21.0	-20.5	-20.2	-25.9	-33.3	-27.5	-29.8
C_2	189.9	180.7	180.0	221.8	291.9	237.4	247.5
T_r	21.1	21.1	21.1	21.1	21.1	21.1	21.1

For mix 2 (ABR = 15.7%), the master curves showed that binder PG 70-22 produces a stiffer mix. These results showed some slight inconsistencies but, in general, the trends are as expected. At the 10 Hz frequency zone, |E*| values cluster together into two groups based on low PG, but PG 70-22 was consistently the stiffest mix. Note that, in 19.0 mm NMAS mixes, |E*| can be affected by the positioning of gauge points. When these points adhere to larger aggregates only, they may experience reduced movement during loading cycles, potentially leading to an increase in the measured modulus, which can add variability and complexity to the results.

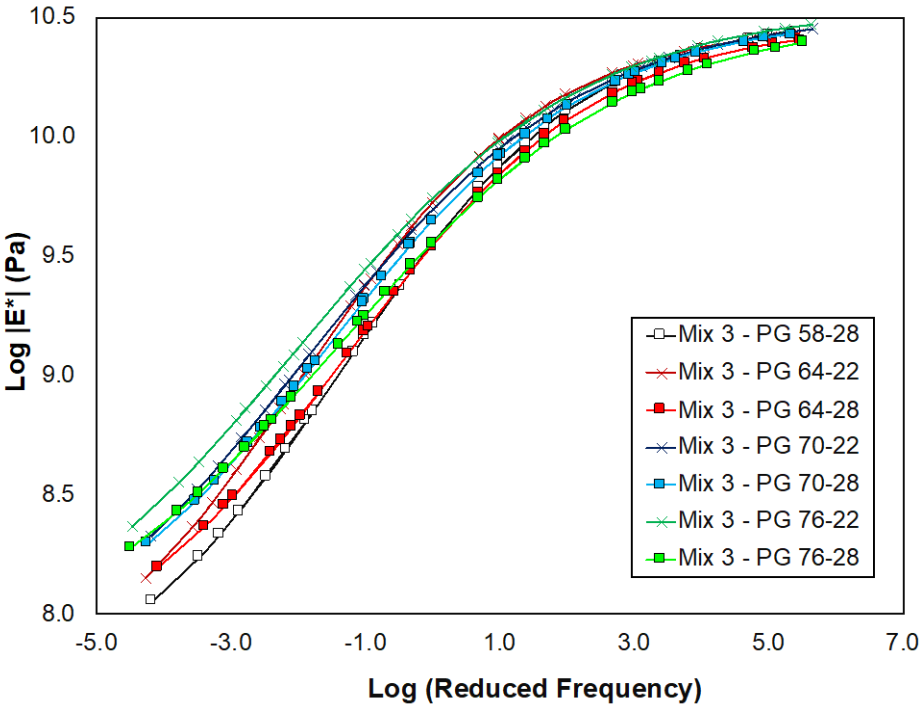

Figure 26. Graph. Master curves for mix 3 (reference temperature = 21.1°C).

Table 7. Sigmoidal and WLF Equations Parameters for Mix 3

Parameter	PG 58-28	PG 64-22	PG 64-28	PG 70-22	PG 70-28	PG 76-22	PG 76-28
α	2.977	2.968	2.782	2.914	2.776	2.875	2.748
β	-0.744	-1.070	-0.680	-0.925	-0.797	-0.942	-0.645
δ	7.540	7.518	7.699	7.615	7.737	7.677	7.757
γ	0.553	0.555	0.539	0.488	0.514	0.468	0.466
C_1	-25.8	-28.4	-23.2	-21.9	-27.3	-30.5	-37.7
C_2	230.4	249.5	207.9	190.4	245.6	256.8	316.6
T_r	21.1	21.1	21.1	21.1	21.1	21.1	21.1

The trends observed in the master curves for mix 3 (ABR of 20.0%) align with expectations. Notably, the use of PG 70-28 asphalt binder yielded mixes with higher stiffness compared to other asphalt binders with low PG -28. Within the 10 Hz frequency zone, |E*| values form two distinct groups based on low PG asphalt binder. However, PG 70-28 consistently exhibited higher stiffness values than mixes made of asphalt binders with low PG -28.

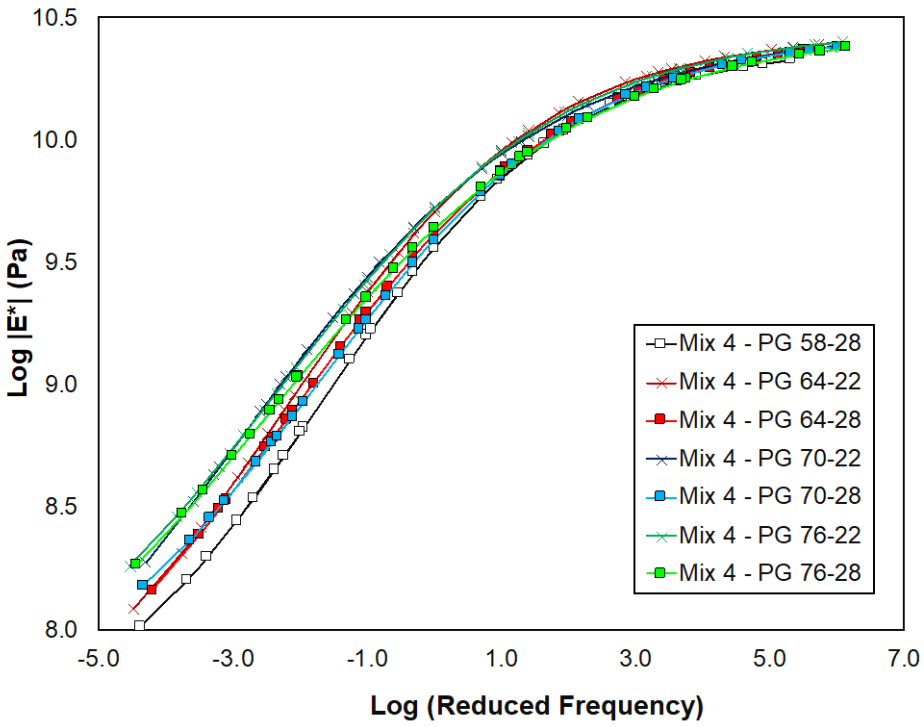

Figure 27. Graph. Master curves for mix 4 (reference temperature = 21.1°C).

Table 8. Sigmoidal and WLF Equations Parameters for Mix 4

Parameter	PG 58-28	PG 64-22	PG 64-28	PG 70-22	PG 70-28	PG 76-22	PG 76-28
α	2.899	3.077	3.172	3.354	2.872	2.971	3.114
β	-0.922	-1.172	-1.032	-1.295	-0.872	-1.116	-1.039
δ	7.489	7.362	7.278	7.094	7.568	7.486	7.342
γ	0.554	0.523	0.471	0.442	0.501	0.474	0.427
C_1	-39.6	-28.3	-26.2	-23.0	-22.2	-25.0	-21.4
C_2	347.6	234.6	227.8	188.1	181.2	198.2	171.4
T_r	21.1	21.1	21.1	21.1	21.1	21.1	21.1

The observed trends in the master curves for mix 4 (ABR of 28.1%) align with expectations. Notably, at the 10 Hz frequency zone, |E*| values exhibit a clear clustering into two groups based on low PG asphalt binder, just like the mixes above. This finding suggests a notable improvement in test repeatability for mix 4. The enhanced repeatability can be attributed to replicates being mixed and compacted on the same day, contrasting with mixes 1–3 where these processes occurred on different days. This improved repeatability underscores the importance of comparing results from these tests with the existing IDOT modulus algorithm. Such a comparison is crucial for guiding updates to design procedures, particularly in terms of incorporating considerations for the combined use of recycled asphalt and polymer-modified asphalt binders.

The existing IDOT modulus algorithm faces limitations concerning temperatures and frequencies. The algorithm is designed exclusively for a frequency of 10 Hz, corresponding to a vehicle speed of 70 mph (common for interstates). As outlined in Chapter 54 of IDOT's *BDE Manual*, the modulus algorithm focuses on this specific frequency over a restricted temperature range, aligning with the design temperatures for the state of Illinois. The designated design temperatures span from 73°F (north) to 81°F (south). Consequently, the following analysis is constrained to this frequency and temperature range. The design modulus is determined solely by the asphalt binder grade in the existing algorithm. This algorithm categorizes asphalt binders into two groups. For PG 64-28 and 70-28, the assumed HMA modulus is lower, ranging from 405 ksi at 82°F to 600 ksi at 73°F. Conversely, for PG 64-22, 70-22, 76-22, and 76-28, the HMA modulus is assumed to vary between 510 ksi at 82°F and 750 ksi at 73°F. The governing equations for these specifications are detailed in Table 9.

Table 9. IDOT Modulus Algorithm (IDOT BDE Chapter 54)

Mix	High PG	Low PG	Equation
IDOT	64	-28	Log E (ksi) = 4.163 - 0.019 x T (F)
IDOT	70	-28	Log E (ksi) = 4.163 - 0.019 x T (F)
IDOT	64	-22	Log E (ksi) = 4.234 - 0.019 x T (F)
IDOT	70	-22	Log E (ksi) = 4.234 - 0.019 x T (F)
IDOT	76	-22	Log E (ksi) = 4.234 - 0.019 x T (F)
IDOT	76	-28	Log E (ksi) = 4.234 - 0.019 x T (F)

One important note is that temperature is expected to increase due to climate change, which is captured in the Federal Highway Administration (FHWA) LTPPBind database, which is part of FHWA's Long-Term Pavement Performance Infopave database. Overall, increasing temperature is anticipated to have a small effect on the design of asphalt binder. However, it would have a significant effect on the modulus value used for pavement design based on the current algorithm. For example, a 3° increase from 73°F to 76°F represents a change of more than 100 ksi for a PG 64-22 binder-based mix. The overall potential effect of making changes to the design algorithm as a whole should consider climate-based changes as well as changes in materials.

Figure 28 graphically represents the superposition of the experimental results derived from the four selected mixes in this study to the current IDOT modulus curves used as input for pavement design. Notably, within the specified temperature range and at a frequency of 10 Hz, the observed trend indicates that the "modern" mixes consistently have a higher stiffness when compared to the values that would be obtained from the *BDE Manual*. This observation highlights the potential for refining the existing IDOT algorithm to accurately capture and reflect the mechanical characteristics of contemporary asphalt mixes. Table 10 defines the functions which describe the modulus and temperature relationships.

In summary, mix 1 had the highest stiffness values, which is likely due to the high ABR and presence of RAS. The design air void content is 4% for "typical mixes" in Illinois. However, previous studies (Carpenter, 2007) indicated that even specimens compacted to 7% air void content (with a corresponding average core air voids of 5.3%) had higher |E*| values than those currently used for design. It could also be argued that for limiting strain criterion pavements, 7% air void content should

be used as a more conservative estimate, because density can vary greatly and consolidation after construction can also vary. In general, low PG was the controlling differential factor for a given mix with different binders. For all binder-mix combinations, low PG -22 binders generated stiffer mixes than low PG -28 ones. This is not consistent with current design procedures in Illinois because: (i) PG 58-28 is currently not considered within the state's algorithm; instead, grade bumping is assumed to be equivalent to current PG, and (ii) PG 64-28 and PG 70-28 may originate mixes with a higher |E*| than ones originating from PG 76-28. PG 76-28 is currently considered to originate mixtures with |E*| closer to the low PG -22 range, according to Chapter 54 of the IDOT's *BDE Manual*. It should be noted that currently IDOT considers PG 58-28 with RAP to be equivalent to PG 64-22 as used by design; however, it was shown to be substantially higher here. It is also notable that no effect was observed for the lower number of design gyrations or finer gradation of mix 4. This finding confirms the consistency of considering, for design purposes, IL-19.0 mixes to have similar and asphalt binder low PG-dependent modulus, as long as air void remains close to the design value.

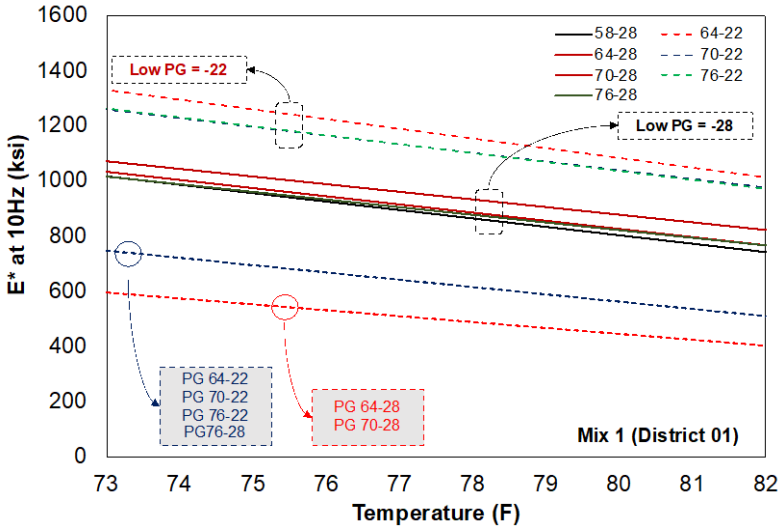

(A) Mix 1 (District 1): Current IDOT design curves are shown at the bottom of the graph

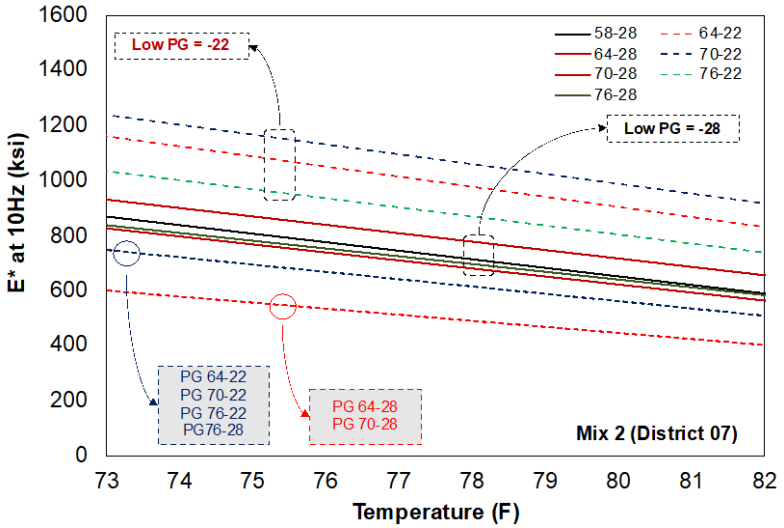

(B) Mix 2 (District 7): Current IDOT design curves are shown at the bottom of the graph

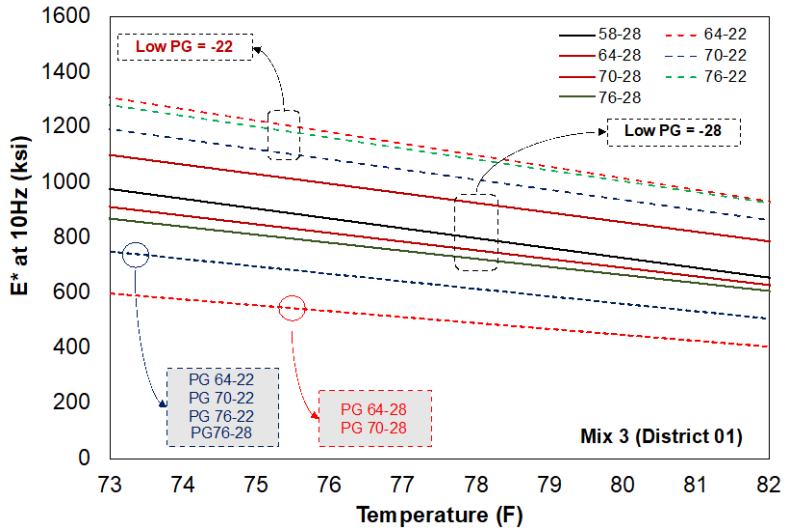

(C) Mix 3 (District 1): Current IDOT design curves are shown at the bottom of the graph

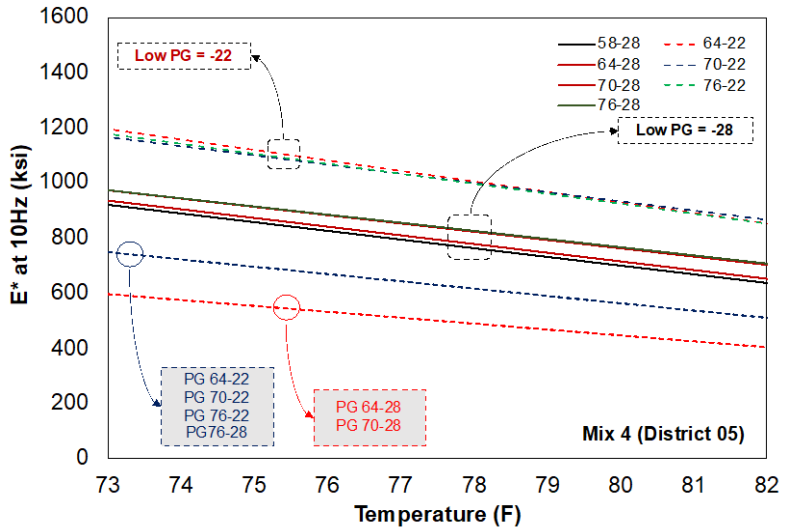

(D) Mix 4 (District 5): Current IDOT design curves are shown at the bottom of the graph)

Figure 28. Graph. Comparison between modern mixes and the IDOT algorithm (based on IDOT BDE Chapter 54 revisions from 2008).

Table 10. Equations for Modern Mixes Tested in This Study

Mix	High PG	Low PG	Equations
1	58	-28	Log E (ksi) = 4.104 - 0.015 x T (F)
1	64	-22	Log E (ksi) = 4.061 - 0.013 x T (F)
1	64	-28	Log E (ksi) = 3.998 - 0.013 x T (F)
1	70	-22	Log E (ksi) = 3.974 - 0.012 x T (F)
1	70	-28	Log E (ksi) = 3.951 - 0.013 x T (F)
1*	70	-28	Log E (ksi) = 4.076 - 0.013 x T(F)
1**	70	-28	Log E (ksi) = 4.004 - 0.013 x T (F)
1	76	-22	Log E (ksi) = 4.006 - 0.012 x T (F)
1	76	-28	Log E (ksi) = 3.979 - 0.013 x T (F)
2	58	-28	Log E (ksi) = 4.280 - 0.018 x T (F)
2	64	-22	Log E (ksi) = 4.217 - 0.016 x T (F)
2*	64	-22	Log E (ksi) = 4.162 - 0.014 x T(F)
2**	64	-22	Log E (ksi) = 4.166 - 0.016 x T(F)
2	64	-28	Log E (ksi) = 4.182 - 0.017 x T (F)
2	70	-22	Log E (ksi) = 4.126 - 0.014 x T (F)
2	70	-28	Log E (ksi) = 4.252 - 0.018 x T (F)
2	76	-22	Log E (ksi) = 4.176 - 0.016 x T (F)
2	76	-28	Log E (ksi) = 4.165 - 0.017 x T (F)
3	58	-28	Log E (ksi) = 4.362 - 0.019 x T (F)
3	64	-22	Log E (ksi) = 4.295 - 0.016 x T (F)
3	64	-28	Log E (ksi) = 4.248 - 0.018 x T (F)
3	70	-22	Log E (ksi) = 4.207 - 0.016 x T (F)
3	70	-28	Log E (ksi) = 4.209 - 0.016 x T (F)
3	76	-22	Log E (ksi) = 4.225 - 0.015 x T (F)
3	76	-28	Log E (ksi) = 4.174 - 0.017 x T (F)
4	58	-28	Log E (ksi) = 4.227 - 0.017 x T (F)
4	64	-22	Log E (ksi) = 4.245 - 0.016 x T (F)
4	64	-28	Log E (ksi) = 4.126 - 0.016 x T (F)
4	70	-22	Log E (ksi) = 4.100 - 0.014 x T (F)
4	70	-28	Log E (ksi) = 4.225 - 0.017 x T (F)
4	76	-22	Log E (ksi) = 4.194 - 0.015 x T (F)
4	76	-28	Log E (ksi) = 4.096 - 0.015 x T (F)

*Plant mix at 4% AV

**Plant mix at 7% AV

LABORATORY ANALYSIS OF PLANT-PRODUCED MIXES

The research team obtained plant mixes for mixes 1 and 2. Subsequently, the loose mixes were reheated and compacted for the analysis of |E*| under two conditions: (i) immediately post-construction (with an air void content of 7%), and (ii) typical service life condition, after post-compaction with traffic (with an air void content reduced to 4%). Mix 1 utilized an SBS-modified PG 70-28 asphalt binder, while mix 2 utilized a PG 64-22 asphalt binder with no polymer modification. The binders for these mixes were sourced from a different supplier than those used in the laboratory mixes.

Figure 29 illustrates the superimposed master curves for plant-produced mixes alongside laboratory specimens with different asphalt binders. The plant-produced mixes exhibit a master curve closer to the laboratory mixes produced with seven different binders. The plant-produced mix has slightly higher stiffness than the laboratory mix of the same PG (Figure 30). This disparity may be a result from the plant mix undergoing slightly more severe aging during the mixing process and the subsequent reheating for compaction. The extended exposure to heat in the plant may mobilize more aged and stiff asphalt binder within the mix. Additionally, the plant mixes had a slightly higher dust correction factor compared to the one obtained in the laboratory. Figure 31 depicts the master curves for both plant and laboratory mixes for source 2. Mixes 1 and 2 exhibit the same stiffness trends. When plotted together, the various mixes show stiffness values remarkably close to each other, with the plant-produced mixes showing slightly higher stiffness. This is reinforced by Figure 32, where the plant-produced mix with 4% air void content is stiffer than its laboratory counterpart. The considerations regarding aged binder mobilization and dust correction factor, previously mentioned for mix 1, are equally applicable to mix 2.

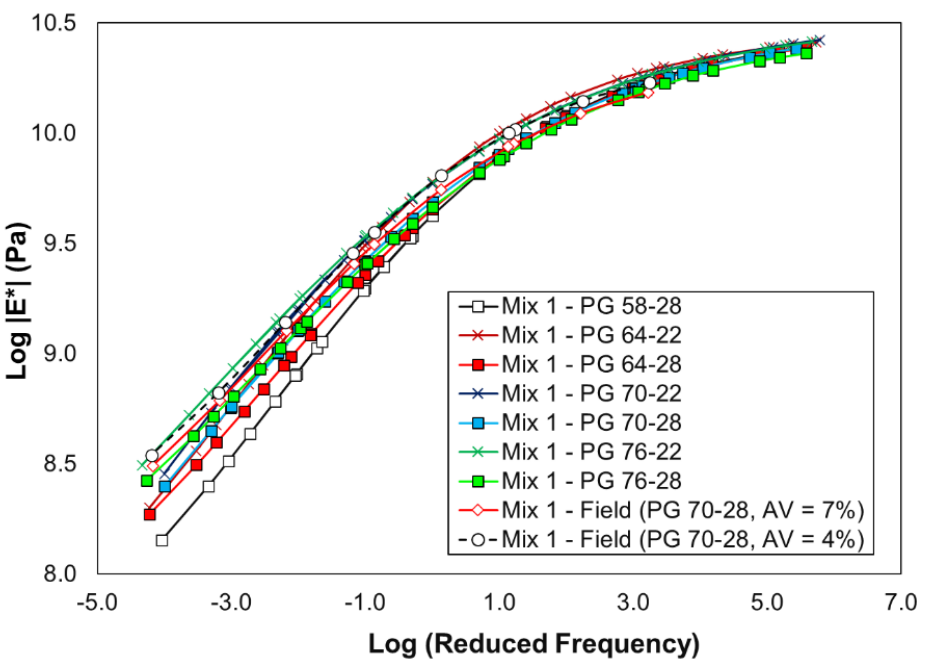

Figure 29. Graph. Master curve comparison between plant-produced and laboratory mixes (mix 1).

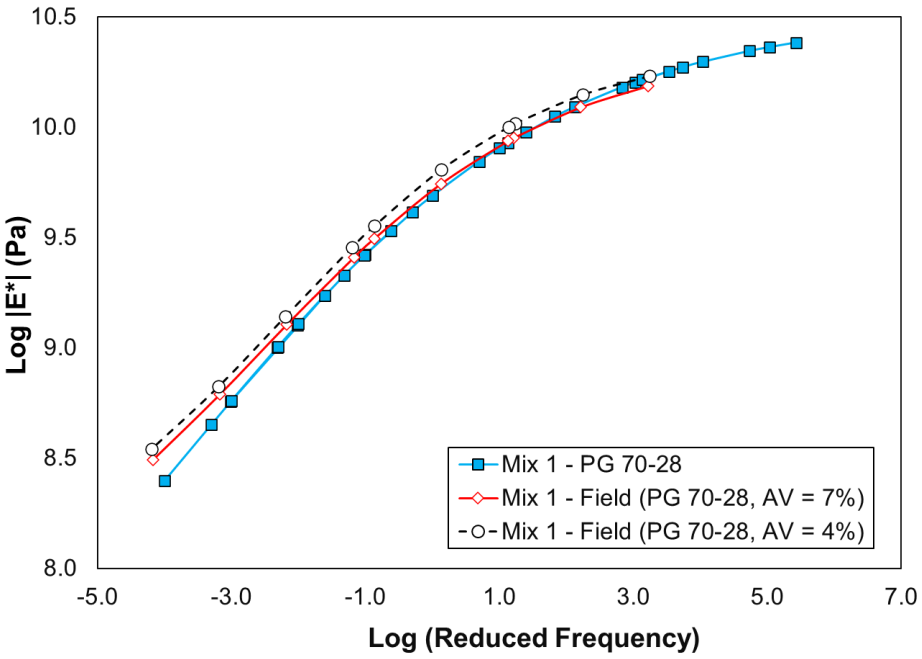

Figure 30. Graph. Master curve comparison between plant-produced and laboratory mixes with the same PG binder (mix 1).

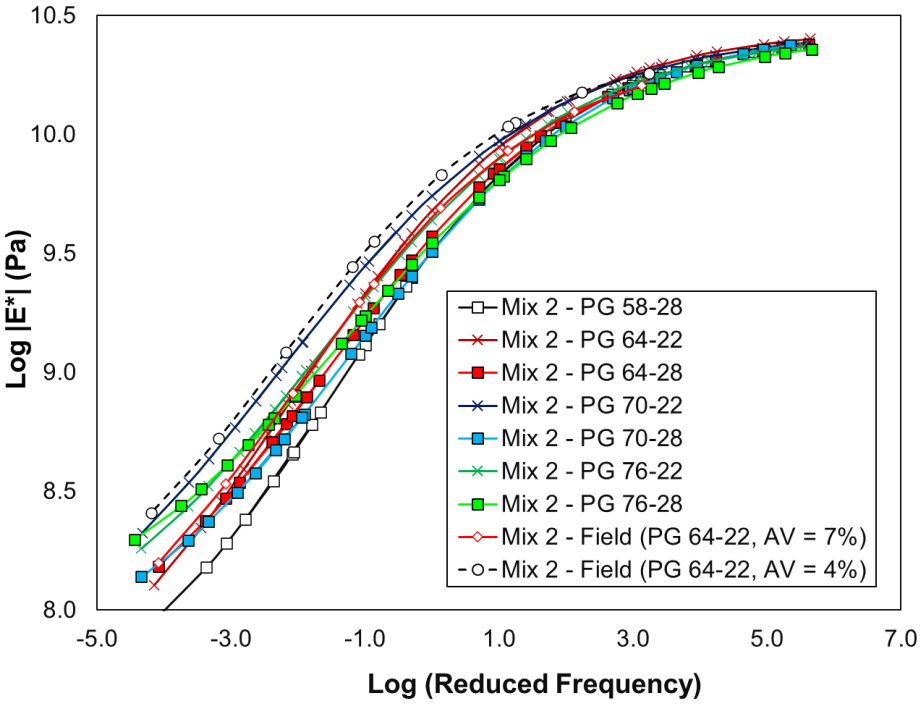

Figure 31. Graph. Master curve comparison between plant-produced and laboratory mixes (mix 2).

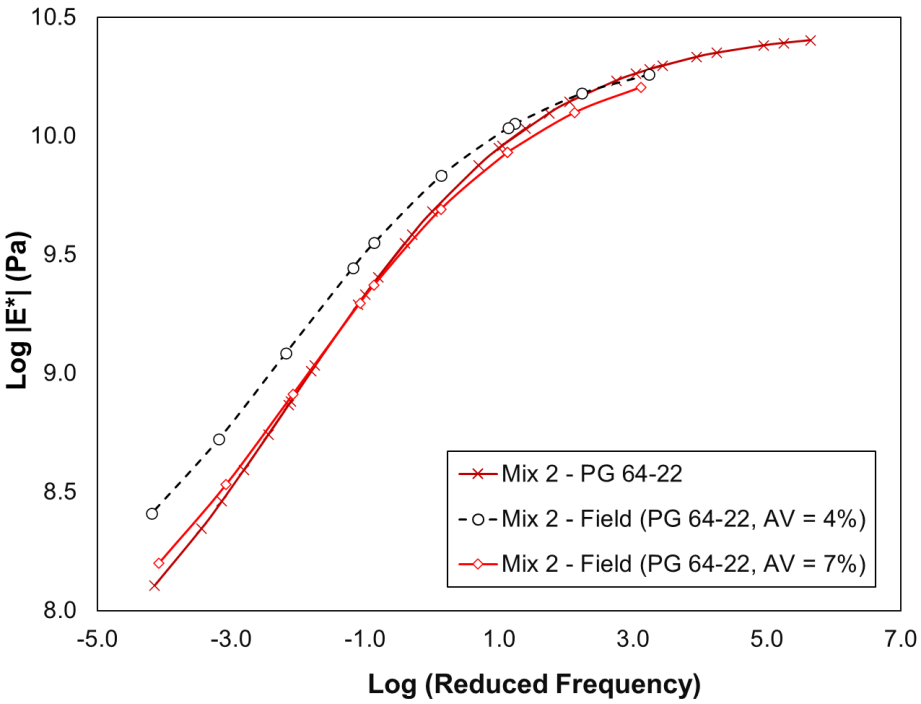

Figure 32. Graph. Master curves comparison between plant-produced and laboratory mixes with the same PG binder (mix 2).

DYNAMIC MODULUS MODELS

All data points derived from dynamic modulus results for various temperatures, frequencies, replicates, and mix/asphalt binder combinations were systematically compared to the predictions generated by different |E*| models. The laboratory results were compared to Witczak and Hirsch models and subsequently evaluated against the ICT BNN model. The Witczak |E*| model showed a R^2 value of 0.570 and a root mean square error (RMSE) of 818 ksi, as shown in Figure 33. In general, better agreement between predicted and measured values is achieved for lower |E*| values, while the dispersion is higher for higher |E*| values. The Hirsch |E*| model showed a R^2 value of 0.433 and a RMSE of 940 ksi, as shown in Figure 33. In general, the model underpredicted the modulus values for all data points, as was also true for the current IDOT modulus algorithm. On the other hand, the ICT BNN model (Asadi et al., 2023) showed excellent fitting to the ground-truth data from the |E*| tests (Figure 34). The BNN model showed a R^2 value of 0.986 and RMSE of 150 ksi, indicating an excellent capacity to predict |E*| values accurately under a wide variety of temperatures, frequencies, asphalt binder PGs, volumetric properties, and other parameters. The data points obtained from the |E*| tests were used as completely unseen test data to assess the robustness of the model and, therefore, were not used as training data, demonstrating the model's overall accuracy in capturing the |E*| of unseen mixes.

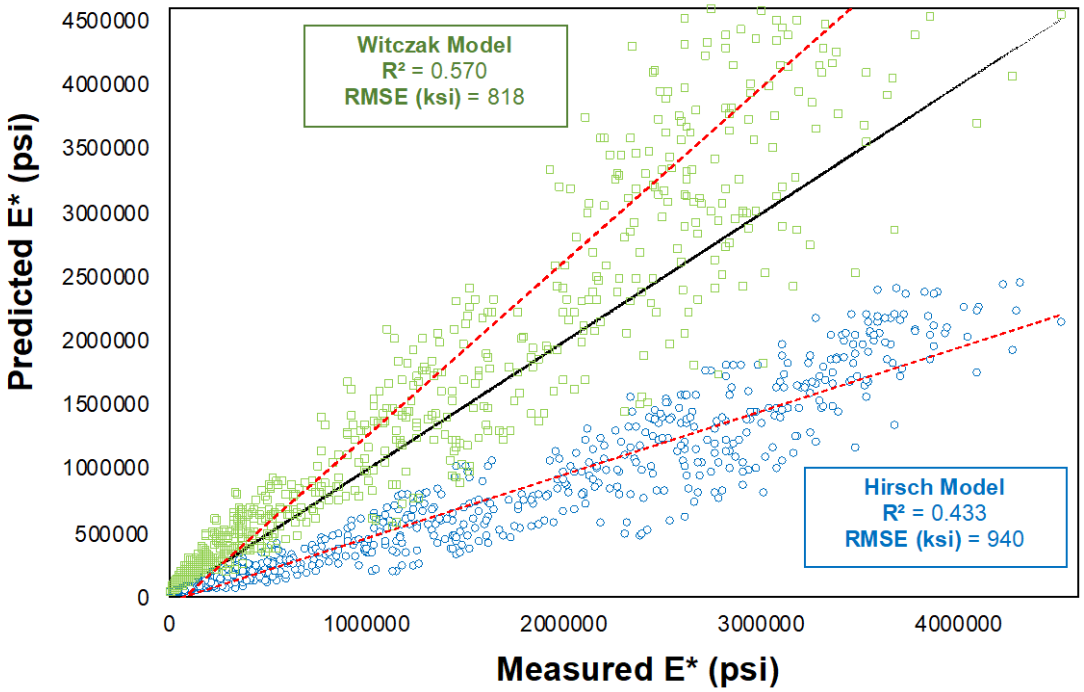

Figure 33. Graph. Measured versus predicted |E*| values for Witczak and Hirsch models.

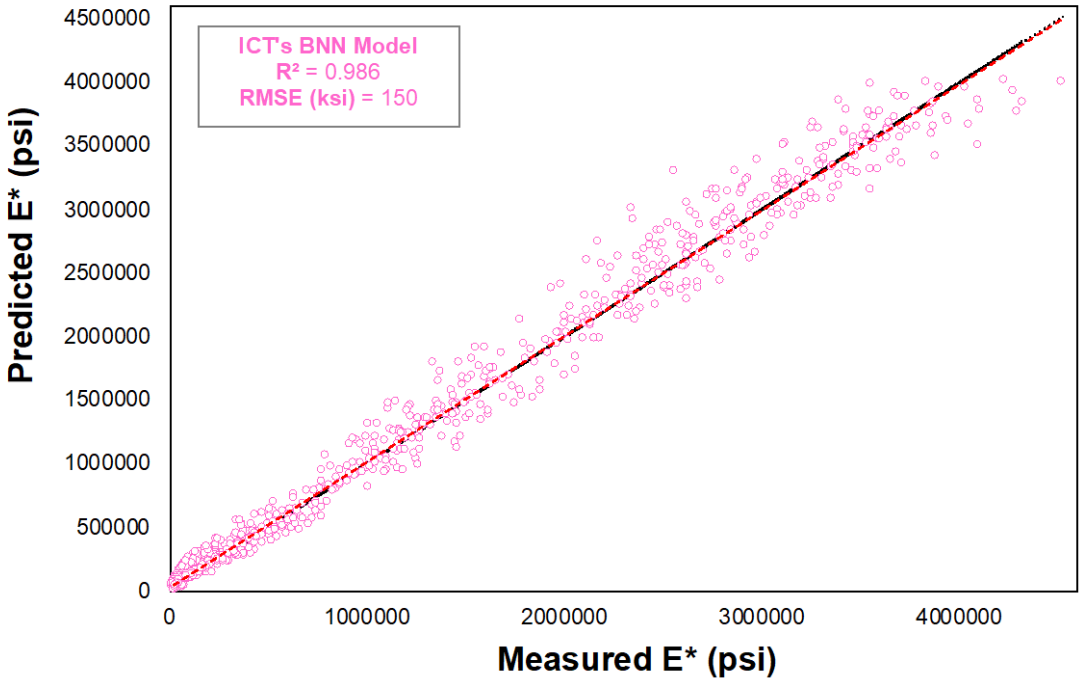

Figure 34. Graph. Measured versus predicted |E*| values for the ICT BNN model.

ULTRASONIC PULSE VELOCITY

The researchers used an AMPT machine to measure |E*| for the four mixes and seven asphalt binders (28 combinations in total) at different temperatures and frequencies to build the respective master curves. At least two replicates were tested for each mixture. For modulus measurements using UPV, velocities were measured directly, while Poisson's ratio (PR) was assumed from typical values for different temperatures (Medina et al., 2018). Table 11 summarizes the PR assumptions. Shift factors (a_T) also need to be assumed to build master curves from UPV modulus measurements. Transducer frequency in UPV ranges from 9 kHz to 100 kHz, much higher than the mechanical loading frequency in |E*| tests. To address this issue, Far et al. (2009) proposed a shift factor prediction tool as an ANN model based on the FHWA LTPP database and shown in Figure 35.

Table 11. Assumed PR Values

Temperature (°C)	4.0	21.0	37.8	54.0	60
PR	0.25	0.28	0.33	0.38	0.39

$$\log a_T = 0.0007\,T^2 + 0.1592\,T + 2.9177$$

Figure 35. Equation. Shift factor prediction tool proposed by Far et al. (2009).

Where: a_T = average shift factor

T = test temperature (°C)

The master curves for each mix and asphalt binder combination obtained from the UPV application are provided in the appendix. In the comparison between the modulus values obtained through the UPV application and the ground-truth data obtained from the AMPT, Figure 36 illustrates a consistent trend where UPV consistently overpredicts the modulus values. However, Poisson's ratio and shift factors are inherent material-specific properties. Once each mix has an individual PR and a_T, master curve prediction errors will ultimately stem from the assumptions for these two parameters. Given that each specimen with modulus measured using UPV had a corresponding actual |E*| test, the actual shift factors could be applied to evaluate the difference between the UPV-measured curves (with predicted and actual shift factors) and the ground-truth modulus. The observed trend is exemplified in Figure 37. For lower frequencies (high temperatures), this correction approximates the UPV-measured data to the ground-truth data, but the difference remains when it comes to higher frequencies.

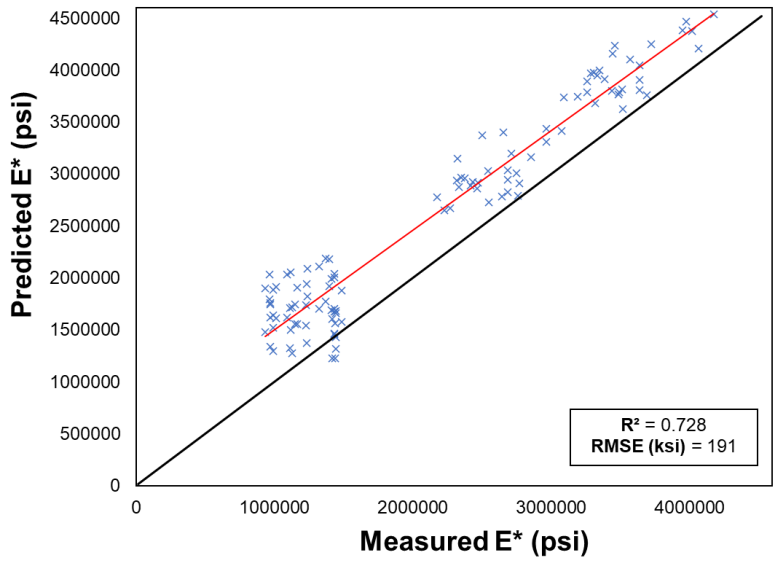

Figure 36. Graph. Comparison between UPV-predicted and measured |E*| results.

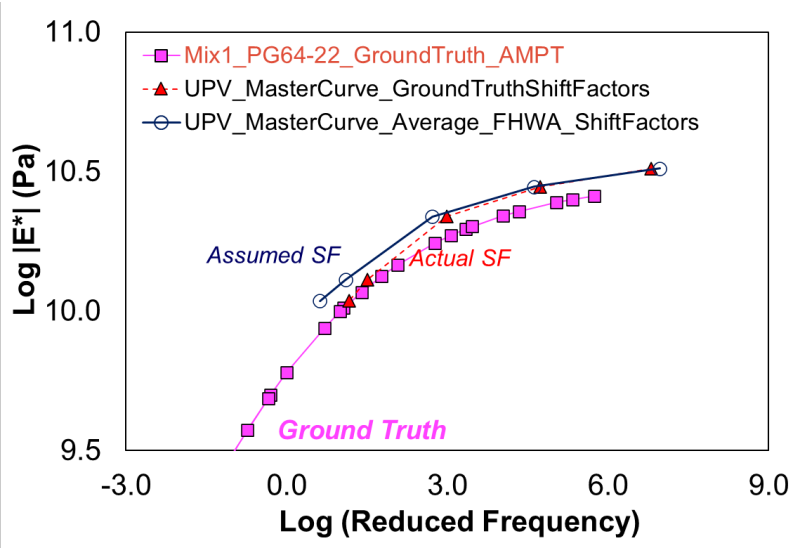

Figure 37. Graph. Shift factor correction trend.

In this context, it can be inferred that the PR assumptions continue to represent a significant source of error for the modulus values measured by UPV. Inhomogeneity can cause other errors, as is often observed for PCC (Saremi et al., 2023), but HMA has more aggregate by percent of total volume than PCC (around 85%), so this may not contribute as substantially to errors. This indicates that PR fluctuates under varying conditions, including temperature and frequency, along with other mix properties like PG, asphalt binder replacement (ABR) value, and air voids (AV). This study made an attempt to "back-calculate" PR using known AMPT |E*| as the elastic modulus in the UPV wave velocity equation with PR as an unknown. Figure 38 illustrates the results, which capture the sensitivity of PR across different mixes, with a comparison made using a no-RAP 19.0 mm NMAS mix with PG 64-22.

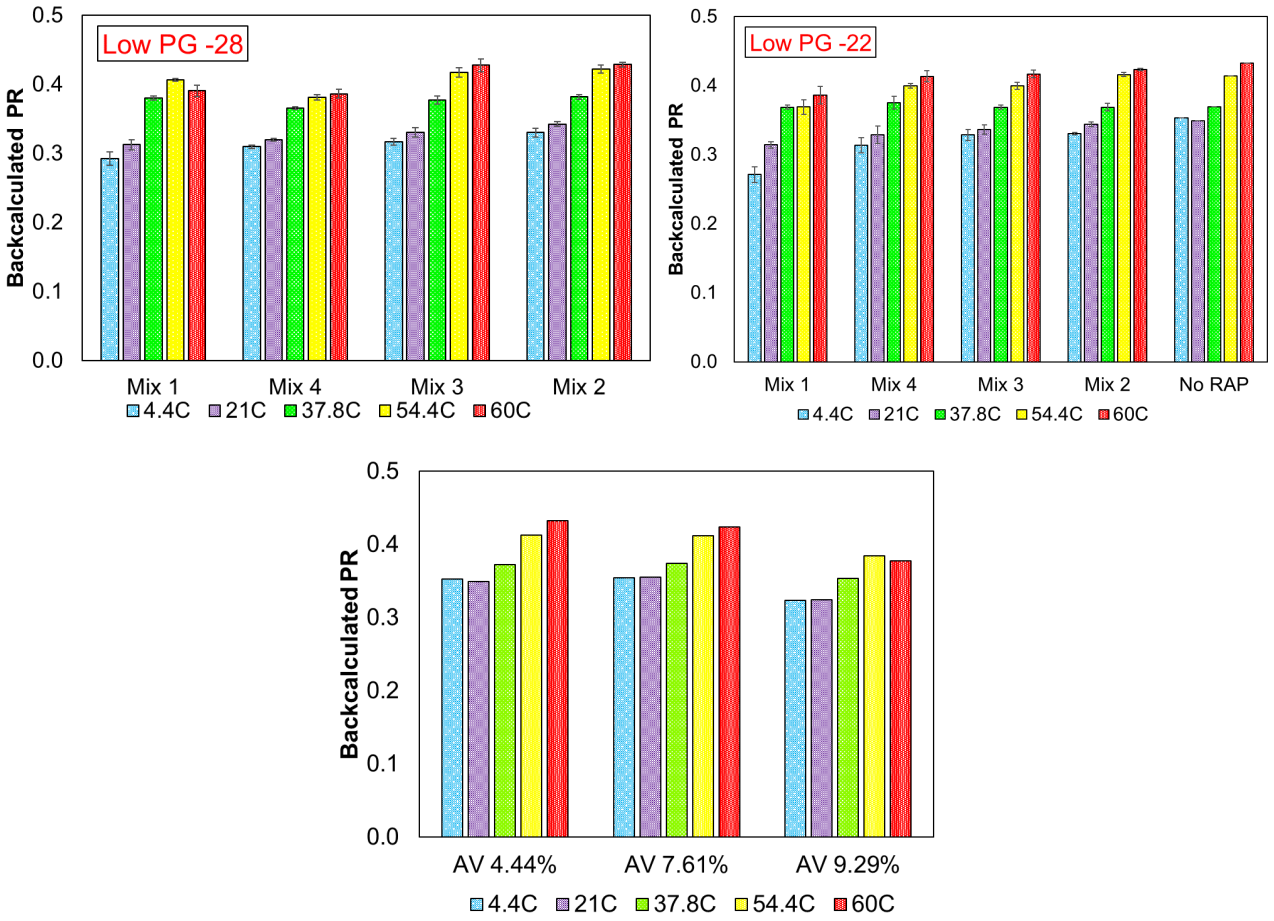

Figure 38. Graph. PR variation with different mixes, temperatures, binder PG, and air voids.

CHAPTER 6: FIELD MODULUS MEASUREMENTS AND STRUCTURAL HEALTH MONITORING BASED ON FWD AND TSD DATA

Table 12 shows data collected during the traffic speed deflectometer (TSD) study for various pavement sections. The effect of temperature must be considered first. The first round of measurements were taken at temperatures colder than the design pavement temperatures in Illinois, while the second round of data were captured at very warm temperatures. Note that some coefficients of variation were very high, especially when the deflections were very low. This was especially critical during the second round of measurements, as it would be expected for deflections to be high at higher temperatures, so the results were counterintuitive. This includes measurements on similar sections of I-57, which were very close together despite the large temperature difference.

Table 12. TSD Data and Analysis

Route	Pavement Structure	Pavement Temperature (°F @4.5 inches)	D_0 (mils)	Coefficient of Variation (CoV) (%)
I-55 Madison County	11.5 inches HMA over rubblized PCC	59	2.9	29%
I-39 McLean County	8 inches HMA over rubblized PCC	57	3.4	30%
US-36 Macomb Bypass	10.75 inches full-depth HMA	69	10.2	26%
I-74 Tazewell/ Woodford County	11.25 inches HMA over rubblized PCC	60	3.4	41%
I-155 Logan County	15 inches full-depth HMA	69	6.3	25%
I-57 Champaign County	11.25 inches HMA over rubblized PCC	57	2.0	31%
I-74 Champaign County	16 inches full-depth HMA	48	3.0	58%
I-70 Effingham County	11.5 inches HMA over rubblized PCC	108	1.5	63%
I-57 Champaign County	11.25 inches HMA over rubblized PCC	83	1.5	50%

Table 13 shows moduli back-calculated from each section. Algorithms for estimating moduli from TSD data were used to estimate tensile strain at the bottom of the HMA layer based on area under pavement profile (AUPP), the subgrade modulus, the known pavement structure, and the relevant temperatures based on the assumption of PG 64-22 asphalt binder. These inputs were placed into an ILLI-PAVE model to determine what modulus would be necessary to achieve that strain. Note that the

final two rows in Table 13 represent excessively high CoV and modulus values (based on the findings presented in Table 12) and were therefore not included as to not introduce results that did not make logical sense. For example, a value of modulus higher at temperature increases is not possible.

Table 13. Back-Calculated Material Properties from TSD Testing

Route	Pavement Structure	Pavement Temperature (°F @4.5 inches)	HMA Strain (micro-strain)	HMA Back-calculated Modulus (ksi)	Subgrade Modulus (E_{RI}) (ksi)
I-55 Madison County	11.5 inches HMA over rubblized PCC	59	45	1541	17.5
I-39 McLean County	8 inches HMA over rubblized PCC	57	35	1945	21
US-36 Macomb Bypass	10.75 inches full-depth HMA	69	126	416	11.1
I-74 Tazewell/ Woodford County	11.25 inches HMA over rubblized PCC	60	52	1365	16.6
I-155 Logan County	15 inches full-depth HMA	69	56	526	11.4
I-57 Champaign County	11.25 inches HMA over rubblized PCC	57	17	1882	18
I-74 Champaign County	16 inches full-depth HMA	48	30	1420	17.1
I-70 Effingham County	11.5 inches HMA over rubblized PCC	108	*	*	17.6
I-57 Champaign County	11.25 inches HMA over rubblized PCC	83	*	*	18.3

*TSD data for these projects was unrealistic and quite variable. As such, back-calculated modulus values were not realistic.

Modulus was observed in two cases to be relatively low at the cold temperatures at which TSD measurements were performed. These measurements were in line with IDOT's design moduli values but were measured at lower temperatures than the mean monthly pavement temperature used in Illinois for the design. The remaining measurements were all much higher than IDOT's existing design moduli values, but this is not unexpected given the additional consolidation over a pavement's lifetime, as well as aging and the already known low values used for design, which are consistent with the previous chapter of this report and previous work on IDOT mixes (Carpenter, 2007). However, overall conclusions are difficult to draw from this data, as the data seem to have high variability at times and are counterintuitive at others. It should be noted that coefficients of variation for deflection measurements were in some cases much higher than is presently acceptable for FWD measurements. Future protocols should also ensure that the temperature at which data are measured is consistent with Illinois design temperatures as much as possible. However, there is promise that this tool will be useful in developing future structural indices for network-level pavement management use on Illinois pavements. This should be pursued in future research.

CHAPTER 7: FATIGUE ANALYSIS

FOUR-POINT BENDING BEAM FATIGUE TEST

1-Second Rest Period Analysis

An experimental matrix was developed to cover different combinations of mixes (1, 2, and 3) and asphalt binders. Each test was conducted first at two low strain levels (70 and 100 microstrain) and a 1-second rest period. The premise assumed was that at 70 microstrain and a 1-second rest period, no damage would be accumulated as a function of load application in the field for 10,000 cycles. The stiffness ratio (SR) obtained for this condition can be assumed as a baseline for the analysis of acceptable SR levels to be considered as a "no damage" accumulation for 10,000 repetitions of load applications. Figure 39 shows the SR values at 70 and 100 microstrain levels.

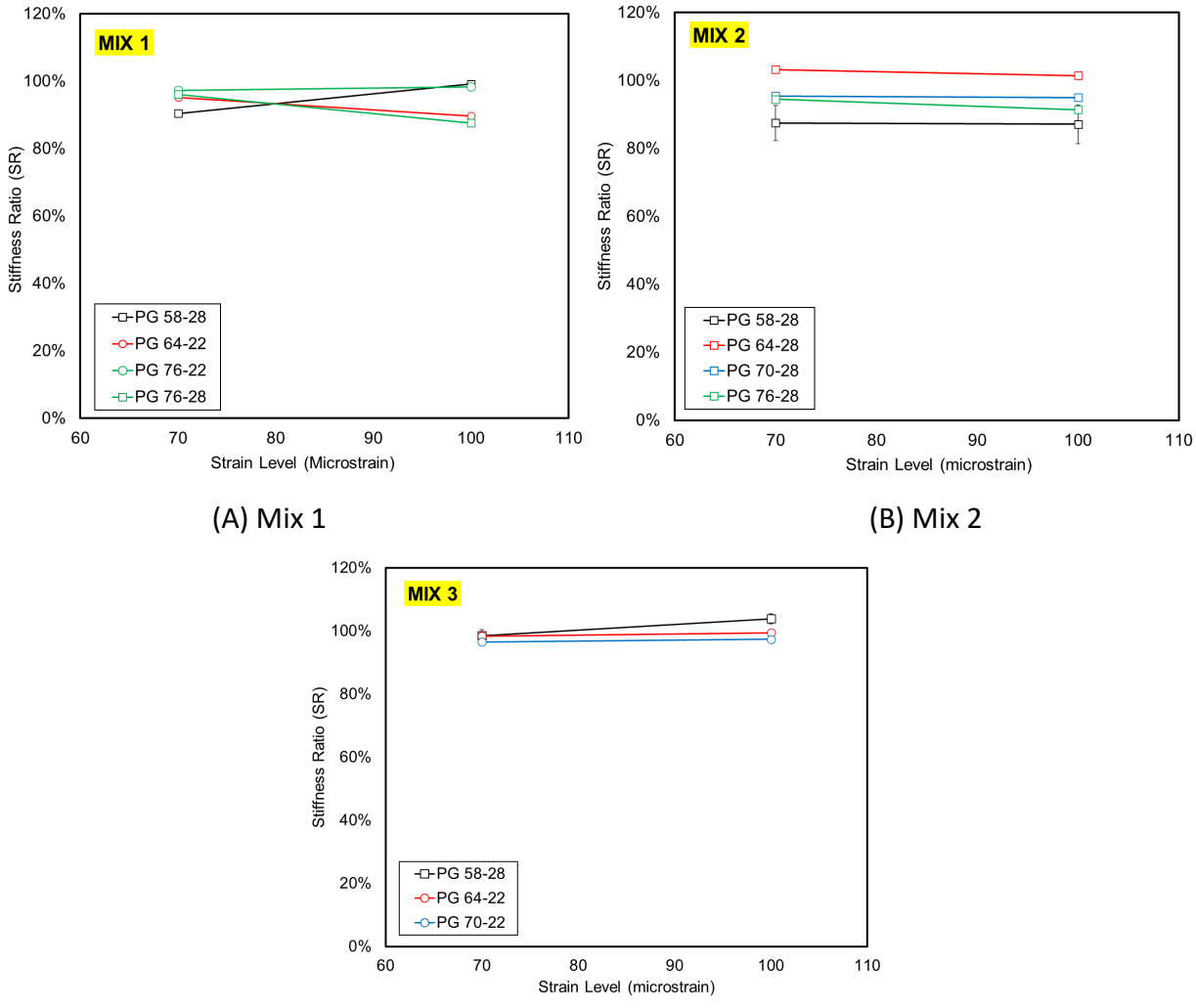

(A) Mix 1

(B) Mix 2

(C) Mix 3

Figure 39. Graph. SR variation from 70 to 100 microstrain strain levels for 1-second rest period.

The experimental results showed that mixes made of PG 58-28 asphalt binder exhibited a relative increase in SR from 70 to 100 microstrain. This phenomenon was particularly pronounced in mixes 1 and 3. One test for mix 2 was excluded due to detected inconsistencies, as depicted in Figure 40. For the cases where a drop in SR was noted between 70 and 100 microstrain, as observed in mix 1 (PG 64-22 and PG 76-28) and mix 2 (PG 76-28), a detailed examination of raw data was conducted to further examine the SR behavior to check for an actual SR drop during load applications. Figure 40 illustrates the flexural stiffness behavior within the 5,000 to 10,000 cycle range for the mentioned samples. The flat linear trend in the graph indicates an absence of damage accumulation between cycles, suggesting that the observed SR decrease is likely due to test instabilities observed in the initial cycles rather than a very low FEL (Figure 41).

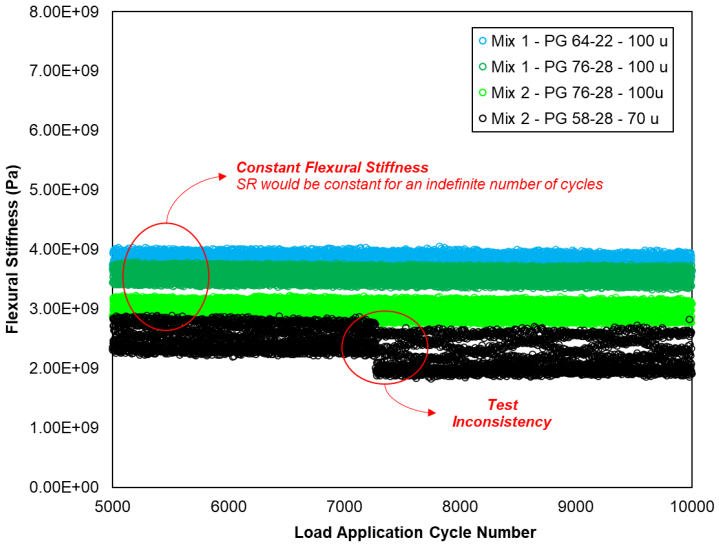

Figure 40. Graph. Raw data analysis for specific cases of 4PBBF test at 1-second rest period.

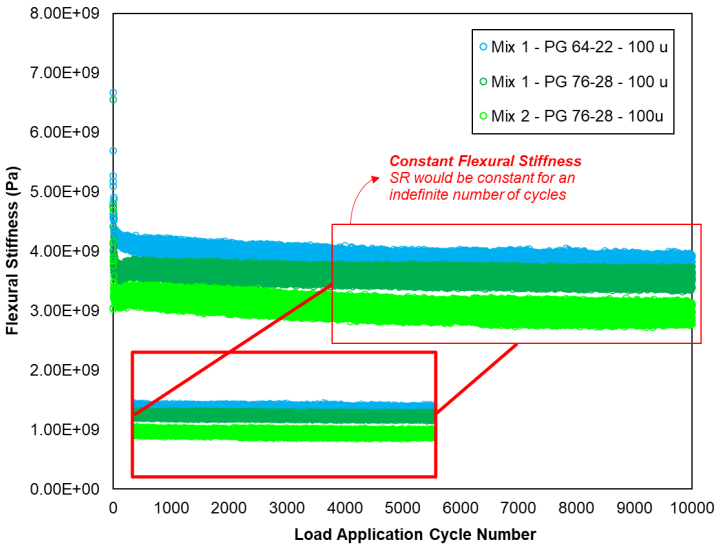

Figure 41. Graph. SR initial drop and subsequent stabilization at the second half of the load application cycles.

0-Second Rest Period Analysis

The experimental protocol for the 0-second rest period considered a range of strain levels spanning from 50 to 500 microstrain (specifically, 50, 70, 90, 100, 125, 150, 175, 200, 250, and 500 microstrain). The purpose of this protocol was to analyze the variation of SR values in relation to the applied strain levels. Given that it is not possible to fundamentally define FEL in a scenario with a reduced number of cycles and 0-second rest period, FEL becomes an engineering concept for which a definition must be set. This concept could be taken as the strain level that would lead to an acceptable SR. Four potential approaches were initially examined (with results shown in Figure 42):

- Acceptable tensile strain (0-second RP) = minimum SR (1-second RP). This represents a scenario where no damage accumulates during subsequent load applications in a stable state.
- Acceptable tensile strain (0-second RP) = strain level that led to the peak SR value among all strain levels tested at 0-second RP.
- Acceptable tensile strain (0-second RP) = strain level that led to SR greater than 90%.
- Acceptable tensile strain (0-second RP) = strain level that led to SR greater than 95%.

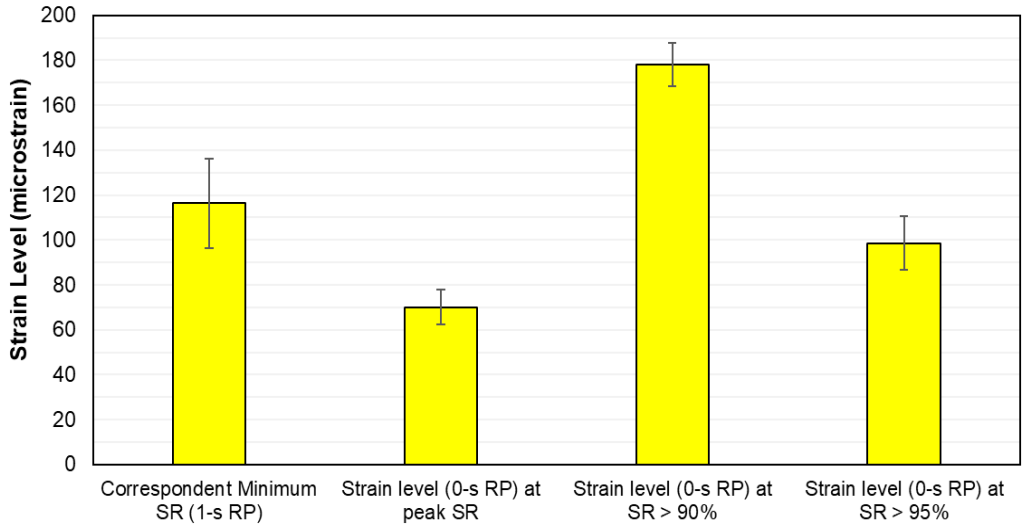

Figure 42. Graph. Analysis of different scenarios of strain levels obtained for acceptable SR values.

Figures 43–45 provide a detailed depiction of the SR variation in relation to increasing strain levels, based on the results obtained for a 0-second rest period. As a general trend, SR tends to decrease as strain levels increase. Particularly at lower strain levels, below 180 microstrain, the SR points exhibit close proximity both to each other and to the 90% SR reference line. This observation aligns with the stiffness results obtained from the dynamic modulus, as follows: for some combinations of mixes and soft asphalt binders (especially ones with PG XX-28), softer mixtures were obtained. Softer mixes are less brittle, and therefore expected to have less damage accumulated in terms of cyclic loading (fatigue). In this regard, results showed that SR values > 90% could be obtained at higher strain levels

for certain combinations of mixes and binders with low PG -28 (e.g., mix 2 with PG 58-28, 64-28, and 70-28, as well as mix 3 with PG 58-28). This was not the case for mix 1 (with 2% RAS) and binders with low PG -22 (generally stiffer at intermediate temperature, 20°C). The inclusion of RAS within the mixes is believed to compromise the potential benefits that could be achieved—specifically, the enhanced ability to retain higher SRs under cyclic loading at normal strain levels when employing softer asphalt binders.

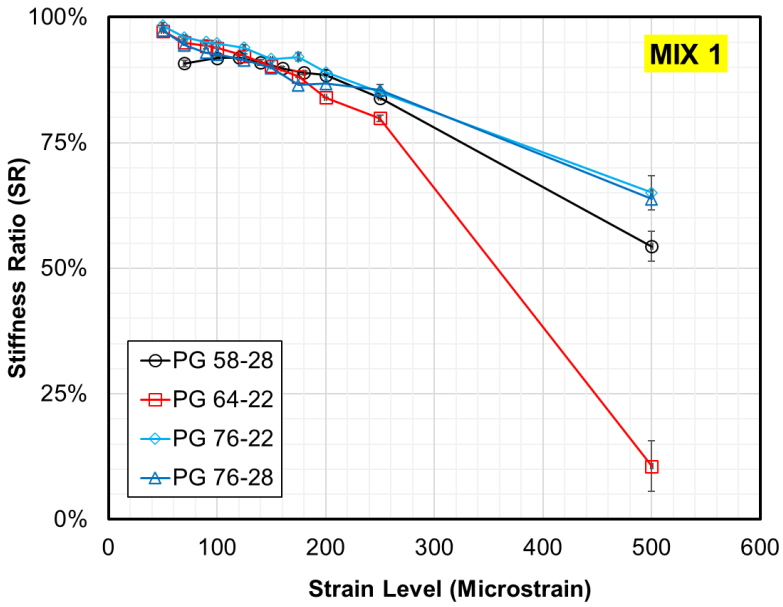

Figure 43. Graph. Stiffness ratio evolution with increasing strain level (mix 1).

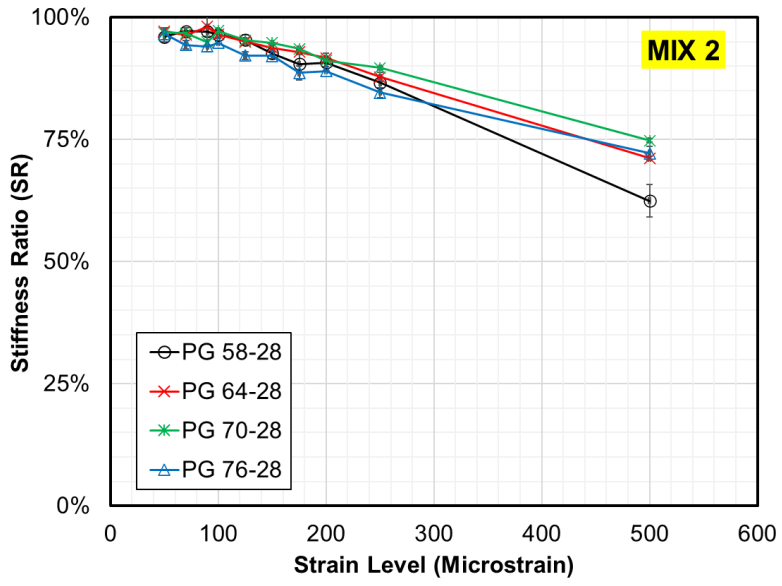

Figure 44. Graph. Stiffness ratio evolution with increasing strain level (mix 2).

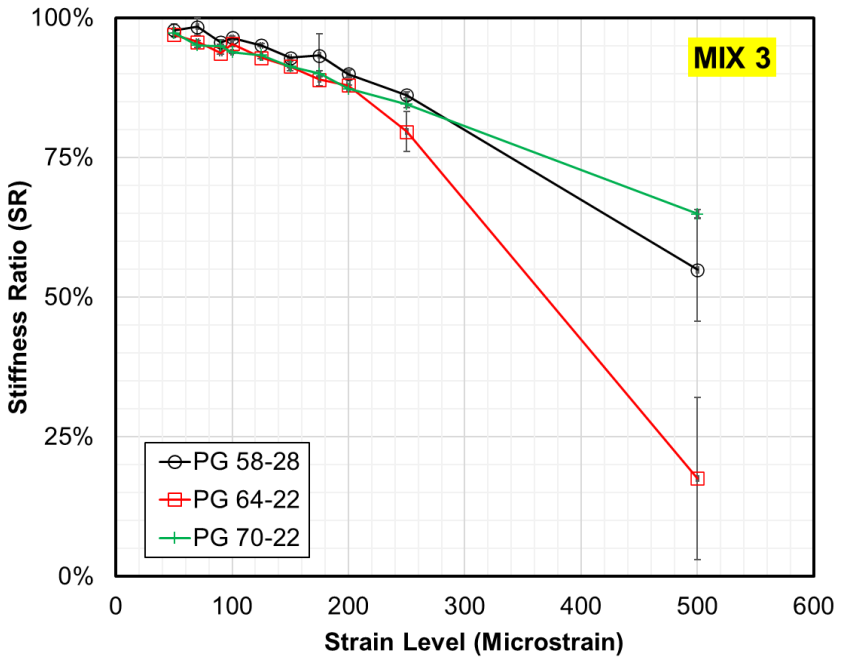

Figure 45. Graph. Stiffness ratio evolution with increasing strain level (mix 3).

Illinois Flexibility Index Test

For the presentation of flexibility index results, the binder nomenclatures were organized in terms of high PG and stiffness, as shown in Table 14. Figure 46 shows the FI values of laboratory-prepared HMA mixtures along with their aging rates (%). The dotted red line indicates the short- and long-term aging FI thresholds of 8 and 5, respectively, that are used in Illinois. For each mixture type, four FI values were computed, and the average was plotted in a bar chart along with error bars.

Table 14. Asphalt Binders' Nomenclature

Asphalt Binder PG	Nomenclature
PG 58-28	A
PG 64-28	B
PG 64-22	C
PG 70-28	D
PG 70-22	E
PG 76-28	F
PG 76-22	G

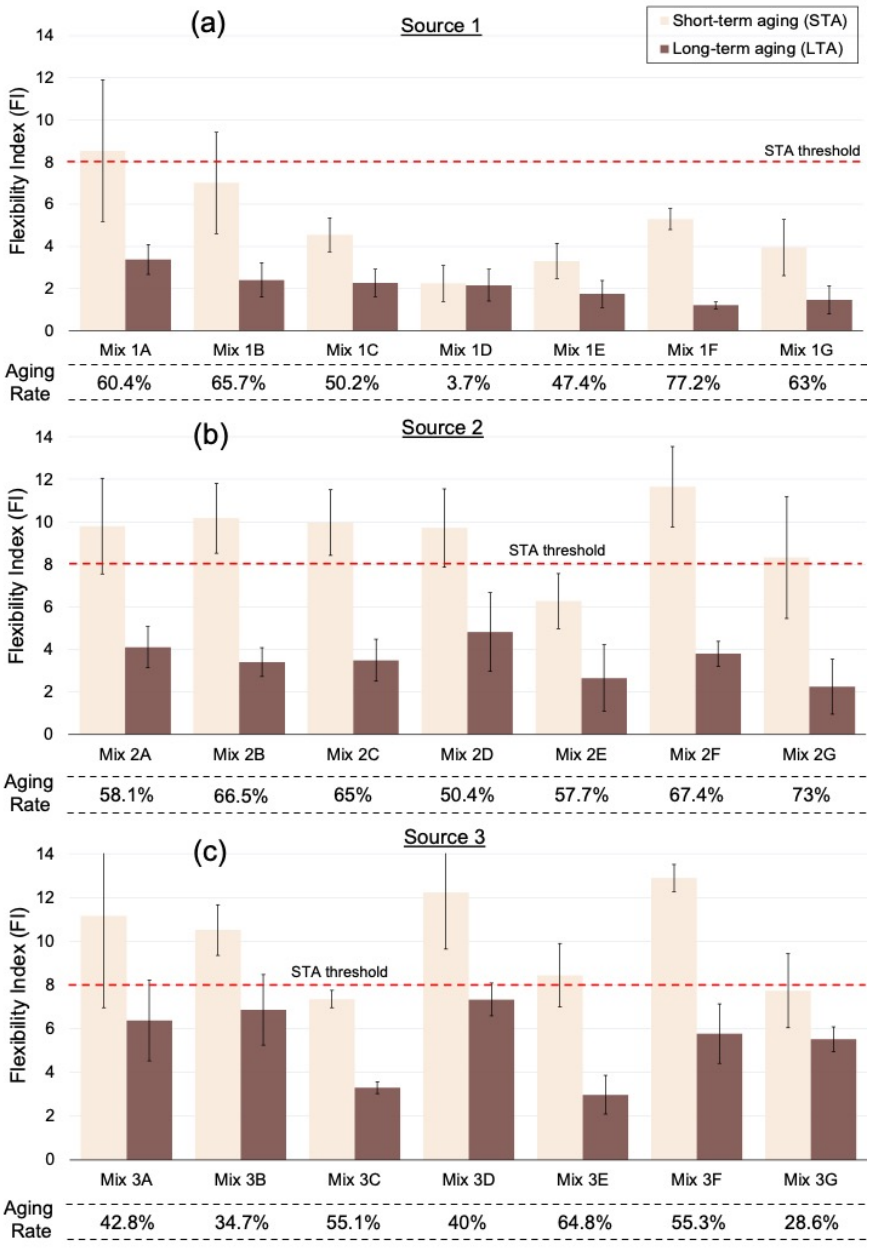

Figure 46. Graph. Flexibility index and aging rate results for mixes 1, 2, and 3.

For source 1, the highest FI values of 8.5 and 3.4 were observed for mix 1A (prepared with PG 58-28 asphalt binder) for STA and LTA, respectively. Mix 1D (PG 70-28) with a FI value of 2.2 in STA and mix 1F with a FI value of 1.2 in LTA showed the lowest FI. This implies that the ranking of FI for LTA specimens did not necessarily agree with that of STA specimens, except for asphalt binder PG 58-28 with the highest FI value in both aging conditions. All mixtures prepared from source 1 material except for mix 1A failed to meet the minimum STA threshold. For LTA, none of the mixes reached a value of 5. The presence of 22% RAP and 2% RAS content in HMA mixtures prepared from source 1 increased the overall brittleness of the mix and, in turn, significantly reduced the FI values. A drop in

FI values with aging was observed and quantified using the aging rate. High sensitivity to aging was observed for mix 1F (PG 76-28) with a 77.2% drop in FI value compared to other mixtures.

For source 2, all HMA mixtures except mix 2E (PG 70-22) satisfied the STA FI threshold. Mix 2F (FI = 11.7) and mix 2E (FI = 6.3) showed the highest and lowest values for STA, respectively, while mix 2D (FI = 4.8) and mix 2G (FI = 2.2) showed the highest and lowest FI values for LTA. A more drastic drop in FI value (73.0%) with aging was observed for mix 2G compared to other mixtures. On average, mixtures prepared from source 2 had better FI values than those prepared from source 1. With a 15% RAP content and no RAS, source 2 had less recycled material content compared to source 1, resulting in better flexibility.

All source 3 HMA mixtures except mix 3C and mix 3G, passed the STA threshold. High FI values of 12.9 and 7.3 were observed for mix 3F in STA and mix 3D in LTA. Mix 3C with a FI value of 7.4 in STA and mix 3E with a FI value of 3 in LTA showed the least flexibility. On average, higher FI values were observed for source 3 HMA mixtures in LTA, compared to sources 1 and 2. Unexpectedly, source 2 HMA mixtures with lesser RAP content and almost similar virgin binder content, as well as similar volumetrics, had lower FI values in LTA compared to source 3. This implies that apart from the recycled material content, the aggregate and RAP sources as well as other mix design parameters potentially contributed to the overall flexibility of the HMA mixture.

To summarize, mixtures prepared from source 1 (22% RAP and 2% RAS) had lower FI values compared to source 2 (15% RAP and no RAS) and source 3 (25% RAP and no RAS). The presence of RAS, a highly oxidized material, is a major contributor to an increase in mix stiffness and reduction in FI values. The changes in the asphalt binder grade had a clear impact on FI values; however, no trend was observed. For example, mixes with the same ABR and the stiffer asphalt binder (mix 1G [N90, 30.3% ABR with PG 76-22]) had significantly lower FI values compared to mixes with softer binder (mix 1A [N90, 30.3% ABR with PG 58-28]). Mixtures prepared from polymer-modified binders with high PG (mix 1F, mix 1G, mix 2F, mix 2G, mix 3E, and mix 3F) had the highest aging rates, reinforcing the findings from the poker chip binder test, although it was not always the case.

CHAPTER 8: CONCLUSIONS, RECOMMENDATIONS AND FUTURE WORK

This research project aimed to address the need for reviewing and updating the Illinois Department of Transportation's mechanistic-empirical flexible pavement design procedures for full-depth asphalt and asphalt over rubblized concrete pavements. The background for this study relates to the evolving hot-mix asphalt technology, for which the existing modulus and fatigue algorithms do not capture the impact of current modified asphalt binders and recycled asphalt on the composition and properties of asphalt mixes used for flexible pavement thickness design. The objectives of this research approached both modulus and fatigue algorithms and design criteria for HMA mixes. The initial focus was on enhancing IDOT's |E*| prediction algorithm to incorporate modern mixes, with extensive testing and comparison against established models. This investigation extended to alternative methods such as ultrasonic pulse velocity nondestructive testing as well as the analysis of field data by means of the traffic speed deflectometer.

This study also aimed to review the current fatigue endurance limit criterion used for design in the state, introducing an adapted four-point bending beam fatigue test protocol under varying rest periods. This criterion holds utmost importance because of its relevance for the final thickness design, which dictates the amount of material needed for construction. If relaxed, it would increase environmental benefits and reduce the overall cost for construction of asphalt pavements assuming that reduced pavement thickness does not lead to reduced performance over the lifespan of the pavement. The significance of this research is underscored by its multi-scale approach, encompassing asphalt binder-level assessments, laboratory tests on mixtures, and field data analysis. By consolidating findings and exploring relationships within this extensive dataset, the project provides valuable insights and recommendations to inform updates to IDOT's pavement design procedures, ensuring they remain aligned with the current state of technology and industry best practices.

Results from the analysis of RTFO-aged binders showed distinct clusters of asphalt binders at the interest frequency range of 10 Hz, demonstrating differences in stiffness among low PG labels of -22 and -28°C. Additionally, the observed reduction in ductility with aging, especially in polymer-modified asphalt binders, underscores the importance of considering the specific characteristics of asphalt binders in pavement design. Given that lower levels of aging are expected to happen with the lower-lift binder course layer, the use of high-ductility SBS-modified binders might result in better anti-cracking performance. The stiffness trends identified in asphalt binders were similarly reflected in HMA samples across the dynamic modulus experimental matrix. Overall, the stiffness of the HMA mixes corresponds with the anticipated behavior based on the characteristics of the asphalt binders. Specifically, when considering the frequency of interest and IDOT's design temperature range, a consistent clustering of mixes in terms of low PG is evident. In summary, the results obtained for the modulus analysis tasks are summarized as follows:

- The typical |E*| values currently used in Illinois are low compared to modern asphalt mixes, which use recycled materials and modified asphalt binders. Increasing the assumed |E*| generally has the potential to result in cost and environmental savings due to decreasing

strains at the bottom of the asphalt layer, allowing for reduced layer thicknesses in full-depth pavement design. However, care should be taken to consider the effects of climate change and potential temperature rises in the state.

- When different asphalt binders are used to produce the same mix, a low performance grade (PG) generally controls the modulus of the mix and is seen to be more critical than high PG or PG spread.

- A BNN model was developed for modulus prediction that substantially outperformed both Witczak and Hirsch models. While Witczak and Hirsch models provided R^2 values of 0.570 and 0.433, respectively, for the ground-truth data, the BNN model provided a R^2 of 0.986. The application of the BNN model is considerably simpler, because there is no need for asphalt binder testing from a specific source, only design PG label. Furthermore, this algorithm includes assessment of RAP content, which previous models did not. Given the good fit of the BNN model to typical modern mixes in Illinois, this can potentially supplement the current algorithm.

- The ultrasonic pulse velocity test can be used for quick screening of HMA |E*|. However, the main drawback of the test is the need for assumptions of Poisson's ratio and shift factors. In this research, the ultrasonic pulse velocity test consistently resulted in predicted |E*| values higher than the ones obtained from actual tests. It was also possible to back-calculate Poisson's ratio based on known |E*| mixes using this technique, which could prove valuable in software like ILLI-PAVE, which requires Poisson's ratio as an input for pavement analysis. Further testing of the ground truth and using field cores, especially where structural testing is performed, could help validate this technique further and provide a new research and investigation tool.

While these findings hold the potential to reduce the design thickness of flexible pavements, it is crucial to assess the impact of recycled materials, which contribute to the stiffening of the mix, on fatigue life. Consequently, the subsequent phase of this study involved a comprehensive fatigue evaluation of the investigated mixes. The objective was to enhance the design of pavement sections by preventing fatigue and ultimately minimizing life cycle costs to only require routine and preventative maintenance. This ongoing task has been continuously refined to yield more reliable results by combining a robust theoretical foundation with simplified laboratory protocols for practical purposes. Inspired by the four-point bending beam fatigue protocol developed in NCHRP report 9-44, adaptations were proposed to the current test standard. These adaptations account for varying strain levels and rest periods within a reasonable test duration. However, the definition of a fatigue endurance limit remains a subject of ongoing research. Challenges on this task include test geometry, loading characteristics, and the viscoelastic behavior of asphalt mixtures, making it unlikely to achieve stiffness ratio (SR) values of 100% due to reduced rest periods and the absence of confinement during the test.

In this context, the current research aims to establish an "acceptable SR < 1" for mixes. This implies that if a mix demonstrates an acceptable drop in SR within 10,000 cycles, with a stabilization trend (flat line) during the last few thousand cycles, it suggests an exceptionally long fatigue life. While this

concept approximates the fatigue endurance limit concept, it is important to note that further in-depth analysis is required to enhance the foundation of these concepts. Among the examined scenarios, the current fatigue endurance limit of 70 microstrain represents the most conservative criterion. This average strain level corresponds to the peak SR value within tests conducted with a 0-second rest period, a particularly critical condition. Realistically, even under platooning conditions, some rest period, even small, is expected to exist. Therefore, the current criteria appear to be conservative. On the other hand, consider a scenario where a 10% drop in SR within 10,000 cycles was considered acceptable (as long as the second half, from 5,000–10,000 cycles of the test protocol, maintains a slope of approximately 0). The allowable strain level could be increased up to 180 microstrain, although this value is very high, and the actual increase should be below this level.

At this time, it is not clear exactly what values should be used for design FEL and modulus. Part of this comes from a need to see more data from a more diverse set of materials, as well as considering shorter but nonzero rest periods to accommodate for truck platooning and other changing load patterns. In addition, modulus uncertainty must be checked and the current IDOT practice should be examined to ensure this approach will not lead to lower-than-expected values affecting the critical strain from a pavement design perspective. These issues will be the subject of future research and will inform a new limiting strain criterion and modulus inputs which can be implemented into IDOT's M-E design methodology.

REFERENCES

AASHTO R 84. (2017). *Standard Practice for Developing Dynamic Modulus Master Curves for Asphalt Mixtures Using the Asphalt Mixture Performance* Tester (AMPT). American Association of State Highway and Transportation Officials.

AASHTO T 321. (2022). *Standard Method of Test for Determining the Fatigue Life of Compacted Asphalt Mixtures Subjected to Repeated Flexural Bending*. American Association of State Highway and Transportation Officials.

AASHTO T 342. (2022). *Standard Method of Test for Determining Dynamic Modulus of Hot Mix Asphalt (HMA)*. American Association of State Highway and Transportation Officials.

AASHTO T 378. (2022). *Standard Method of Test for Determining the Dynamic Modulus and Flow Number for Asphalt Mixtures Using the Asphalt Mixture Performance Tester (AMPT)*. American Association of State Highway and Transportation Officials.

Airey, G. D. (2003). Rheological properties of styrene butadiene styrene polymer modified road bitumens. *Fuel*, 82(14), 1709–1719. https://doi.org/10.1016/S0016-2361(03)00146-7

Al-Khateeb, G., Shenoy, A., Gibson, N., & Harman, T. (2006). A new simplistic model for dynamic modulus predictions of asphalt paving mixtures. *Journal of the Association of Asphalt Paving Technologists*, *75*.

Al-Qadi, I. L., Elseifi, M., & Carpenter, S. H. (2007). *Reclaimed asphalt pavement—A literature review* (Report No. FHWA-ICT-07-001). Illinois Center for Transportation.

Al-Qadi, I. L., Said, I. M., Ali, U. M., & Kaddo, J. R. (2022). Cracking prediction of asphalt concrete using fracture and strength tests. *International Journal of Pavement Engineering*, *23*(10), 3333–3345.

Alvarez, C., & Thompson, M. R. (1998). Mechanistic Empirical Evaluation of the Mn. *Road Mainline Flexible Pavement Sections, Transportation Engineering Series*, (97).

American Association of State Highway and Transportation Officials. (1993). *AASHTO Guide for Design of Pavement Structures*, 4th Edition with 1998 Supplement. AASHTO.

American Association of State Highway and Transportation Officials. (2008). *Mechanistic-empirical pavement design guide: A manual of practice*. AASHTO.

Arabani, M., Kheiry, P. T., & Ferdosi, B. (2009). Laboratory evaluation of the effect of HMA mixt parameters on ultrasonic pulse wave velocities. *Road Materials and Pavement Design*, *10*(1), 223–232. https://doi.org/10.1080/14680629.2009.9690189

Asadi, B., Hajj, R., & Al-Qadi, I. L. (2023). Asphalt concrete dynamic modulus prediction: Bayesian neural network approach. *International Journal of Pavement Engineering*, 24(2).

ASTM C597-22. (2022). *Standard Test Method for Ultrasonic Pulse Velocity Through Concrete*.

Bari, J., & Witczak, M. W. (2005). Evaluation of the effect of lime modification on the dynamic modulus stiffness of hot-mix asphalt: Use with the new mechanistic–empirical pavement design guide. *Transportation Research Record*, *1929*(1), 10–19.

Batioja-Alvarez, D., Lee, J., & Haddock, J. E. (2019). Understanding the Illinois flexibility index test (I-FIT) using Indiana asphalt mixtures. *Transportation Research Record*, *2673*(6), 337–346.

Bech, N., & Vandenbossche, J. M. (2023). Relationship between backcalculated dynamic modulus, estimated dynamic modulus, and fatigue damage in asphalt concrete. *International Journal of Pavement Engineering*, *24*(2), 2068549.

Behnood, A., & Daneshvar, D. (2020). A machine learning study of the dynamic modulus of asphalt concretes: An application of M5P model tree algorithm. *Construction and Building Materials*, *262*, 120544. https://doi.org/10.1016/j.conbuildmat.2020.120544

Bennert, T. (2009). *Dynamic modulus of hot mix asphalt* (Report No. FHWA-NJ-2009-011). New Jersey Department of Transportation.

Birgisson, B., Roque, R., & Page, G. C. (2003). Ultrasonic pulse wave velocity test for monitoring changes in hot-mix asphalt mixture integrity from exposure to moisture. *Transportation Research Record*, *1832*(1), 173–181. https://doi.org/10.3141/1832-21

Birgisson, B., Sholar, G., & Roque, R. (2005). Evaluation of a predicted dynamic modulus for Florida mixtures. *Transportation Research Record*, *1929*(1), 200–207.

Blundell, C., Cornebise, J., Kavukcuoglu, K., & Wierstra, D. (2015, June). Weight uncertainty in neural network. In *International conference on machine learning* (pp. 1613–1622). PMLR.

Bonnaure, F., Gest, G., Gravois, A., & Uge, P. (1977). New method of predicting the stiffness of asphalt paving mixtures. In *Association of Asphalt Paving Technologists Proc* (Vol. 46).

Carpenter, S. H. (2007). *Dynamic modulus performance of IDOT mixtures* (Report No. FHWA-ICT-07-008. Illinois Center for Transportation.

Carpenter, S. H., & Shen, S. (2006). Dissipated energy approach to study hot-mix asphalt healing in fatigue. *Transportation Research Record*, *1970*(1), 178–185. https://doi.org/10.1177/0361198106197000119

Carrillo, J., Ramirez, J., & Lizarazo-Marriaga, J. (2019). Modulus of elasticity and Poisson's ratio of fiber-reinforced concrete in Colombia from ultrasonic pulse velocities. *Journal of Building Engineering*, *23*, 18–26. https://doi.org/10.1016/j.jobe.2019.01.016

Ceylan, H., Gopalakrishnan, K., & Kim, S. (2008). Advanced approaches to hot-mix asphalt dynamic modulus prediction. *Canadian Journal of Civil Engineering*, *35*(7), 699–707. https://doi.org/10.1139/L08-016

Christensen, R. (1982). *Theory of viscoelasticity*. 2nd ed. Academic.

Christensen Jr, D. W., Pellinen, T., & Bonaquist, R. F. (2003). Hirsch model for estimating the modulus of asphalt concrete. *Journal of the Association of Asphalt Paving Technologists*, 72.

Clark, R. (1958). Practical results of asphalt hardening on pavement life. *Journal of the Association of Asphalt Paving Technologists*, *27*, 196–208.

Daniel, J. S., Richard Kim, Y., & Lee, H. J. (1998). Effects of aging on viscoelastic properties of asphalt-aggregate mixtures. *Transportation Research Record*, *1630*(1), 21–27. https://doi.org/10.3141/1630-03

Darabi, M. K., Kola, R., Little, D. N., & Garg, N. (2020). Time-dependent Drucker-Prager-Cap model coupled with PANDA (Pavement Analysis Using Nonlinear Damage Approach) to predict rutting performance of flexible pavements. *Construction and Building Materials*, *244*, 118326. https://doi.org/10.1016/j.conbuildmat.2020.118326

Di Benedetto, H., Sauzéat, C., & Clec'h, P. (2016). Anisotropy of bituminous mixture in the linear viscoelastic domain. *Mechanics of Time-Dependent Materials*, *20*(3), 281–297.

Doyle, P. (1958). Cracking characteristics of asphalt cement. *Proc of Assoc of Asphalt Paving Technologists*, *27*, 581–597.

Far, M. S. S., Underwood, B. S., Ranjithan, S. R., Kim, Y. R., & Jackson, N. (2009). Application of artificial neural networks for estimating dynamic modulus of asphalt concrete. *Transportation Research Record*, (2127), 173–186.

Ferry, J. D. (1980). *Viscoelastic properties of polymers*. John Wiley & Sons.

Filonzi, A., Komaragiri, S., Hajj, R., Trevino, M., Hazlett, D., Mahmoud, E., & Bhasin, A. (2022). A method to evaluate the tensile strength and ductility of asphalt binders using a thin confined film. *International Journal of Pavement Engineering*, 1–12.

Flintsch, G. W., Ferne, B., Diefenderfer, B., Katicha, S., Bryce, J., & Nell, S. (2012). Evaluation of traffic-speed deflectometers. *Transportation Research Record*, *2304*(1), 37–46.

Garcia, G., & Thompson, M. (2007). *HMA dynamic modulus predictive models (a review)* (Report No. FHWA-ICT-07-005). Illinois Center for Transportation.

Glover, C. J., Davison, R. R., Domke, C. H., Ruan, Y., Juristyarini, P., Knorr, D. B., & Jung, S. H. (2005). *Development of a new method for assessing asphalt binder durability with field validation* (Report No. FHWA/TX-05/1872-2). Texas Transportation Institute.

Hernandez, J. A., Gamez, A., & Al-Qadi, I. L. (2016). Effect of wide-base tires on nationwide flexible pavement systems: Numerical modeling. *Transportation Research Record*, *2590*(1), 104–112. https://doi.org/10.3141/2590-12

Illinois Department of Transportation. (2016). *Bureau of design and environment manual*.

Illinois Department of Transportation. (2021). *Manual of Test Procedures for Materials*.

Illinois Department of Transportation. (2022). *Standard Specifications for Road and Bridge Construction.*

Illinois Department of Transportation. (2023). *Special Provision 80441.*

Isied, M. M., & Souliman, M. I. (2019). Integrated predictive artificial neural network fatigue endurance limit model for asphalt concrete pavements. *Canadian Journal of Civil Engineering*, *46*(2), 114–123. https://doi.org/10.1139/cjce-2018-0051

Jiang, Z. Y., Ponniah, J., & Cascante, G. (2006). Improved ultrasonic pulse velocity technique for bituminous material characterization. *Transportation Association of Canada*.

Katicha, S., Flintsch, G., & Diefenderfer, B. (2022). Ten years of traffic speed deflectometer research in the United States: A review. *Transportation Research Record*, *2676*(12), 152–165

Kim, Y. R., Underwood, B., Far, M. S., Jackson, N., & Puccinelli, J. (2011). *LTPP computed parameter: Dynamic modulus* (Report No. FHWA-HRT-10-035). Federal Highway Administration.

Lasemi, Z. (2015). Illinois industrial minerals: An overview. In *Proceedings of the 47th forum on the Geology of industrial minerals* (pp. 173–181). Illinois State Geological Survey, Prairie Research Institute.

Lippert, D. L., Wu, S., Ozer, H., Al-Qadi, I. L., Meister, J. F., Renshaw, G., Barry, M. K., Said, I. M., Murphy, T., Espinoza Luque, A. F., Safi, F. R., Trepanier, J. S., & Vespa, J. W. (2017). *Construction and performance monitoring of various asphalt mixes in Illinois: 2016 interim report* (Report No. FHWA-ICT-17-003). Illinois Center for Transportation.

Ma, J., Nawarathna, H. M., & Hesp, S. A. (2022). On the sustainable use of recycled plastics in flexible asphalt pavements. *Journal of Cleaner Production*, *359*, 132081.

Mata, R., Ruiz, R. O., & Nuñez, E. (2023). Correlation between compressive strength of concrete and ultrasonic pulse velocity: A case of study and a new correlation method. *Construction and Building Materials*, *369*, 130569. https://doi.org/10.1016/j.conbuildmat.2023.130569

Medina, J. R., Underwood, B. S., & Mamlouk, M. (2018). Estimation of asphalt concrete modulus using the ultrasonic pulse velocity test. *Journal of Transportation Engineering, Part B: Pavements*, *144*(2), 04018008. https://doi.org/10.1061/JPEODX.0000036

Miao, X., Lasemi, Z., Mikulic, D. G., & Falter, M. (2016). Directory of Illinois mineral producers, and maps of extraction sites. *Circular no. 584*.

Mohammad, L. N., Kim, M., Raghavendra, A., & Obulareddy, S. (2014). *Characterization of Louisiana asphalt mixtures using simple performance tests and MEPDG* (Report No. FHWA/LA. 11/499). Louisiana Department of Transportation and Development.

Mohanraj, K., Filonzi, A., Mahmoud, E., & Bhasin, A. (2023). Field validation on the use of poker-chip test to predict cracking in flexible pavements. *Journal of Transportation Engineering, Part B: Pavements*, *149*(2), 1–11. https://doi.org/10.1061/JPEODX.PVENG-1202

Monismith, C., Secor, K., & Blackmer, E. (1961). Asphalt mixture behavior in repeated flexure. *Journal of the Association of Asphalt Paving Technologists*, 30.

Nguyen, Q. T., Di Benedetto, H., Nguyen, Q. P., & Hoang, T. T. N. (2021). Effect of time–temperature, strain level and cyclic loading on the complex Poisson's ratio of asphalt mixtures. *Construction and Building Materials*, *294*, 123564. https://doi.org/10.1016/j.conbuildmat.2021.123564

Olivier, A., Shields, M. D., & Graham-Brady, L. (2021). Bayesian neural networks for uncertainty quantification in data-driven materials modeling. *Computer Methods in Applied Mechanics and Engineering*, *386*, 114079.

Pal, P. (2019). Dynamic Poisson's ratio and modulus of elasticity of pozzolana Portland cement concrete. *International Journal of Engineering and Technology Innovation*, *9*(2), 131–144.

Papazian, H. S. (1961). *The response of linear viscoelastic materials in the frequency domain* (Doctoral dissertation, The Ohio State University).

Prowell, B. D. (2010). *Validating the fatigue endurance limit for hot mix asphalt* (Vol. 646).

Transportation Research Board.

Pundit Lab (2017). Operating Instructions for Ultrasonic Instrument.

Romero, P., & VanFrank, K. (2019). *Balanced asphalt concrete mix performance in Utah, phase III: Evaluation of field materials using BBR and SCB-IFIT tests* (No. UT-19.15). Utah Department of Transportation, Research Division.

Rowe, G., Baumgardner, G., & Sharrock, M. (2009). Functional forms for master curve analysis of bituminous materials. In *Advanced testing and characterization of bituminous materials*, two volume set (pp. 97–108). CRC Press.

Saremi, S. G., Goulias, D. G., & Akhter, A. A. (2023). Non-destructive testing in quality assurance of concrete for assessing production uniformity. *Transportation Research Record*, *2677*(1), 1259–1275. https://doi.org/10.1177/03611981221103871

Schapery, R. A. (1984). Correspondence principles and a generalized J integral for large deformation and fracture analysis of viscoelastic media. *International Journal of Fracture*, *25*(3), 195–223.

Shen, S., & Carpenter, S. H. (2005). Application of the dissipated energy concept in fatigue endurance limit testing. *Transportation Research Record*, *1929*, 165–173.

Shen, S., & Carpenter, S. H. (2006). *Dissipated energy concepts for HMA performance: Fatigue and healing* (Vol. 67, No. 11).

Shen, S. (2006). *Dissipated energy concepts for HMA performance: Fatigue and healing*. University of Illinois at Urbana-Champaign.

Si, Z., Little, D. N., & Lytton, R. L. (2002). Characterization of microdamage and healing of asphalt concrete mixtures. *Journal of Materials in Civil Engineering*, *14*(6), 461–470.

Singh, D., Zaman, M., & Commuri, S. (2013). Artificial neural network modeling for dynamic modulus of hot mix asphalt using aggregate shape properties. *Journal of Materials in Civil Engineering*, *25*(1), 54–62. https://doi.org/10.1061/(ASCE)MT.1943-5533.0000548

Singhvi, P., Mainieri, J. J. G., Ozer, H., Sharma, B. K., Al-Qadi, I. L., & Morse, K. L. (2022). Impacts of field and laboratory long-term aging on asphalt binders. *Transportation Research Record*, *2676*(8), 336–353. https://doi.org/10.1177/03611981221083614

Sultana, S., & Bhasin, A. (2014). Effect of chemical composition on rheology and mechanical properties of asphalt binder. *Construction and Building Materials*, *72*, 293–300. https://doi.org/10.1016/j.conbuildmat.2014.09.022

Tavassoti-Kheiry, P., Boz, I., Chen, X., & Solaimanian, M. (2017). Application of ultrasonic pulse velocity testing of asphalt concrete mixtures to improve the prediction accuracy of dynamic modulus master curve. *Proceedings, Airfield and Highway Pavements*.

Van Velsor, J. K., Premkumar, L., Chehab, G., & Rose, J. L. (2011). Measuring the complex modulus of asphalt concrete using ultrasonic testing. *Journal of Engineering Science & Technology Review*, *4*(2).

Williams, M. L., Landel, R. F., & Ferry, J. D. (1955). The temperature dependence of relaxation mechanisms in amorphous polymers and other glass-forming liquids. *Journal of the American*

Chemical Society, *77*(14), 3701–3707.

Witzcak, M. W. (2002). *Simple performance test for Superpave mix design* (Vol. 465). Transportation Research Board.

Witczak, M., El-Basyouny, M., & El-Badawy, S. (2007). *Incorporation of the new (2005) |E*| predictive model in the MEPDG*. NCHRP 1-40D Final Report.

Witczak, M. W., & Fonseca, O. A. (1996). Revised predictive model for dynamic (complex) modulus of asphalt mixtures. *Transportation Research Record*, *1540*(1), 15–23.

Witczak, M. W., Mamlouk, M. S., Souliman, M., & Zeiada, W. (2013). *Laboratory validation of an endurance limit for asphalt pavements*. Transportation Research Board.

Witczak, M. W., & Root, R. E. (1974). Summary of complex modulus laboratory test procedures and results. In *Fatigue and Dynamic Testing of Bituminous Mixtures*. ASTM International.

Yan, C., Zhang, Y., & Bahia, H. U. (2020). Comparison between SCB-IFIT, un-notched SCB-IFIT and IDEAL-CT for measuring cracking resistance of asphalt mixtures. *Construction and Building Materials*, *252*, 119060. https://doi.org/10.1016/j.conbuildmat.2020.119060

Zhu, Z., Singhvi, P., Ali, U. M., Ozer, H., & Al-Qadi, I. L. (2020). Quantification of the effect of binder source on flexibility of long-term aged asphalt concrete. *Transportation Research Record*, *2674*(9), 605–616. https://doi.org/10.1177/0361198120930717

Zhang, J., Alvarez, A. E., Lee, S. I., Torres, A., & Walubita, L. F. (2013). Comparison of flow number, dynamic modulus, and repeated load tests for evaluation of HMA permanent deformation. *Construction and Building Materials*, *44*, 391–398. https://doi.org/10.1016/j.conbuildmat.2013.03.013

APPENDIX

DYNAMIC MODULUS PHASE ANGLE CURVES

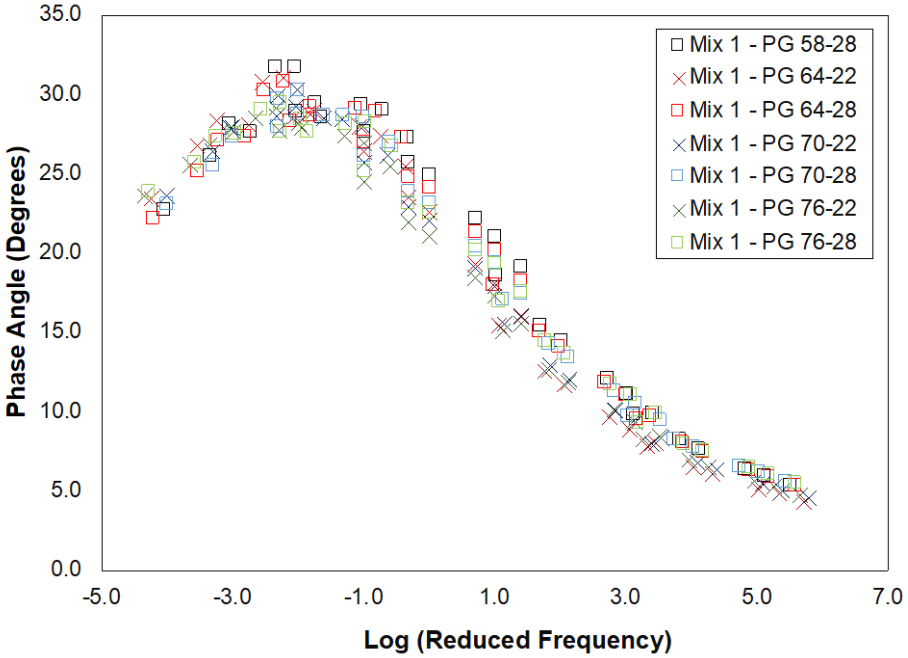

Figure 47. Plot. Phase angle curves for mix 1 (reference temperature = 21.1°C).

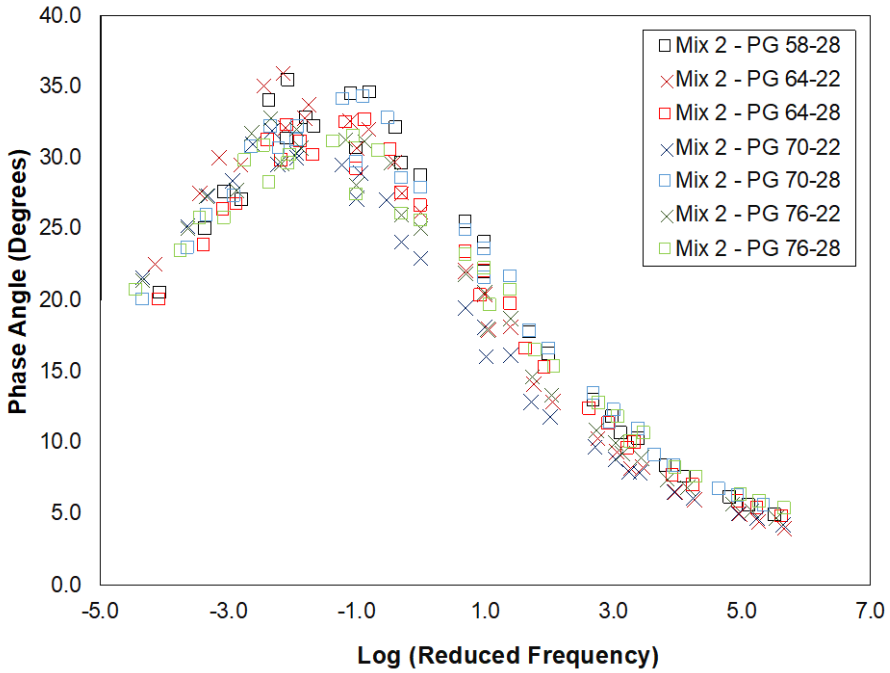

Figure 48. Plot. Phase angle curves for mix 2 (reference temperature = 21.1°C).

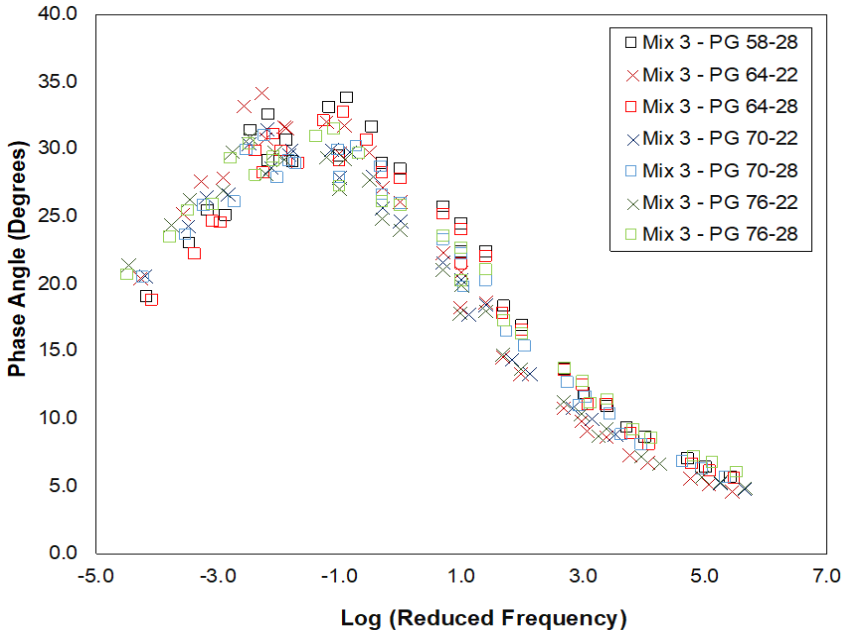

Figure 49. Plot. Phase angle curves for mix 3 (reference temperature = 21.1°C).

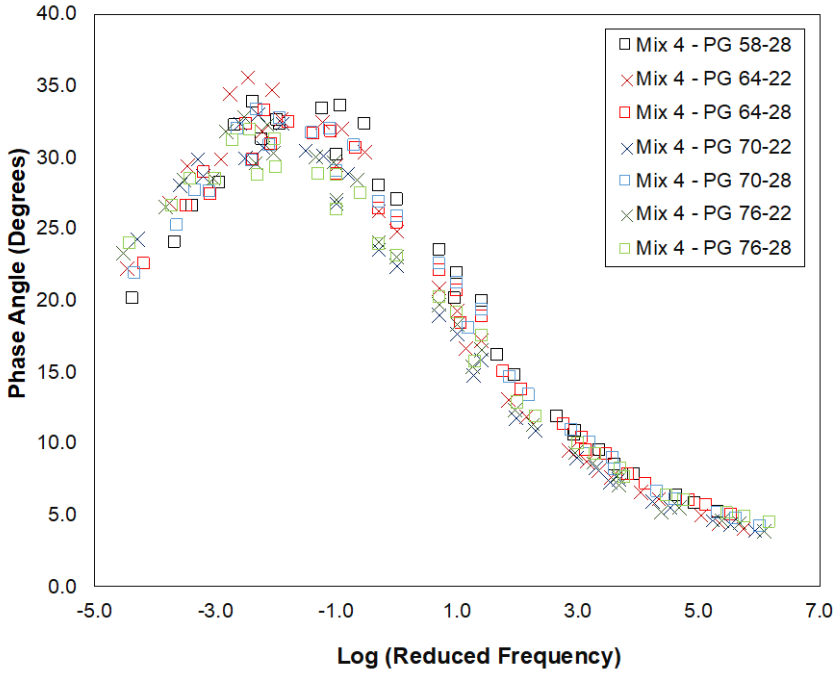

Figure 50. Plot. Phase angle curves for mix 4 (reference temperature = 21.1°C).

DYNAMIC MODULUS BLACK-SPACE DIAGRAMS

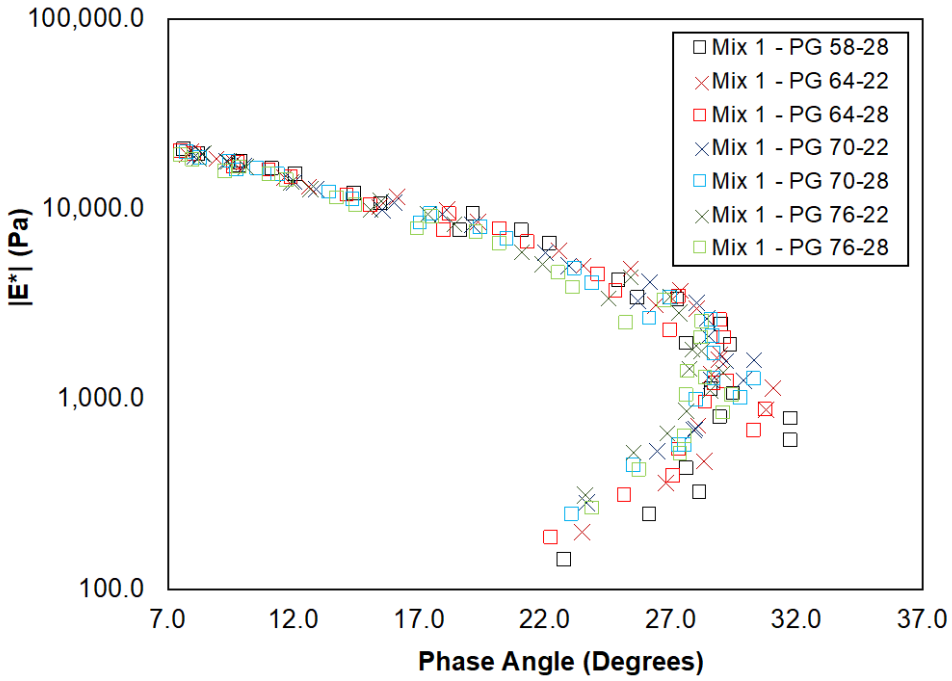

Figure 51. Plot. Black space diagram curves for mix 1 (reference temperature = 21.1°C).

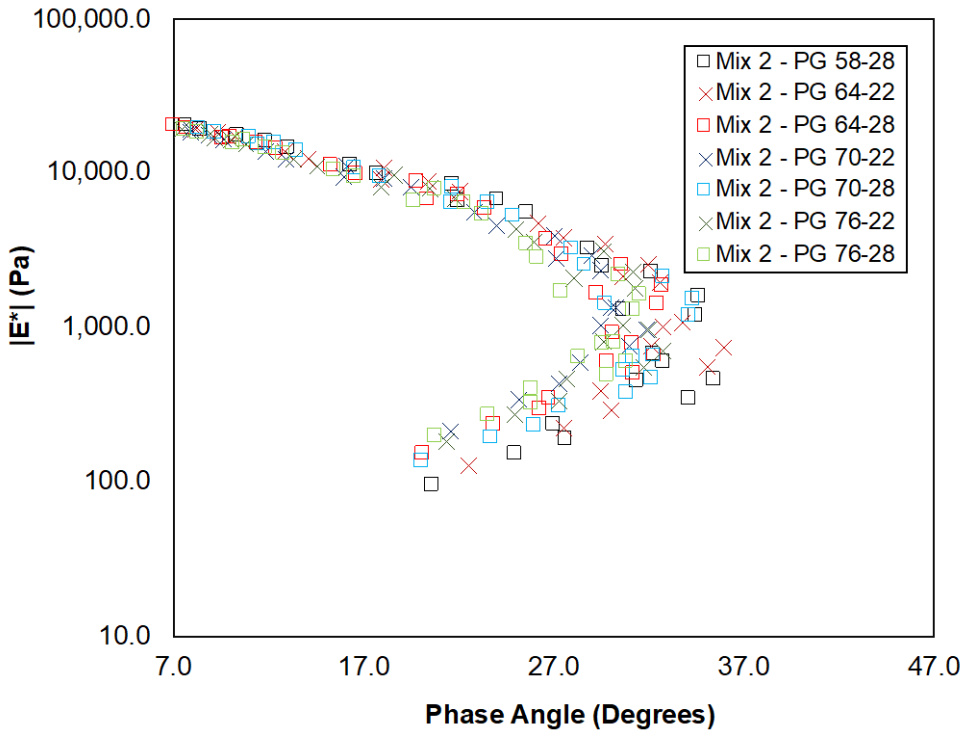

Figure 52. Plot. Black space diagram curves for mix 2 (reference temperature = 21.1°C).

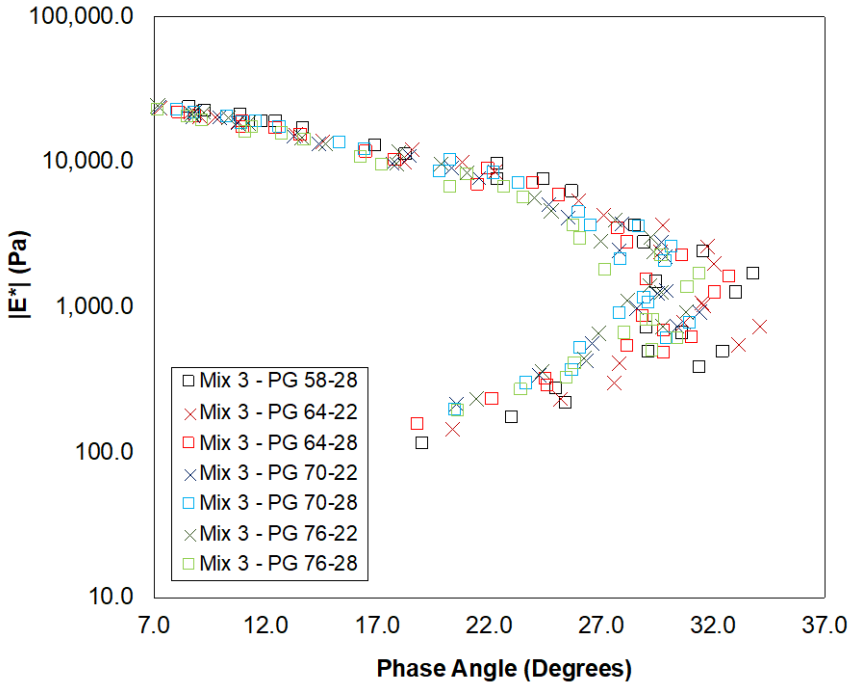

Figure 53. Plot. Black space diagram curves for mix 3 (reference temperature = 21.1°C).

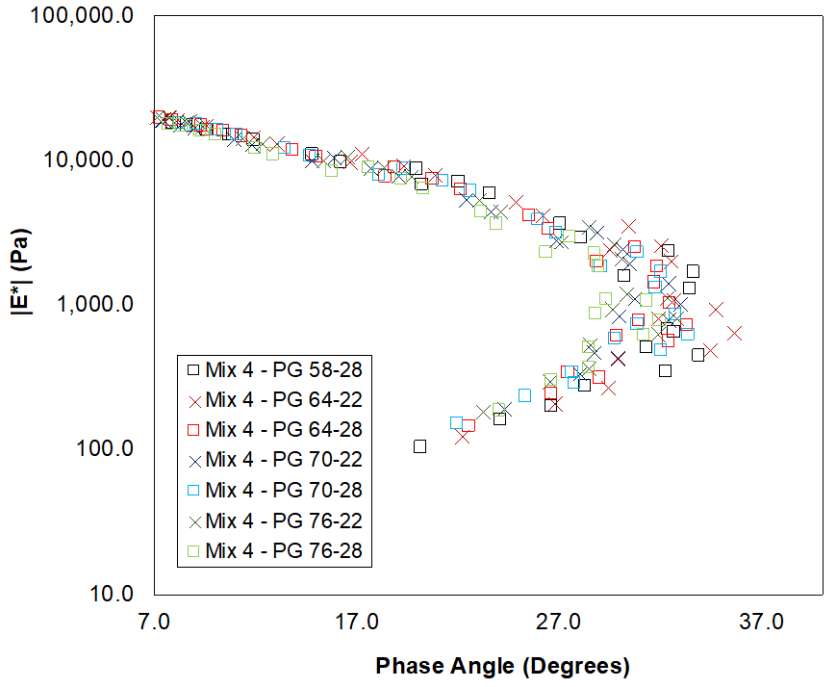

Figure 54. Plot. Black space diagram curves for mix 4 (reference temperature = 21.1°C).

UPV MASTER CURVES

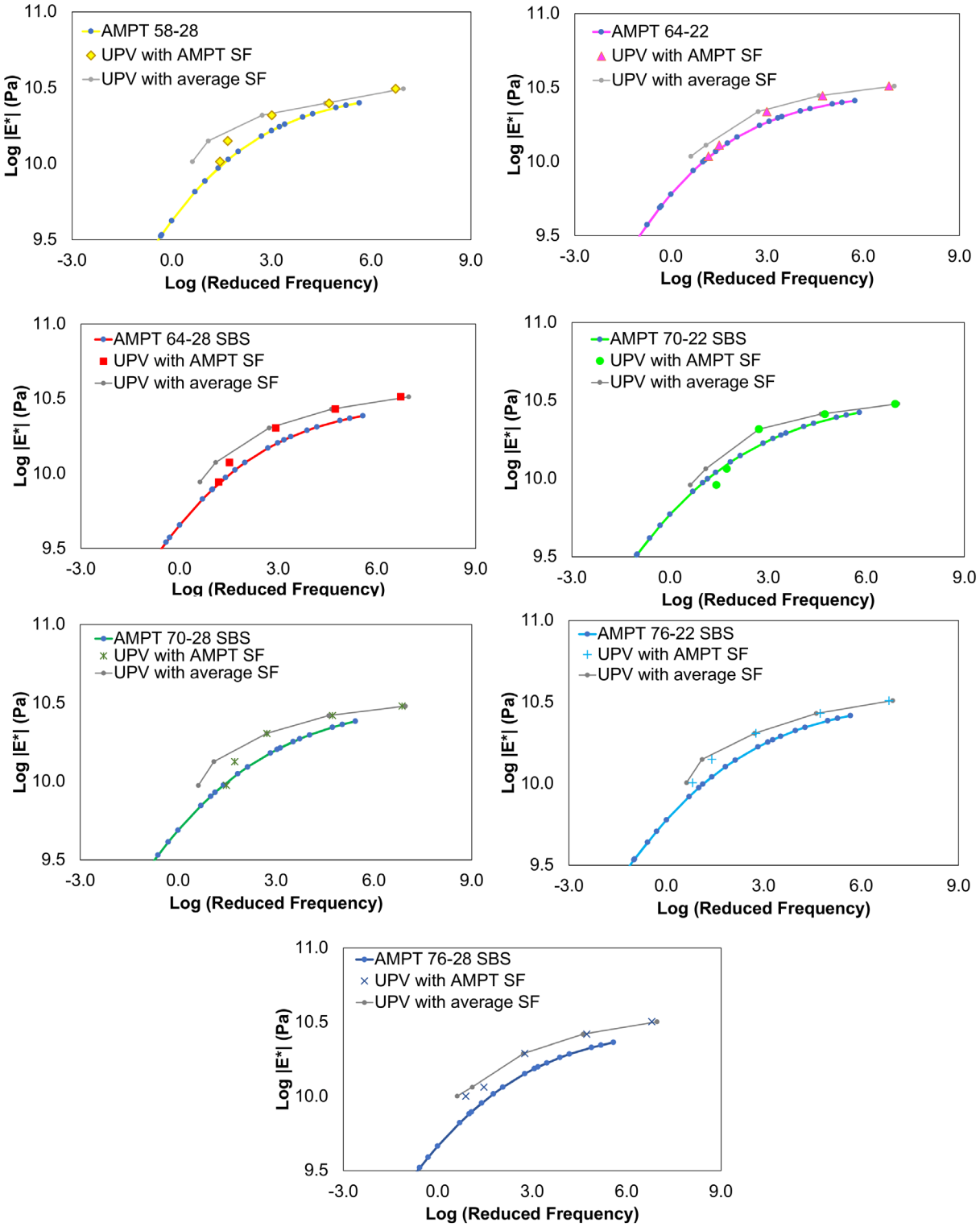

Figure 55. Graph. AMPT and UPV-derived master curves for mix 1 (reference temperature = 21.1°C).

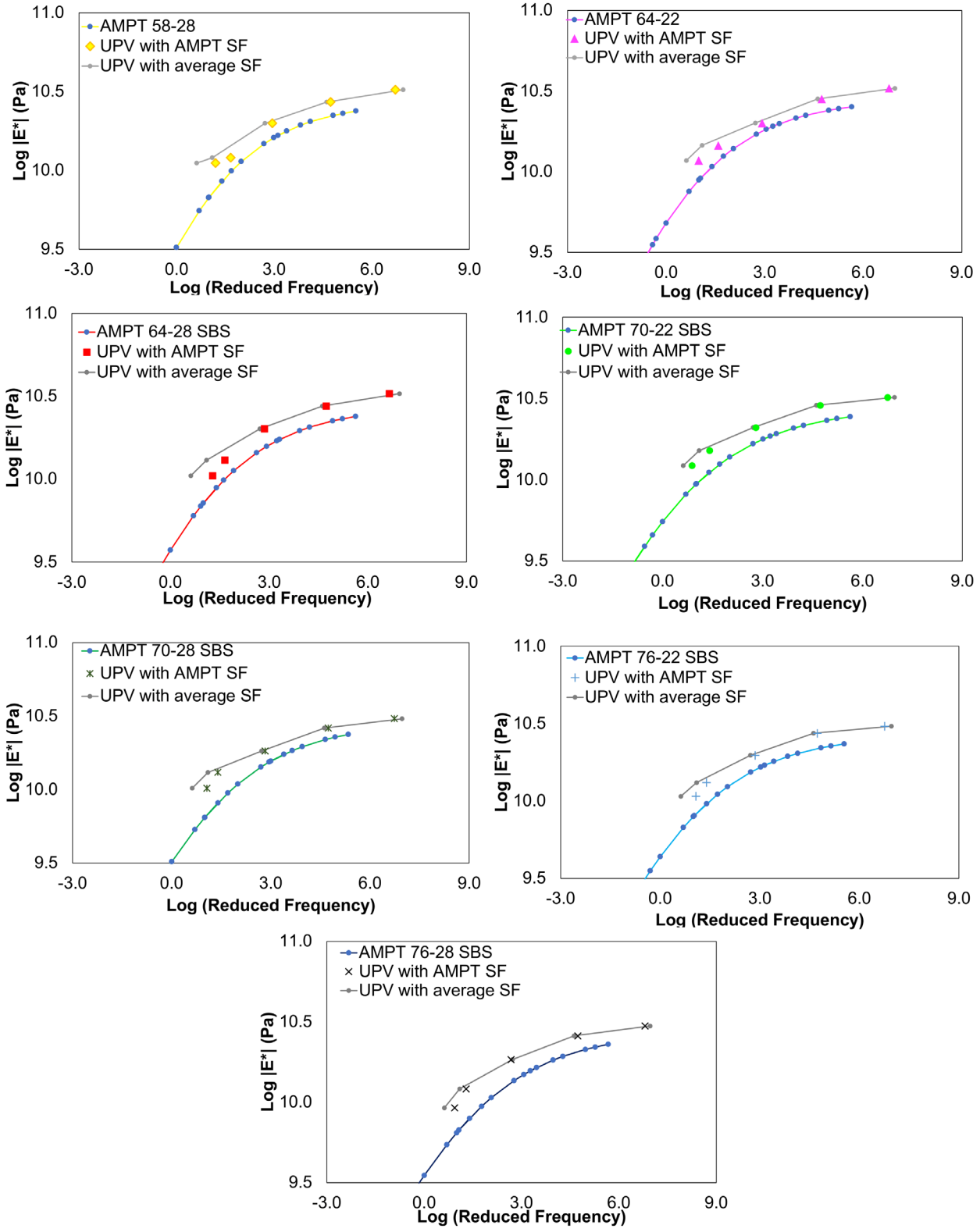

Figure 56. Graph. AMPT and UPV-derived master curves for mix 2 (reference temperature = 21.1°C).

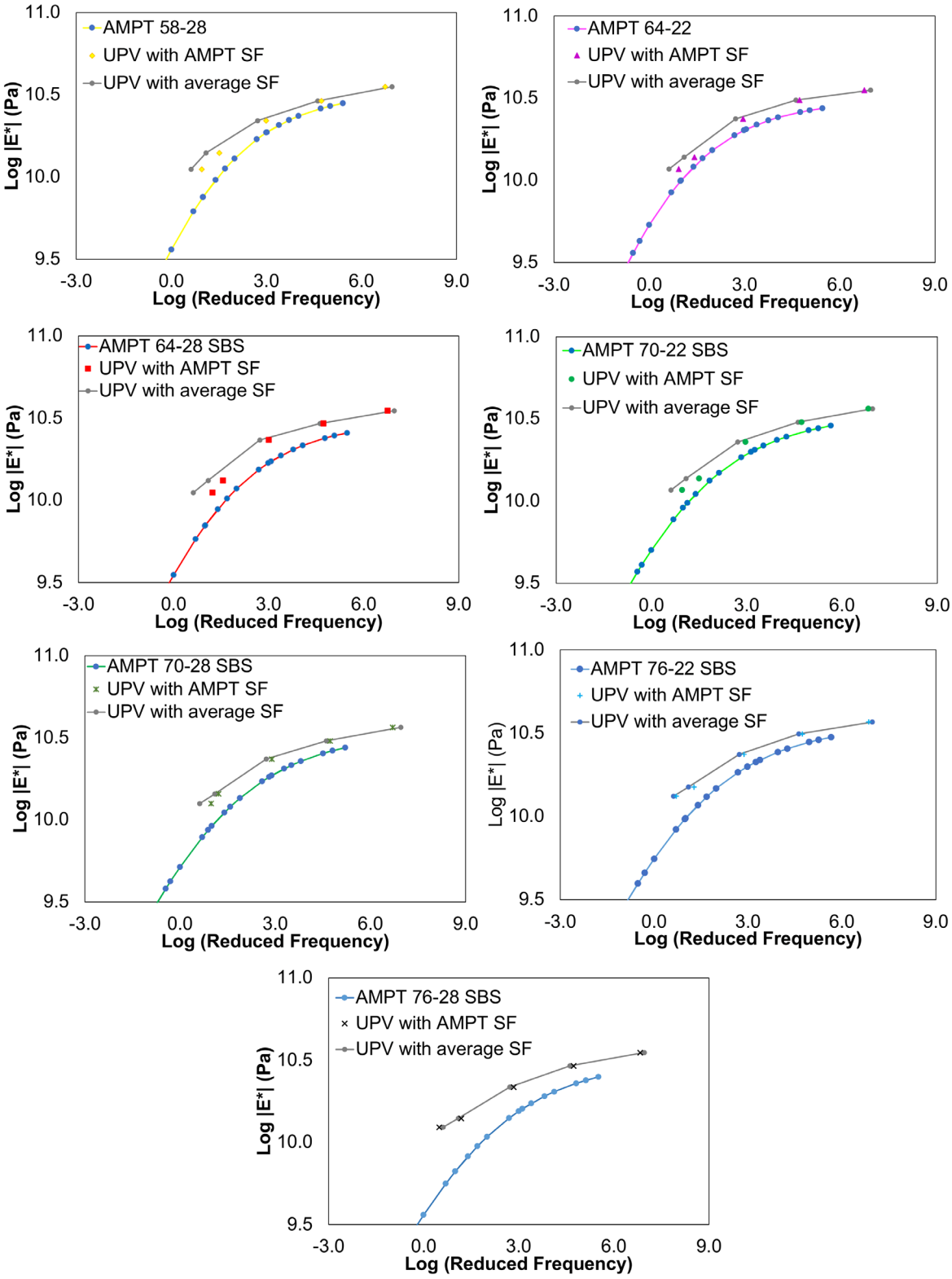

Figure 57. Graph. AMPT and UPV-derived master curves for mix 3 (reference temperature = 21.1°C).

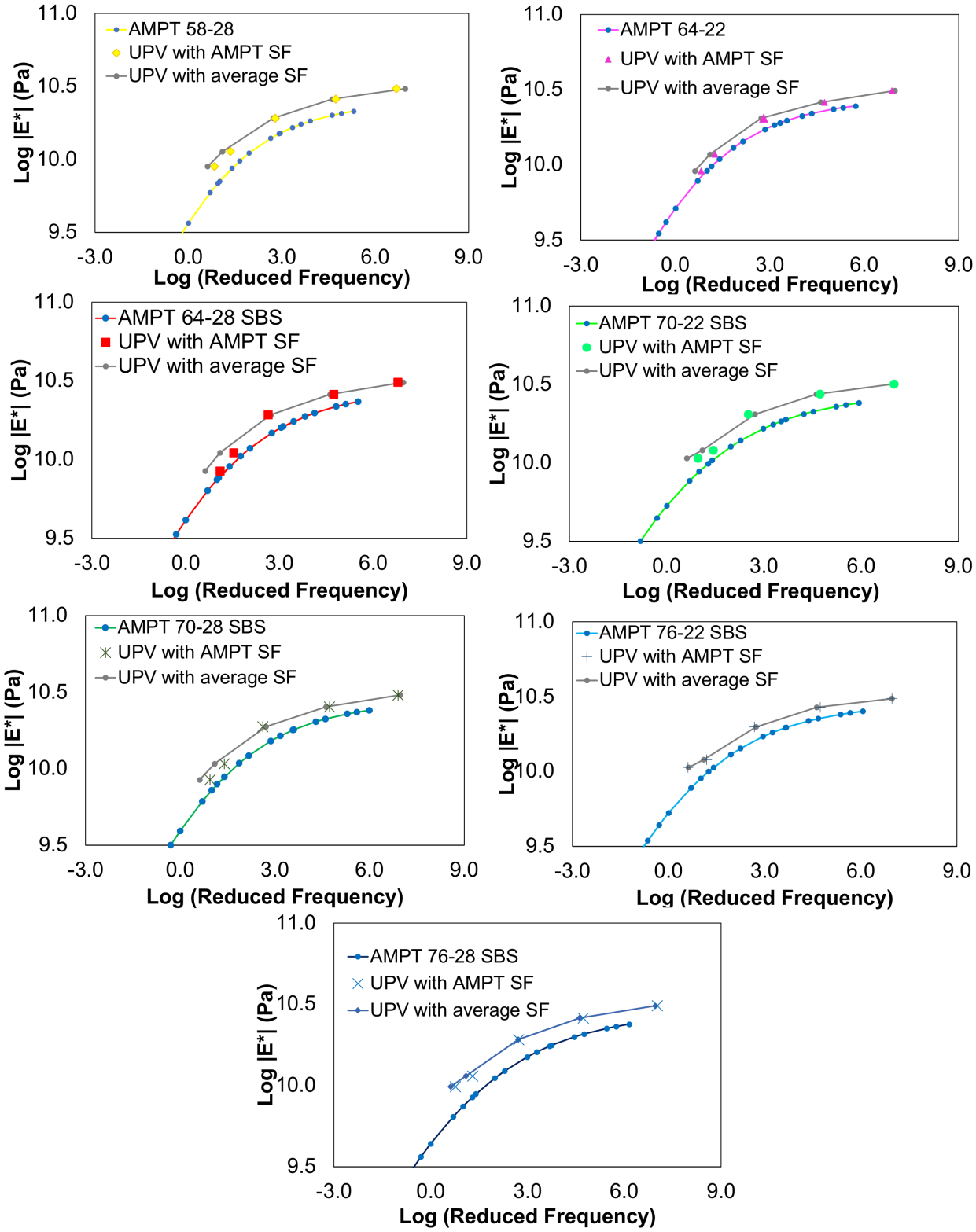

Figure 58. Graph. AMPT and UPV-derived master curves for mix 4 (reference temperature = 21.1°C).

STRAIN-LEVEL ANALYSIS FOR DIFFERENT ASSUMPTIONS REGARDING SR

Table 15. Strain Levels Associated with a "No Damage" Baseline Scenario from the 1-second Rest Period Analysis

Mix	Binder	Minimum SR at 1-second RP ("no damage")	Correspondent strain level at 0-second RP
1	58-28	90	160
1	64-22	90	150
1	76-22	97	50
1	76-28	88	150
2	58-28	87	250
2	64-28	101	Min
2	70-28	95	150
2	76-28	91	150
3	58-28	98	70
3	64-22	98	Min
3	70-22	97	50

Table 16. Strain levels Associated with Different "Acceptable SR" Premises

Mix	Binder	Strain level (0-s RP) at peak SR	Strain level (0-s RP) at SR > 90%	Strain level (0-s RP) at SR > 95%
1	58-28	120	160	Min
1	64-22	50	150	70
1	76-22	50	175	100
1	76-28	50	150	50
2	58-28	90	200	125
2	64-28	90	200	125
2	70-28	100	250	150
2	76-28	50	150	100
3	58-28	70	200	125
3	64-22	50	150	100
3	70-22	50	175	90


Illinois Department
of Transportation


ILLINOIS